

UNIVERSITY OF MELBOURNE

SCHOOL OF MATHEMATICS AND STATISTICS

THE BLOCKCHAIN PROPAGATION PROCESS: A MACHINE
LEARNING AND MATRIX ANALYTIC APPROACH

Aapeli Vuorinen

supervised by
Professor Peter Taylor

A thesis submitted for the degree of
Master of Science

May 17, 2019

Abstract

Blockchain, spearheaded by the Bitcoin cryptocurrency, is a novel, emerging technology that allows a distributed network of users to synchronise and maintain a decentralised, global ledger of transactions with no central control or authority. One key part of this technology is the process by which blocks and transactions propagate through the underlying network of users, allowing them to come to a consensus on the state of the ledger and advance the blockchain. In this thesis, we explored the propagation process for Bitcoin within the mathematical framework of matrix analytic processes by performing an observational experiment to collect data and fitting phase-type distributions to this dataset.

It is well known that the propagation delay of blocks is a key limiting factor in the efficiency and scalability of blockchain technology. It is imperative that the network reaches an overall consensus on the current state of the chain of blocks at regular epochs. If blocks propagate faster through the network, then this happens faster and the time between blocks can be decreased. This means that the blockchain can then process more events as well as verify those events faster. Additionally, recent work on a strategy known as selfish-mining has shown that adversarial miners can take advantage of this delay to inflate their share of mining rewards.

We set out to model the block propagation process of Bitcoin blocks. To do so, we set up a distributed, large-scale observational experiment by creating a global data collection system for observing the block propagation process. We collected data on the propagation patterns of 14810 blocks over 5 months from November 2018 until March 2019, and created a novel tool for observing the blockchain from several geographically diverse locations.

We fitted Coxian phase-type distributions of a varying number of phases to the data and performed model selection, finally choosing a model with $p = 4$ phases. We used a variant of the EM-algorithm originally introduced by Asmussen, and made improvements to the computational run-time of the algorithm. We present the final parameter estimates of our model and discuss the merits and shortcomings of this approach.

This thesis makes three contributions. The first is an open dataset of Bitcoin block propagation data which we have cleaned and pre-processed to include additional covariates extracted from the blockchain. We present a short exploratory data analysis of patterns in the dataset in Part III. Our second contribution is a phase-type model for the block propagation delay, which we discuss in Part II. Finally, we have made an incremental improvement to the EM-algorithm for fitting phase-type distributions by parallelising it and reducing its memory footprint, which is particularly useful for very large, “big data” datasets. We also believe that our exposition describing the Bitcoin ecosystem in Part I is of value.

We have created an accompanying website at <https://bitcoin.aapelivuorinen.com/>, which contains complementary material, the cleaned dataset, the source code for data collection, and our improved phase-type fitting algorithm.

Acknowledgments

I wish to express my gratitude towards Peter Taylor for his patient, inspiring supervision, and for providing me with direction when I needed it through insightful comments and criticism.

I would like to thank my good friend and mentor, Yoni Nazarathy for his continuous encouragement, support, and guidance over the past years, both in mathematics and in life.

Finally, I would like to thank the friends and family who supported me through this endeavour.

Contents

Abstract	1
Acknowledgments	2
1 Introduction	5
1.1 Outline of the thesis	7
I Bitcoin	8
2 Overview of the Bitcoin ecosystem	9
2.1 Overview of cryptographic primitives	10
2.1.1 Digital signatures	10
2.1.2 Cryptographically hash functions	10
2.1.3 Proof-of-work schemes	11
2.1.4 Merkle trees	12
2.2 The structure of the blockchain	12
2.2.1 Addresses and wallets	12
2.2.2 Transactions	13
2.2.3 Blocks and the mining process	13
2.2.4 51 % attacks and double spending	16
2.2.5 Application-Specific Integrated Circuits	17
2.2.6 Mining pools	17
2.2.7 The block size limit and SegWit transactions	18
2.3 The Bitcoin protocol	18
2.3.1 Protocol messages	18
2.3.2 Nodes and peers	18
2.3.3 Peer discovery	19
2.3.4 Control messages: <code>version/verack</code> , <code>ping/pong</code> , <code>getaddr/addr</code>	19
2.3.5 Data messages: <code>inv</code> , <code>getdata</code> , <code>tx</code> , <code>block</code> , <code>getheaders/headers</code>	19
2.3.6 The transaction propagation process	20
2.3.7 The block propagation process	20
3 Data collection and the bitcoin-crawler	21
3.1 Overview	21
3.2 The <code>bitcoin-crawler</code>	21
3.3 The global data collection system	23
3.4 Blockchain data and mining pools	23
3.5 Cleaning of nonsensical data	24
4 The dataset	25
4.1 Overview of the dataset	25
4.2 Accompanying website and source code	27
II Mathematical modelling	28
5 Mathematical preliminaries	29
5.1 Continuous time Markov chains	29
5.2 Phase-type distributions	31
5.2.1 Examples of phase-type distributions	32
5.2.2 Coxian distributions	33
5.3 The expectation-maximisation algorithm	33
5.4 Fitting phase-type distributions to data	35
5.5 Properties of the algorithm	37
5.6 Akaike's Information Criterion	38
5.7 MapReduce	38

6	Computational aspects of phase-type fitting	39
6.1	The integral $\mathbf{\Gamma}$	39
6.1.1	The <code>EMpht.c</code> program	40
6.1.2	The <code>EMpht.jl</code> program	41
6.1.3	Uniformisation methods	41
6.2	Our program	43
6.3	Computation of the conditional expectations	43
7	Phase-type fits to propagation delays	44
7.1	Method	45
7.2	Model selection	45
7.3	Discussion	46
7.3.1	Basic statistics	47
7.3.2	Interval-censoring and censoring of the tail	48
7.3.3	Interpretation as propagation delay	48
7.3.4	Further extensions	48
III	Exploratory Data Analysis and Further Questions	50
8	Patterns in the dataset	51
8.1	Inter-arrival times of blocks	51
8.2	Difference between timestamp in the block header and the arrival time	52
8.3	Empty and full blocks, size and weight	53
8.4	Block size and number of transactions	55
8.5	Empty blocks and mining pools	55
8.6	Causes of delay	56
8.7	Delay and location	58
	Conclusion	62
IV	Appendices	63
A	Maximum likelihood estimators for transition rates and initialisation probabilities of a Markov chain	64
B	Computation of conditional expectations	66
C	Computations for the integral $\mathbf{\Gamma}$ as the exponential of a block matrix	69

Chapter 1

Introduction

Bitcoin, conceived by Nakamoto in 2008 [1], is a decentralised electronic payment system that introduced the concept of a blockchain. Often referred to as a cryptocurrency, Bitcoin relies on asymmetric cryptography to manage addresses which act as containers for Bitcoins, and to authorise transactions from one such address to another using digital signatures. These transactions are broadcasted onto a public network where several entities operate as “miners”; working to bundle these transactions together into blocks in exchange for a reward. Miners continuously work on solving a computationally difficult problem, and each time a miner finds a solution to the problem, a new block is mined. The difficulty of this computational problem, known as the proof-of-work, is regularly adjusted so that blocks occur on average every ten minutes. Each block references the last block in the chain, constructing a succession of blocks known as the blockchain.

Outside of the research community, Bitcoin has seen high uptake due to its innovative, decentralised design which renders control by any entity impossible, and the ideals of distributed self-governance in the absence of trust that it represents. However, its exchange rate has been a source of intense speculation and coupled with its high volatility, slow transaction times, and high fees, the ability of Bitcoin to act as a currency or stable store of value is limited. In addition, a lack of control by regulatory authorities has led to a surge of Bitcoin’s use in illicit transactions, which in turn drives it further away from legitimate industry.

Nonetheless, as it matures, blockchain technology continues to draw increased interest from the technology sector, with several startups and established enterprises alike exploring blockchain technology as a solution to their business needs. Technical problems still exist with tying together the boundary between real world events and the self-governing blockchain, as well as in scalability and efficiency. Several iterations of blockchains have been proposed and created since Bitcoin, implementing new and exciting features such as smart contracts, allowing intricate custom logic to be implemented on a blockchain.

Blockchain itself, an inventive human construct, has given rise to a multitude of interesting phenomena, attracting researchers from many fields to study it from several perspectives and approaches. Research on the emerging behaviour and properties of blockchain lies at the intersection of several communities, including the applied probability and modelling community, the game theoretic community, the networking and topology inference community, as well as the distributed systems and database community within computer science. These areas often overlap, giving rise to fruitful discussions between different communities and cultivating cross collaboration across fields of research. A unique property of blockchain is that the full history of transactions and events that were accepted into the ledger are readily available, which opens up further avenues for research.

From a probabilistic modelling perspective, the blockchain structure and the processes underlying its construction present several interesting questions to be studied. This includes the block arrival process which is modelled in [2], and double spending attacks as modelled in [3]. Other extensions exploring the behaviour of systems similar to blockchain have been proposed, such as those where the rate of blocks being produced is much higher than the rate at which the network can propagate those nodes to every node to reach a consensus, leading to a random tree structure instead of one resembling a chain with occasional branches.

The incentives underpinning the mining process, coupled with the rare yet considerable reward for mining a block, make the process an interesting construct to study from the angle of game theory. One interesting model for miner behaviour is the selfish-mine strategy introduced in [4], and further studied by Göbel et al. under the presence of propagation delay in [5]; who show that miners can inflate their share of mining rewards using this strategy. Others have studied the behaviour of mining pools, groups of miners who band together share the burden and rewards in order to reduce the variance in the revenue of their mining operations. In [6], the authors examine the dynamics of mining pools the framework of cooperative game theory. The reward from mining blocks will eventually disappear, presumably as miners should be rewarded from transaction fees. The implications of having blocks without an intrinsic reward are studied in [7].

The control packets and the structure of the ad-hoc, peer-to-peer network underlying blockchains are fundamentally different from those of other pre-existing networks such as the internet. This provides an exciting challenge for the networking community in attempting to infer the topology of the network. Much research has been done on revealing the topology of the underlying network using both active and passive methods; for instance, a method exploiting the Bitcoin protocol was developed in [8], in [9] inference was performed using a Bayesian approach, and in [10] a timing analysis based method was developed. It is a rapidly evolving field, with the Bitcoin protocol being continuously adjusted to counteract each new inference technique soon after it is published.

Finally, blockchain is studied by the distributed systems and databases community in computer science, who are mainly interested in the scalability and efficiency of the system as a database and distributed system. The work in this field ranges from modelling blockchain as a distributed system as in [11], to proposing new consensus protocols to overcome the limitations of the current proof-of-work solutions. Several authors have studied Byzantine fault-tolerance as an alternative, see [12] for an overview of recent developments. Approaches to overcome scalability issues in blockchain currently consist of two major branches: using sharding to distribute the blockchain across the network as in [13], and using off-chain transaction networks to reduce the amount of data stored on the main network. The Lightning network currently in development for Bitcoin is an example of the latter.

The aim of this work is to explore aspects of the block propagation process of Bitcoin, in particular, the structure of delays, and the time taken for the network to reach consensus. To this end, we performed a large-scale observational experiment and collected data on the propagation patterns of 14810 blocks between November 2018 and March 2019. We then fitted several phase-type models to this data, discussing the fits and producing an estimate of the delay distribution. In the last part, we have also made an effort to further explore the collected data and open up new research questions that may be investigated using it, by performing an exploratory data analysis.

The contributions of this thesis are threefold. Firstly, we created both a tool and an open, high quality dataset for studying the Bitcoin network. Secondly, we produced estimates and fits of the propagation delay using phase-type distributions. Finally, we made a small improvement to the algorithm for fitting phase-type distributions by increasing its performance for extremely large datasets.

1.1 Outline of the thesis

We begin in Part I by discussing the concepts underlying Bitcoin, and the system we developed to observe the propagation process. Chapter 2 provides a thorough explanation of the Bitcoin ecosystem and in Chapters 3 and 4 we explain our data collection and cleaning methodology, and give an overview of the dataset. We hope that Part I is of value to a general audience.

In Part II we perform our mathematical modelling. In Chapter 5 we introduce the concept of phase-type distributions and develop the theory of maximum likelihood parameter estimation for this family of distributions using the EM-algorithm, while also discussing model selection using Akaike's information criterion and the MapReduce paradigm for data processing. Furthermore, in Chapter 6 we survey recent literature and new improvements on fitting phase-type distributions. Finally, in Chapter 7 we present our phase-type fits and discuss the various ways of extending the model.

Part III consists of a further exploration of the dataset from a less rigorous perspective through an exploratory data analysis. We present some interesting patterns we observed and discuss further research questions that could be investigated from this data.

Part I

Bitcoin

Chapter 2

Overview of the Bitcoin ecosystem

Bitcoin is an electronic payment system introduced in 2008 in [1] and implemented several months later in 2009 as the Bitcoin reference client [14]. It is interesting for its decentralised design which allows it to operate without a central clearing house or a universally trusted authority. This is achieved through a novel and technically creative incentive structure which ties together each entity taking part in the Bitcoin community allowing it to follow a set of predefined rules while operating autonomously.

Bitcoin itself is comprised of two parts. The first consists of the blockchain data structure, a distributed ledger of transactions, as well as the rules guiding its evolution dictating how the ledger advances. These rules are known as the consensus rules. The second part is the network protocol which allows users on the network to transmit this information between one another, and keep the blockchain synchronised between users. Computers connected to the network are referred to as nodes, and two computers connected to each other are called peers of each other. This thesis touches on both aspects of Bitcoin, and in some sense, it can be seen as studying the intersection and interplay of the two.

When a new block is mined or a new transaction is created, the information contained in it must be transmitted by the underlying network protocol to all the nodes in the network. However, this process is not instantaneous due to processing and network delays, which leads to a propagation delay: the time between when a new object is introduced to the network and when it reaches a given node. We call the time at which a new block is mined the block arrival time, or if talking about a particular location, then the block arrival time refers to the time at which the block was first observed at that location.

The propagation delay is extremely important. In the case of a newly mined block, an increased delay leads to the network as a whole taking longer to reach consensus. Due to the nature of the blockchain, it is not enough for a block to be mined for it to be immutably in the chain. As shown by Nakamoto in the original Bitcoin paper [1], the probability of an adversary who wishes to overwrite the blockchain succeeding drops off exponentially with the number of blocks that they are trying to overwrite. One should therefore only consider a transaction or block permanently confirmed after it is several blocks deep in the blockchain. This means that it takes several times the block inter-arrival time for a transaction to be processed. This hinders the scalability and adoption of blockchain, as a blockchain system with a long block inter-arrival time can include fewer transactions per unit time and takes a longer time to process each transaction.

With an increased propagation delay, certain types of predictable delays may make topology inference tractable, allowing well-funded adversaries to correlate transactions with nodes on the network, corroding the pseudonymity of Bitcoin users. In a sense, imperfections in the underlying network

protocol may leak information about the users of the Bitcoin ecosystem built on top of it.

This chapter is largely based on the source code of the Bitcoin reference client in [14], as well as the author's experience with blockchain and Bitcoin.

2.1 Overview of cryptographic primitives

This section gives an overview of the cryptographic primitives and ideas used in Bitcoin. The system relies heavily on asymmetric cryptography through elliptic curve cryptography to sign and verify transactions; and on cryptographically secure hash functions for its proof-of-work feature. The latter is additionally used in a special structure called a Merkle tree, also discussed in this section.

2.1.1 Digital signatures

Elliptic curve cryptography is a central building block of Bitcoin. It allows users to securely and independently sign a transaction when they wish to transfer Bitcoins, proving that they authorised it, akin to the purpose of real-world signatures on cheques. These elliptic curve digital signatures exploit properties of groups defined on elliptic curves over Galois fields to construct a scheme for digitally signing a piece of binary data using asymmetric key pairs; that is, pairs of keys consisting of a private and a public component. As we only give a high-level overview of the primitives, interested readers are referred to [15] and [16] for a thorough introduction to elliptic curve cryptosystems and [17] for details on the elliptic curve parameters used in Bitcoin.

An asymmetric cryptographic scheme consists of two routines, one for signing data and one for verifying a signature. These routines require the use of an asymmetric key pair, consisting of a private key to be safeguarded by the user, and the public key against which a signature is verified. The private key consists of a randomly generated number, from which the public key is derived. The signing routine can be seen as a function which takes as its inputs a private key and binary data to be signed and outputs a digital signature. The verification routine on the other hand takes a digital signature, binary data, and a public key and returns a binary value indicating whether the signature matches the data and public key or not.

Asymmetric cryptosystems are generally constructed by way of a trapdoor function: a function that is easy to compute given either the public key or the private key, and easy to invert given the private key, but whose inverse is intractable unless one possesses also the private key. In the case of elliptic curve cryptography, the underlying trapdoor function is the discrete logarithm on the Galois field at hand [15]. Importantly, the security of these cryptosystems relies on it really being difficult to compute the inverse of the trapdoor function without the private key, which relies on the assumption that $P \neq NP$; one of the major unsolved problems in theoretical computer science. Furthermore, if $P = NP$, then this inverse can be computed in polynomial time, breaking most asymmetric cryptosystems in use.

2.1.2 Cryptographically hash functions

Bitcoin uses cryptographically secure hashing extensively in its proof-of-work construct and the way it refers to objects. A general hash function is any function that takes an arbitrary length binary string and outputs a fixed size binary string. Hash functions are used in several areas of computer science such as hash tables and non-cryptographic checksums, where one generally hopes they are fast and that values rarely map to the same output. Cryptographic hash functions¹ are a subset of hash functions

¹Again, the theoretical existence of such functions relies on $P \neq NP$.

that make them appropriate for use in cryptography by having the following additional properties:

1. the input is completely uncorrelated to the output, so even a small change in the input completely scrambles the output;
2. given an arbitrary hash, it is computationally infeasible to find an input that matches this hash;
and
3. it is computationally infeasible to find two inputs with the same hash.

These functions are useful in the verification and attestation of information. For instance, suppose we had a large blob of data that needed to be transferred from one location to another. Computing a cryptographic hash of the content before and after the transfer would then provide us with a convenient way of verifying that each bit was correct, meaning we only need to verify n bits for a hash of length n instead of all the bits in the data. A common use of hashing is in signing full documents: digitally signing long binary documents tends to be extremely slow if not impossible, so instead the document is cryptographically hashed, and that short binary string is signed instead.

Most objects referred to in Bitcoin are identified by the hashes of their contents, a property known as content-addressability. For instance, a transaction has a canonical encoding as a certain binary string, and so instead of having some form of transaction number or other reference, transactions are referred to by the hash of their canonical encoding. Similarly, a block has a canonical encoding, and so each block is also referred to by its hash. This referencing method only works because it is computationally infeasible to create a new transaction or block with the same hash. The hashing algorithm used in Bitcoin for content-addressability is the double **SHA-256** hash.

2.1.3 Proof-of-work schemes

The first property of cryptographic hash functions means that the output should be completely random. That is, the output for any set of distinct inputs should be uniformly and independently distributed over the possible outputs of that hash function (a binary string of fixed length n can be identified with a non-negative integer between 0 and $2^n - 1$).

We can use this property to construct a “proof-of-work” scheme. Suppose we would like another user to prove that they have performed a certain amount of work before accepting some data from them; for instance to fight email spam. We may proceed as follows: the user first takes the hash of their data and affixes to it a random binary string called a nonce. They then compute some predefined cryptographic hash of this concatenated data, which is some integer between 0 and $2^n - 1$. If this result is lower than some predefined difficulty threshold, then we accept the data. Otherwise, we require that the user changes the nonce and repeats the computation until producing a valid hash. By altering the difficulty threshold, we can adjust the expected number of computations that the user must perform before producing acceptable data, hence probabilistically “proving” that they have performed a certain amount of work. An additional advantage of this is that we do not even need to receive the data from the user in order to decide whether they satisfied the proof-of-work requirement. Rather, we need only receive and check the hash of a short binary string, an inexpensive computation, after which we can instruct the user to transmit to us the whole data.

This idea of proof-of-work was introduced in [18] in 1997 and has been adopted for a variety of uses such as email spam protection. It is central in the Bitcoin mining process where it acts to limit the rate at which blocks are mined as well as to randomly allocate blocks to miners, discussed later in Section 2.2.3.

2.1.4 Merkle trees

An important data structure used in Bitcoin blocks is the Merkle tree. They allow us to combine the hashes of a set of objects in a convenient way, while making each individual hash easily accessible and usable. A Merkle tree is a complete binary tree of hashes, where each leaf node corresponds to the hash of one object. Each internal node is the hash of the concatenation of the hashes of its two descendants, all the way to the root node, whose hash is referred to as the hash of that Merkle tree, or the Merkle hash of a collection of data. If any hash in the set of objects were to be changed, then each hash above it would change, and the root hash of the Merkle tree would change. The added convenience of using a Merkle tree is as follows: if there are n objects to be hashed, then verifying or attesting that one particular hash belongs in the tree requires computing and transmitting only $\lceil \log_2(n) \rceil$ hashes. If the hashes were instead concatenated and that binary string hashed, then this operation would require n hashes. Figure 2.1 illustrates a Merkle tree consisting of four transactions.

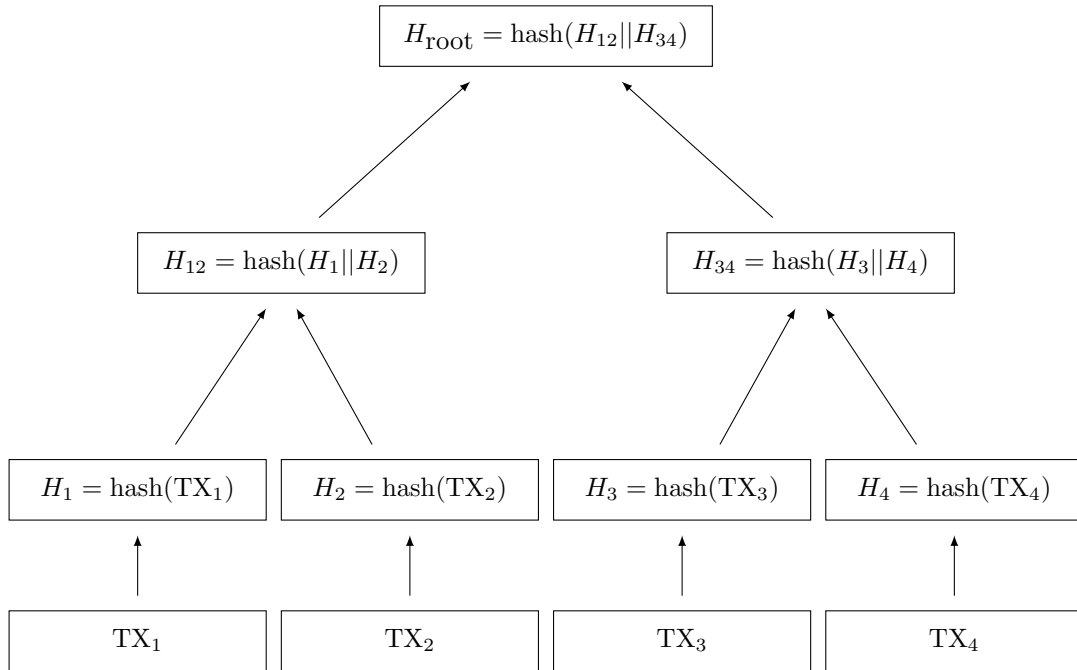


Figure 2.1: A Merkle tree consisting of four transactions. $||$ denotes concatenation.

2.2 The structure of the blockchain

2.2.1 Addresses and wallets

Bitcoin itself does not have a concept of an identity. Instead, Bitcoins are held in and transferred between Bitcoin addresses. To create a new address, a user generates a private key and a corresponding public key. They then compute a hash of this public key, which identifies the Bitcoin address². There is no action resembling opening an account with Bitcoin: anyone can create millions of empty addresses with virtually no effort, and these only become visible to the rest of the users when Bitcoins are transferred into those accounts.

²The exact hash depends on what kind of transactions the address will be used for.

A user will generally have a Bitcoin wallet: a collection of Bitcoin addresses for different uses. There exist several programs that manage Bitcoin wallets and will automatically generate and manage multiple addresses for receiving and sending Bitcoins. This is partly for increased privacy, but also to protect the user in the case of an unforeseeable break or improper implementation of the cryptographic primitives used by Bitcoin³.

2.2.2 Transactions

When a user wishes to transfer Bitcoins from their wallet to another wallet they create a transaction object. This transaction object is essentially an instruction to move Bitcoins from one address to another, and is cryptographically signed with the private key corresponding to the sending address⁴. This allows anyone with the complete transaction data to verify that this transaction was indeed authorised by the user controlling that address: they will need to extract the public key, signature, and sending address from the transaction, then cryptographically verify that the signature corresponds to that public key and that the public key corresponds to the sending address. Transactions often also include a transaction fee, which incentivises miners to include them in new blocks, discussed in Section 2.2.3.

This cryptographical signing of transactions makes it possible to prove that a user authorised the transfer of Bitcoins from their address to some other address without a central authority like a bank; however, this does not stop that user from sending out a transaction spending Bitcoins they do not really have or from sending a given Bitcoin multiple times, known as double spending⁵. To overcome these two issues, there must exist some globally accessible ledger of all past transactions. In Bitcoin, this ledger is the blockchain.

2.2.3 Blocks and the mining process

To prevent Bitcoins from being created out of thin air and to prevent double spending, Bitcoin employs a decentralised database known as the blockchain which contains a full ledger of all confirmed transactions. This database is incrementally updated through a process known as mining, discussed in Section 2.2.3.

A block is a data structure containing two sections: a header and the data itself. The data section consists of a list of transactions assembled in a Merkle tree whose hash is included in the header. The header contains four pieces of information of interest to us: the hash of the last block in the chain, the hash the Merkle tree of transactions in the block, the approximate timestamp at which the block was mined, and an arbitrary integer called a nonce which is related to the mining process⁶. See Figure 2.2 for a simplified illustration of the block structure. Ignoring for the moment some additional fields in the block header⁷, the hash is essentially calculated as

³The public key of a Bitcoin address need not be made public to the network until Bitcoins are spent, only a hash is made public. If a break in the elliptic curve cryptography were to be found, it would require the public key which would be hidden using this method.

⁴In reality, the underlying Bitcoin system uses a concept of inputs and outputs, which are manipulated by scripts through a simple stack-based, non-Turing complete programming language. Transactions are hence a collection of scripts that unlock inputs to create new “unspent” outputs. This is largely an artefact of the evolution of Bitcoin, and in practice, the vast majority of scripts adhere to a small set of standard formats.

⁵It is possible to create a type of digital currency without a blockchain that does not allow creating coins out of thin air; however, this is still prone to double spending. This idea is actually discussed in the original whitepaper [1] and precedes Bitcoin.

⁶The block header also contains `nBits`, a measure of the mining difficulty, and `nVersion`, the block version, which is used in updates to the Bitcoin rules and protocol.

⁷The actual hash is `hash(nVersion||hashPrevBlock||hashMerkleRoot||nTime||nBits||nNonce)`.

$$H_n = \text{hash}(H_{n-1} || H_{\text{root}} || \text{Timestamp} || \text{Nonce}), \quad (2.1)$$

where H_n is the hash of block n , H_{root} is the hash of the Merkle tree of transactions as in Figure 2.1, and $||$ indicates concatenation. Figures 2.3 and 2.4 illustrate this relationship and how the blockchain emerges from it.

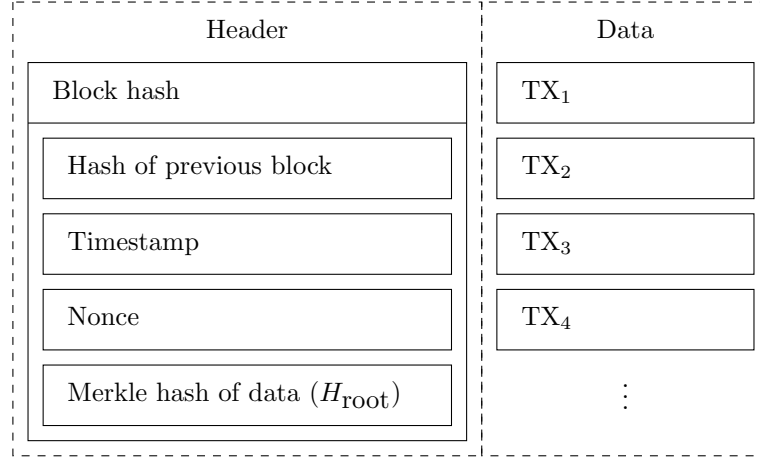


Figure 2.2: The simplified block data structure

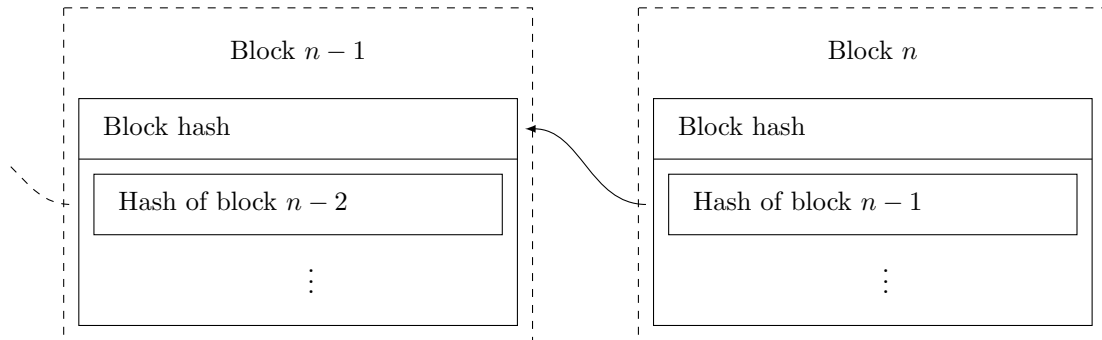


Figure 2.3: Links in the blockchain

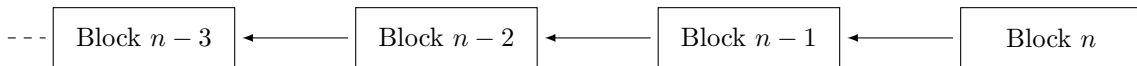


Figure 2.4: The blockchain

In order to mine valid blocks a miner must operate a full Bitcoin node. A full node is a server that maintains a current copy of the full blockchain and validates new blocks as it receives them from the network, conjoining them to its own replica of the chain. Without doing this, transactions that it creates might be invalid due to being based on an outdated view of the balances of addresses. In addition, blocks it mines will not be on the longest chain of blocks and will therefore be rejected by other nodes on the network. For mining, the node needs to also receive and keep track of all currently

unconfirmed transactions being broadcasted onto the network in what is known as the memory pool, or mempool.

Now to mine Bitcoins, the miner assembles a block template; a data structure identical to a block but without a valid proof-of-work. To do this, it combines together a set of unconfirmed transactions from its memory pool whose combined size is under the predefined size limit of a block. Ostensibly the miner will choose transactions that maximise its reward from the transaction fees, incentivising users to add higher fees into their transactions to receive priority service. Then to turn this block template into a valid block, the miner attempts to find a proof-of-work hash, whose difficulty is defined by the current mining difficulty. If the miner finds a valid hash, then it should swiftly attempt to broadcast the newly mined block forward and get it propagated to the whole network before someone else finds another block (unless attempting a selfish-mine strategy, or similar).

The mining difficulty is deterministically adjusted approximately every two weeks⁸ using the block timestamps of the latest blocks in order to keep the arrival rate of new blocks being mined approximately constant at one new block every 10 minutes.

To incentivise miners to perform this work in validating transactions and advancing the blockchain, miners are entitled to a block reward for finding a new block. When a miner successfully mines a new block, they may include a transaction transferring new Bitcoins equivalent to the current block reward to any addresses of their choosing. This transaction is called the coinbase transaction and occurs first in each block. Currently this reward is at 12.5 Bitcoins per block and is set to half every 210000 blocks (which corresponds to approximately 4 years), until eventually being set to zero once a total of 21 million Bitcoins have been mined. This incentive in turn means that there is economic competition in providing the service, and there tends to be a large number of competing miners active at any given time. The coinbase transaction contains an empty input that can be almost arbitrary⁹ and is commonly used by miners to include their mining signature, a string which advertises the miner that mined that block.

According to the Bitcoin rules, miners should always mine on the longest chain they are aware of. The length of a chain of blocks is given by the amount of chainwork on that chain: the expected number of hashes required to produce the blocks in the current chain¹⁰. Not mining on top of this longest chain would cause the blocks of the miner to not have as much chainwork as the longest chain, and according to consensus rules, would be dropped by any other miners, effectively wasting the effort of the miner mining on the wrong chain. This incentivises miners to quickly validate new blocks as they receive them, and to mine on the longest chain.

Validating blocks is a simple process whereby a node verifies that the block contains a valid proof-of-work, that the block header is correct, and that each transaction included in the block is valid and correctly signed. The verification of digital signatures is the most computationally intensive in comparison to the other verification tasks.

When two miners happen to find blocks at almost the same time, a fork in the blockchain can occur, whereby a portion of the network believes that one of the blocks represents the current longest chain of blocks, while another part of the network believes another block makes up the longest chain. This is illustrated in Figure 2.5. This happens when a miner mines a block on the stale chain before it learns about a new block, an artefact of the block propagation delay. In the case of a fork, each

⁸The mining difficulty is adjusted every 2016 blocks, which corresponds to 2 weeks if blocks occur every 10 minutes.

⁹The latest version of the protocol requires this input to contain the block height, in order to stop two coinbase transactions from being identical and hence having the same transaction hash, but other than that, this input script can be arbitrary.

¹⁰To illustrate, suppose we had a list of integers between 0 and $2^{64} - 1$. One can compute the expected number of independent uniform random variables on the integers from 0 to $2^{64} - 1$ that need to be sampled to realise a list of integers which is uniformly bounded by the original list.

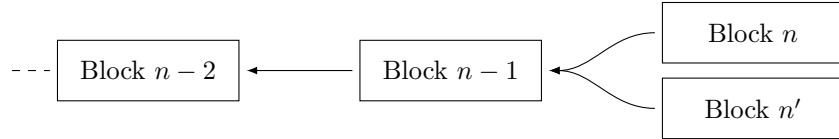


Figure 2.5: A fork in the blockchain

miner will mine on the block they received first, ignoring other blocks at the same height. Eventually, another miner will find a block on one of the branches and propagate it across the network, at which point the miners mining on the wrong chain will see a longer chain, and switch to that chain, resolving the fork. The leftover block is known as an orphan. This is illustrated in Figure 2.6.

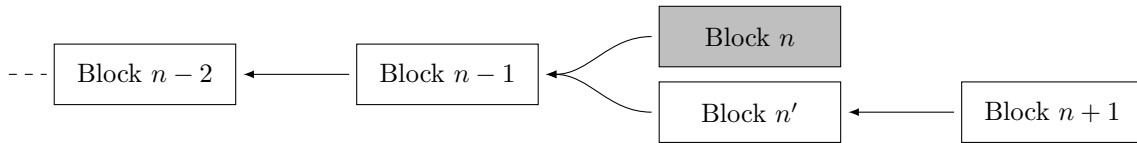


Figure 2.6: Resolution of a fork in the blockchain with the orphan block shaded

Forks can occur for other reasons as well, such as the selfish-mine strategy introduced in [4] and explored further in [5] under the effects of propagation delay. In such a case, an adversarial miner mines blocks on top of the longest chain, but instead of advertising new blocks as it finds them, hides them and mines a longer, private chain. When that node then observes that the rest of the network has mined another block, they reveal the next block in their private chain and attempt to quickly flood the network with it. If they have superior infrastructure and can perform this faster than the other node takes to propagate through the network, they can have their block be accepted instead of the one mined by the rest of the network. This way, the adversarial miner gets a head start on new blocks in their private chain, and can inflate their share of the rewards.

The mining process can be seen in two different ways. As one interpretation, it is a process whereby a node is selected at random to process the next batch of transactions; with the probability of finding a block being proportional to the processing power that that node contributes to the network. Another interpretation of this process is that of a literal mining process, where any node doing work finds a block (which grants them a reward) with some low probability, depending on how much effort is put into the mining activity. However, the process is not equivalent to real mining, as the probability of finding a block is adjusted periodically to make sure the total number of blocks is kept approximately constant over time, despite fluctuations in total mining power.

2.2.4 51 % attacks and double spending

Controlling the mining process does not give the miner the ability to transfer arbitrary Bitcoins between addresses. However, if one entity is able to dominate the mining process, they are able to delay or even deny the confirmation of any transactions of their choosing, simply by not including them in blocks. They may also engage in attacks known as double spending.

One version of double spending is when a miner with a sufficiently large proportion of mining power creates a transaction and allows it to be confirmed, then takes possession of a good or service paid for by that transaction; but immediately mines another block at the same height as the previous block without that transaction. If they have a sufficiently large proportion of the hashing power on

the network, they can keep on producing blocks on top of this later block until it eventually takes over the main blockchain, effectively erasing the transaction previously confirmed¹¹. This is generally known as a 51 % attack, referring to the fact that one entity requires over 50 % of mining power to perpetually sustain this kind of attack on the blockchain. In the event of one entity controlling the majority of mining power, they could always keep mining their own chain that would stay the longest, and ignore any other blocks found by others, in practice keeping the network continuously under their control. However, an entity need not control the majority of hashing power to succeed with high probability in replacing a block; controlling the majority of hashing power just means that they eventually succeed every time.

2.2.5 Application-Specific Integrated Circuits

Once a block template has been assembled and its corresponding header computed, the operation of finding a small enough hash to satisfy the proof-of-work requirement is a fairly straightforward operation. It requires having the binary data for the header, computing a cryptographic hash, comparing this to a threshold, and repeating this process while slightly modifying the header each time. Originally this work was done on commodity central processing units (CPU) found in desktop computers. However, given the embarrassingly parallel¹² nature of the hashing problem, it was soon discovered that this was an ideal computation to be performed on a graphics processing unit (GPU), and soon the rate at which a commodity GPU could compute hashes surpassed that of CPUs by several orders of magnitude.

In the past few years, there has been increased work in offloading this computation to dedicated hardware with circuits specifically engineered for the task. These application-specific integrated circuits (ASIC) drastically reduce the cost and energy requirements per hash, by removing a large portion of hardware overhead. Due to the high research and development cost, as well as a high unit cost associated with such dedicated hardware, the technology is developed by a handful of advanced companies with the expertise to develop such technology and the capital to amortise these costs into their operation. Even though this hardware is sold to the rest of the mining community, some fear that this centralises control of the mining process. Some newer cryptocurrencies attempt to dwarf the development of ASICs and force people to use commodity processors by introducing hashing algorithms that cannot be easily computed via dedicated circuitry. This can be done, for instance by making a hashing algorithm memory-hard, so that the proof-of-work requires large amounts of memory to be quickly computed, or by making the proof-of-work space-hard, requiring for instance that the hash accommodate information from a large number of random blocks in the history of the blockchain, so that a device without the full blockchain cannot quickly compute it.

2.2.6 Mining pools

Due to the extremely low probability of finding a small enough hash to qualify for a new block, and the historically ever-increasing aggregate hashing power of the network, the probability of finding a block on any given piece of mining hardware over the lifetime of that hardware is small. In order to reduce this risk, a number of mining pools have formed. These pools band together and aggregate the hashing power from several miners, then share the rewards in order to reduce the variance in

¹¹Generally the adversary will confirm into this alternate blockchain another transaction spending the same outputs, in order to make sure that transaction cannot be confirmed into the blockchain at any future time.

¹²In computer science, a problem is called embarrassingly parallel if it is trivial to perform that problem in parallel while introducing almost no overhead.

their mining operations¹³. This however, increases centralisation and means that these mining pools generally control large proportions of mining power, often up to a third of the network. This is a worrying fact, as mining pools are rarely run with much transparency and the entities controlling the pool often get to single-handedly choose what gets accepted into a block and what does not.

2.2.7 The block size limit and SegWit transactions

In late 2017, an update called SegWit, or segregated witness, was activated on the Bitcoin network to somewhat alleviate scalability issues as well as some security issues. Before this, the block size limit for Bitcoin was defined to be one million bytes, and was measured as the size of the serialised block. The SegWit update introduced an additional data section called “witness data” which is not needed in determining the validity of certain parts of transactions, and thus can be discarded in some cases. Due to this, the block size is now computed differently, in particular, parts of a transaction that belong to the segregated witness data count for only one quarter of the size of normal data, and a new unit, called a “weight” unit (or “weight byte”) was introduced. For normal transactions and non-segregated witness data, one byte of data is equal to four weight units, whereas for segregated witness data, one byte counts for only one weight unit. The block limit was also redefined and is now 4 million weight units.

2.3 The Bitcoin protocol

This section outlines the general Bitcoin protocol, but some details are specific to the Bitcoin Core client as at version 0.17.1 [14].

2.3.1 Protocol messages

The Bitcoin network is an ad-hoc, peer-to-peer, decentralised network. Each entity willing to participate in the mining or verification of transactions must operate a full node. The network protocol is comprised of several short messages, transmitted on top of raw TCP sockets, by default on port 8333. These messages are preceded by a short message start sequence, followed by the message name, the message data, and a checksum. There is only one class of messages, so there is no protocol-level distinction between control messages and data messages. The protocol is a broadcast protocol: once a transaction or block has been received by a computer, it attempts to quickly broadcast that object to each of its peers that are missing it.

2.3.2 Nodes and peers

A computer connected to the Bitcoin network is called a node of the network. Two nodes that are connected to each other are peers of each other. Hence the network consists of a set of nodes and a set of peer-links.

¹³Interesting aside: when mining for a mining pool; it is not at first obvious how to prove to the pool that one is performing a certain amount of mining work on behalf of that pool. Many mining pools have introduced innovative ways to prove this, such as a pay-per-share scheme where miners participating in the pool produce weaker “proofs” that they are mining for the pool: during the normal course of mining, a miner will inevitably stumble across block hashes that are close to the real requirement but not quite low enough, such as differing by a few orders of magnitude. If the miners submit these to the mining pool which checks that the block is the one that the pool needs mined; then they can both verify that the miner is working for that pool, as well as estimate the proportion of mining power contributed by that miner. Furthermore, once a miner finds a valid block, they are incentivised to send it to the pool, as they will get some proportion of the reward (possibly weighted by the proportion of shares submitted by them).

2.3.3 Peer discovery

A full Bitcoin node is a server connected to the Bitcoin network that maintains an up-to-date copy of the full blockchain, while continuously receiving, verifying, and relaying transactions and blocks from its peers.

When a new Bitcoin node joins the network, it must first establish an initial connection by finding some peers. This is facilitated by a list of “good” nodes hardcoded into every release of the Bitcoin client¹⁴. Upon starting afresh, a node will randomly pick some nodes from this list and establish connections to them. Once a node has bootstrapped using this list of nodes, it will continuously grow its list of good nodes by connecting to random nodes it receives from its peers and similarly advertise the list to its peers. The sharing of information about nodes is done through the **addr** message, which contains a list of address and port combinations of nodes, as well as a list of the capabilities of that node.

When two nodes connect to each other, the procedure starts with a peer handshake. The connecting node establishes a TCP socket to the second node, then sends a **version** message. This message contains information about the node address and port, as well as its capabilities. The receiving node in turn replies with a **version** message. Both nodes acknowledge they have received the version message with **verack** messages, completing the version negotiation and connection establishment.

2.3.4 Control messages: version/verack, ping/pong, getaddr/addr

The protocol contains a selection of messages required for a node to control and maintain connections and keep a current list of healthy peers.

The **version** and **verack** messages are used in the initial handshake, as outlined in the section above. The **version** message contains a selection of information about the node, such as the protocol version that node is running, the services it offers (such as whether it supports an upgraded, compact way of transmitting blocks), the software name and the version that it is running, as well as network information like the address and port of the sending and receiving nodes [14]. A **verack** message acknowledges a previously received **version** message.

To confirm that a peer is still connected and responding, a node may send a **ping** message to that node. This message contains only a random number used to label the corresponding **pong** message that repeats the number, confirming that the peer is still connected and functioning.

In order for nodes to maintain a current list of healthy nodes, each node regularly sends an **addr** message to each of its peers. This message contains a list of nodes, along with the majority of the contents of their most recent **version** message. Additionally, a node may send a **getaddr** message to its peers to request an **addr** message. During the course of its operation, a node regularly establishes “feeler” connections to some of the nodes in its list of nodes not currently connected to, to check their version information and make sure these nodes are healthy and ready to be connected to in case it needs to connect to more peers.

2.3.5 Data messages: inv, getdata, tx, block, getheaders/headers

When a node wishes to inform a peer of blocks or unconfirmed transactions that it has but the peer might not have, it sends an **inv** message. This contains a list of transaction or block hashes. The

¹⁴One of the core Bitcoin developers operates a crawler that records information on the various nodes available on the network including their uptime and health. These are then occasionally filtered and compiled into the source code as good bootstrapping nodes, that is, nodes good for fresh clients to connect to [19].

peer will then check its memory pool and database to decide whether or not it has these objects. To request them, it sends a **getdata** message, asking for a list of objects from that peer.

Upon receiving a **getdata** request, a node replies with either a **tx** message to send a transaction, or a **block** message to send a single block.

To accelerate the block propagation process, the protocol also contains a **getheaders** message which requests only the header of a block, as well as the **headers** message which in turn only contains the header of the block. This is vital for decreasing the block propagation delay.

The latest protocol versions contain some enhancements to block messages, known as compact blocks, which allow a node to only transmit the parts of a block that their peer does not currently have, achieved using bloom filters.

2.3.6 The transaction propagation process

When a node generates a new unconfirmed transaction, it advertises it to its peers using an **inv** message. Once those peers then ask for the transaction using a **getdata** message, it sends it through with a **tx** message.

The client includes a selection of countermeasures to topology inference of the network. One such countermeasure is the delaying of propagation of transactions by a random Poisson variate to make it non-trivial to infer its peers.

2.3.7 The block propagation process

When a client receives an **inv** message for a block, it replies with a **getheaders** request for the block header of that block. It then verifies that the header is valid, in that the hash is correct, and that the hash is lower than the threshold. If this is correct, it sends out **inv** messages to all of its peers who do not already know about the block, then simultaneously attempts to download the block by sending a **getblock** request.

Upon receiving a new block, newer clients send a **cmpctblock** message, which contains only the data of a block that the peer does not already have.

When a node on the network mines a new block, it is in its best interest to get that block propagated through the whole network as quickly as possible, in case another node also finds a block at a similar time, forking the network, and possibly causing the original miner's block to be discarded.

Chapter 3

Data collection and the bitcoin-crawler

In this chapter we give a detailed overview of the `bitcoin-crawler` and our setup for the experiment.

3.1 Overview

To analyse the underlying Bitcoin network, we set up an observational experiment to collect data about the block propagation process. We provisioned servers in nine geographically separated datacentres in locations around the world, which ran a custom software called `bitcoin-crawler` that we created for this project.

In total, we provisioned 9 observational nodes, 1 master server, and 1 full Bitcoin node to collect additional covariates. The full data collection system comprises of over 1000 lines of code and was used to collect over 137 gigabytes of data.

Although the Bitcoin blockchain contains an immutable store of all data required to verify and process transactions, it does not contain information about the process by which the network reached consensus and how particular blocks were mined and propagated. In particular, we are interested in the block propagation process and the path that newly mined blocks take to reach every network on the node, as well as the delays associated with this. In a sense, this information is ephemeral. We therefore needed to actively monitor the network by collecting and storing this information. In order to get a comprehensive, real-time overview of the process, we needed to build a large system with enough servers to receive data from the majority of nodes on the network.

This process was technically challenging both as it required an in-depth knowledge of the Bitcoin protocol and software engineering, but also because it required the cost-effective deployment and management of a number of servers that collected data in tandem in a large-scale, distributed manner.

This chapter outlines a tool called the `bitcoin-crawler` that we developed for the task, the system of servers we deployed, and the data we collected, as well as some other aspects pertaining to the data collection process.

3.2 The bitcoin-crawler

At the heart of the data collection was the `bitcoin-crawler`. This is a custom multi-threaded software that we specifically developed for this project using the Python programming language. The

bitcoin-crawler imitates a full Bitcoin node by implementing a subset of the Bitcoin protocol but contains custom logic to maintain connections to many more peers than a regular node, as well as logging code to store the data of interest for later aggregation and analysis. The program uses the **python-bitcoinlib** library by Todd [20] for some Bitcoin specific computations like serialisation.

The **bitcoin-crawler** starts by discovering its own IP addresses, which are required in connecting to peers on the Bitcoin network. Each server was running on a dual-stack network supporting both IPv4 and IPv6. The node does this by querying the master server which replies back with the addresses.

In order to stay connected to the network, the **bitcoin-crawler** requires an up-to-date list of addresses of possible peers to connect to similar to a normal Bitcoin node. Initially, it starts with the same hard-coded list of well-known, good addresses embedded into the reference client (see Section 2.3.3 for further discussion). Once the **bitcoin-crawler** has bootstrapped itself through these nodes, it learns about new addresses from its peers by periodically sending out **addr** messages.

When started, the program randomly chooses an address from this list of good addresses and spawns a new thread to handle that address. The main thread keeps connecting to new random addresses from this list whenever it needs to connect to more peers. After some experimentation on how many peers we could connect to while keeping system load manageable, we chose to maintain 700 connections per server.

Once a new thread is spawned, that thread establishes a Bitcoin connection to its peer by performing the initial handshake and agreeing on version parameters as specified in the protocol. When the connection has been established, the thread performs three functions. The first is to log all **ping** and **pong** messages, as well as messages advertising blocks (a subset of **inv** messages). This is the data we collected and analysed in this project and is added to a global list of messages to be stored to disk. The second function is to periodically send out an **addr** message to query that peer for new addresses, which are then merged into the global list of potential addresses to connect to. Finally, the thread maintains the connection by sending out and replying to necessary protocol messages. In our implementation, this includes sending out **inv** messages every two minutes with our best guess of the most recent block; as well as **ping** messages every thirty seconds to make sure the peer does not disconnect due to inactivity. The thread also replies to incoming **ping** messages with a corresponding **pong** message.

In order to not be marked as an outdated or stale node, we need to occasionally send out **inv** messages with a current block hash to peers. However, as we did not maintain a full Bitcoin node through the whole experiment and did not have current information on the blockchain on each server, we had to guess it somehow. To do this, the **bitcoin-crawler** maintains a rolling buffer of the last 200 blocks observed and advertises the most common of those to its peers. After experimenting, this seemed to work adequately.

The main thread contains a buffer for data to be saved to disk. When a thread needs to write to this structure, it acquires a lock for it, and appends its data to the end of the buffer. Once this buffer is full, the main thread acquires a lock on the structure and writes the data to disk and the buffer is emptied.

Programming the **bitcoin-crawler** was a time-consuming task and took several weeks to finish. Another approach would have been to take an existing Bitcoin client and operate full nodes, or to modify an existing client to perform only the functions we require. However, the former would have been too expensive as a full node has large overheads, demanding a large amount of processing power and several hundred gigabytes of storage space; and the latter would have been a very time-consuming endeavour and would most likely have taken longer to complete.

3.3 The global data collection system

In order to collect a sample of data from the global Bitcoin network and to get a comprehensive overview of the underlying network and propagation process, we deployed servers running the `bitcoin-crawler` at 9 geographically diverse locations around the world.

Each server was numbered from 1 to 9 for easy of identification. They were hosted on the Amazon Web Services (AWS) Elastic Compute Cloud (EC2), on a variety of `t2.nano` and `t3.nano` instance types and ran Ubuntu 18.04 LTS. The servers were assigned Elastic IP addresses, and a DNS hierarchy hosted on Route 53 was set up to simplify server management. The servers were managed using SSH. This information along with the AWS regions is summarised in Table 3.1 and Figure 3.1.

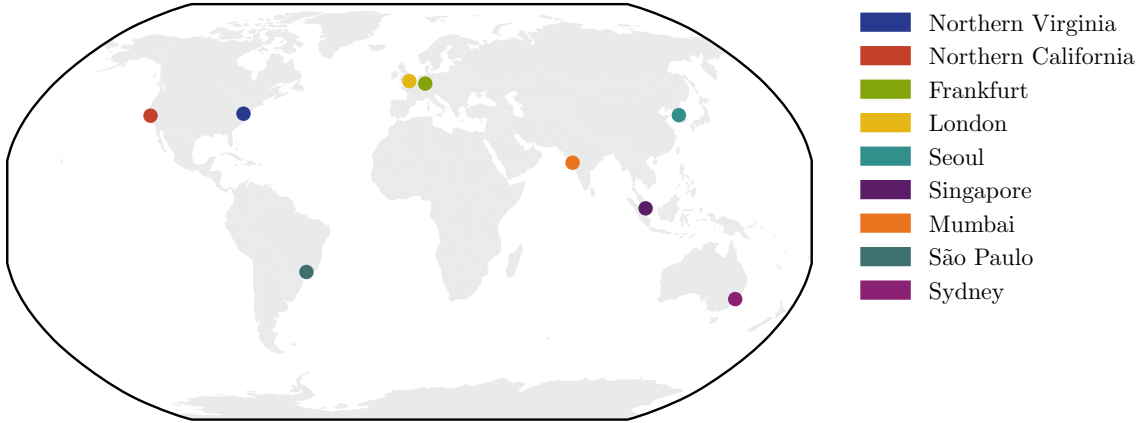


Figure 3.1: Map showing locations of observational nodes

Number	Location	Region	Instance type
1	Northern Virginia	us-east-1	t3.nano
2	Northern California	us-west-1	t3.nano
3	Frankfurt	eu-central-1	t3.nano
4	London	eu-west-2	t3.nano
5	Seoul	ap-northeast-2	t2.nano
6	Singapore	ap-southeast-1	t3.nano
7	Mumbai	ap-south-1	t2.nano
8	São Paulo	sa-east-1	t3.nano
9	Sydney	ap-southeast-2	t3.nano

Table 3.1: The locations used for data collection

A master server was provisioned to regularly copy data from each server into the master datastore, as well as to serve information about IP addresses for the observational servers. In addition, the server ran a PostgreSQL server and scripts to process the data.

3.4 Blockchain data and mining pools

To complement the real-time Bitcoin data, a full Bitcoin node was provisioned to extract data from the blockchain itself. This was required to verify which blocks ended up being included in the final blockchain and to classify blocks into mining pools through the coinbase transaction and the embedded mining signature (refer to Section 2.2.3 and Section 2.2.6). The blockchain data was also used to

compute the size and number of transactions for each block, among other covariates. This data was extracted by calling the Bitcoin Remote Procedure Call (RPC) interface and saving the results into files that were processed by various scripts. In particular, the coinbase transaction input was extracted from the block, decoded into UTF-8, and matched against a number of patterns known to identify mining pools.

3.5 Cleaning of nonsensical data

Once the data had been collected, it was cleaned to remove any invalid data points.

The Bitcoin client has a rigorous battery of built-in techniques to disconnect from misbehaving and adversarial peers. It maintains a tally of violations and once a peer passes a certain number of violations, it is blocked. This is imperative for real nodes, as it is very easy to provision a server with a reasonable budget that could connect to almost every node on the network and send spoofed messages or poisoned data. If the client was unable to appropriately and sternly block these peers, the whole network would be intimately exposed to a number of denial of service attacks.

Early on in our data collection we judged that implementing techniques to block nodes was unnecessary for our program. This is because the vast majority of nodes on the network already block these adversarial nodes, and so they have little incentive to spam the minority of custom nodes that do not. Nevertheless, we found that some proportion of data was still nonsensical, and occasionally we would encounter a fake block hash in our data.

We also removed orphaned blocks from our dataset (see Section 2.2.3). These are themselves of interest when studying the mining process in general, but we did not include them in our dataset, as they possibly have a different propagation pattern to non-orphaned blocks which we did not model.

To clean the collected corpus, we computed from the blockchain data a list of blocks that had been accepted into the blockchain during the collection period. We then removed any data points that did not overlap with this list. Approximately 16.5 % of data was removed in the cleaning step.

Chapter 4

The dataset

4.1 Overview of the dataset

In total, we collected in excess of 137 gigabytes of data. This chapter gives a brief overview of the cleaned dataset presented through a discussion and some summary figures and tables.

Our main dataset contains one row for each `inv` message observed by an observational node (see Section 2.3.5). Each block generally appears several times from different peers, and often even several times per peer, as a peer may be connected to several of our observational nodes. In total, the dataset contains approximately 20.6 million messages regarding 14810 unique blocks, which we collected between November 2018 and March 2019.

Table 4.1 shows a sample from the main dataset. The `block` column contains the block hash and has been truncated in the table for clarity. The `time` column is the time of that observations and is recorded in Unix time, that is, in seconds since January 1st, 1970. The `node` and `node_location` columns correspond to values in Table 3.1 and identify which one of our nine observational nodes received that message. Finally, the `peer_ip` and `peer_port` values contain the IP address and port of the peer that sent the message.

The most common observation location was Northern Virginia. We do not know why there was such a disparity in the number of observations by location, but we speculate it might be because of a large number of nodes in that region with fast internet connections¹. The proportions observed at each location are shown in Figure 4.1.

Table 4.2 shows a sample of the blockchain data that complements the main dataset. This dataset contains one row for each block that was mined during our experiment. Again, the `block` column contains the block hash and has been truncated. The `size` column gives the real size of the block in its

¹Virginia contains possibly the largest amount of cloud infrastructure in the world, due mainly to historical reasons relating to its proximity to Washington and funding from the United States Government.

block	time	node_id	node_location	peer_ip	peer_port
0000...563df98	1542887007.19418	4	London	62.152.58.16	9421
0000...fda7919	1543748261.60442	9	Sydney	52.198.169.28	8333
0000...10c9e85	1544975472.21318	1	Northern Virginia	2a01:4f8:191:4174::2	8333
0000...f219fca	1547242755.84717	1	Northern Virginia	47.88.192.215	8333
0000...64dd0e6	1547487249.97776	4	London	108.56.233.194	8333
0000...ff3b14d	1547900706.97837	6	Singapore	117.52.98.78	8333
0000...11eeae7	1549261393.32542	6	Singapore	81.209.69.107	8333
0000...aa713e3	1549319396.6256	1	Northern Virginia	144.76.5.41	8433
0000...5cf4059	1550359795.0164	1	Northern Virginia	54.64.245.84	8333
0000...91f5404	1551099161.4188	1	Northern Virginia	185.186.209.210	8333

Table 4.1: A sample extract from the dataset

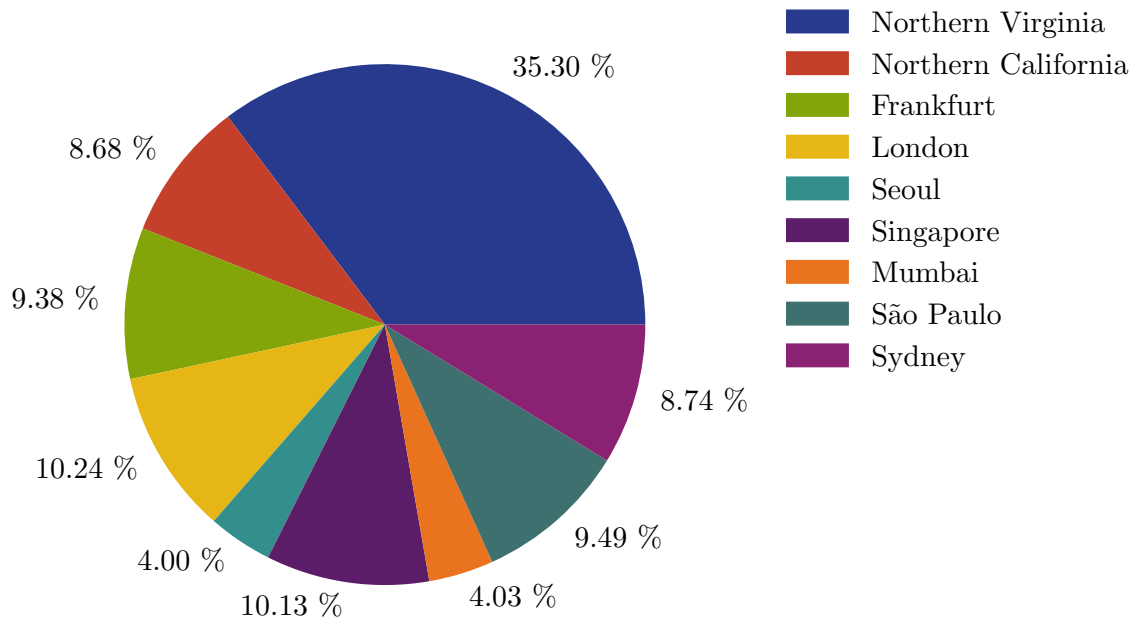


Figure 4.1: Proportion of block messages by location

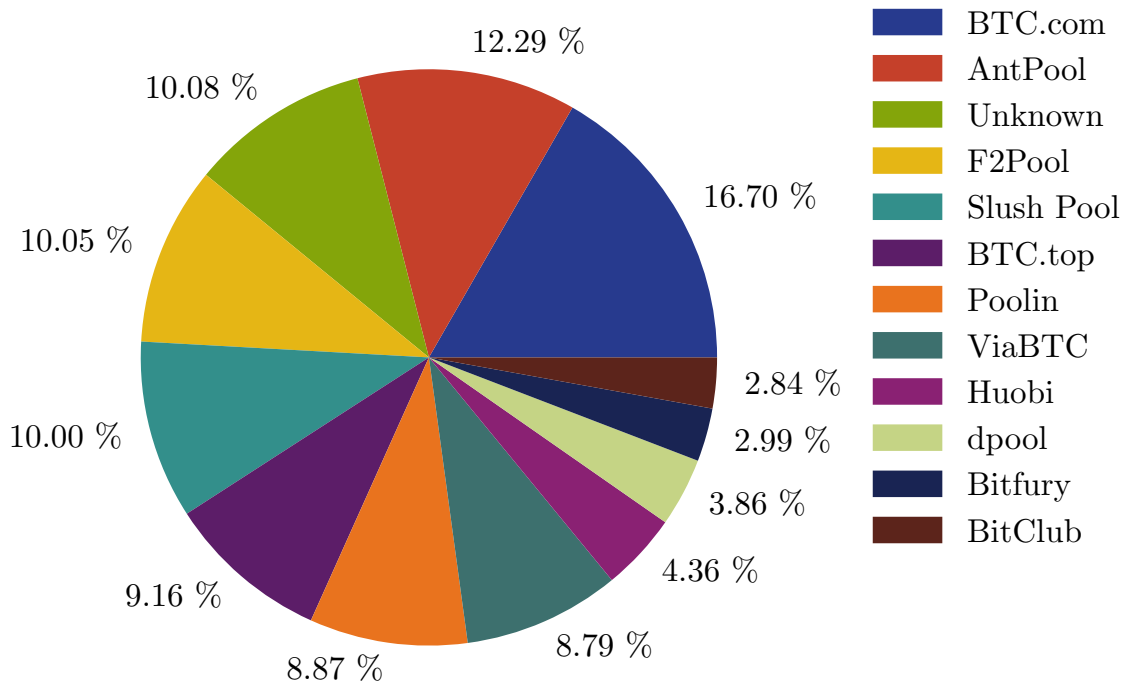


Figure 4.2: Proportion of blocks mined by mining pool

canonical encoding or when transmitted on the wire as a full block. **weight** is the weight of the block as described in Section 2.2.7. The **height** column is the height of the block in the blockchain, and **time** is the Unix time of the block as it appears in the block timestamp, which is often very inaccurate

block	size	weight	height	time	nonce	bits	nTx	pool
0000...f6048dd	1191087	3993369	550706	1542627049	1206282193	172a4e2f	1900	Slush Pool
0000...b4373a9	154481	534173	553369	1544510774	3681510874	1731d97c	305	Unknown
0000...f9dd7e9	649274	2359871	555601	1545843940	4123099930	17371ef4	648	Unknown
0000...3984206	1283944	3993127	559626	1548178688	2688550637	172fd633	3133	AntPool
0000...f1735ea	1262291	3993185	559645	1548188137	2421018921	172fd633	2524	BTC.com
0000...ea10bc7	559802	1993133	562220	1549670573	2587934320	17306835	476	AntPool
0000...18574e1	697494	2340000	562268	1549698426	1796028615	17306835	1700	Poolin
0000...2316419	1288903	3993037	562793	1550026180	1918332176	172e6f88	2873	BTC.top
0000...2df3348	1134403	3993103	564931	1551302350	2869178554	172e5b50	2040	BTC.com
0000...a101cf8	1317204	3992916	565279	1551493180	1664069908	172e5b50	3273	Slush Pool

Table 4.2: A sample extract from the blockchain data

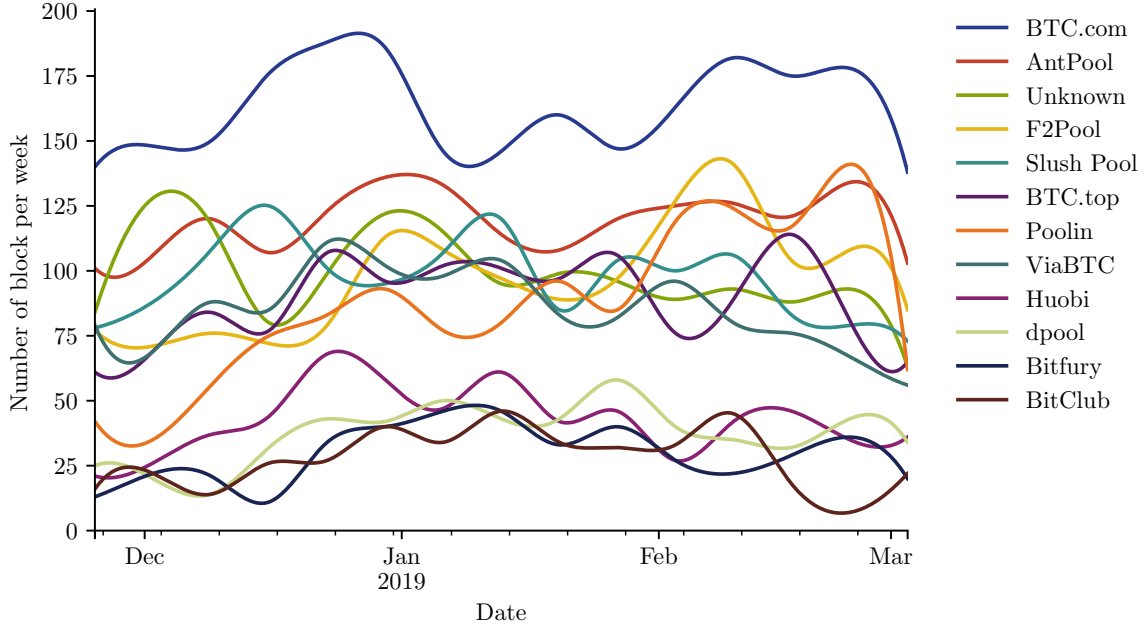


Figure 4.3: Number of blocks mined by each pool over time

(see a discussion in Section 8.2). The **nonce** is the block nonce as discussed in Section 2.2.3. **bits** is the mining difficulty threshold encoded using a special Bitcoin encoding scheme. Finally, **nTx** is the total number of transactions in that block, and **pool** is the name of the mining pool that we believe mined the block. Figure 4.3 shows the proportion of blocks mined by each mining pool.

To use this dataset, one would generally perform a join on the two tables; that is, for each observation, one ought to match up the block hashes between the two tables to get the covariates relating to that block from the blockchain table.

This is only a short overview of the dataset. For a further discussion of the data and trends within it, see Part III, in which we explore several interesting phenomena and patterns we discovered in the dataset.

4.2 Accompanying website and source code

We have made the data available online at <https://bitcoin.aapelivuorinen.com/>. This website also includes other interesting complementary material, the source code for the **bitcoin-crawler** and the fitting algorithm, and the final fits to be discussed in Part II.

Part II

Mathematical modelling

Chapter 5

Mathematical preliminaries

In this part, we develop the theory of parameter estimation for phase-type distributions via the EM-algorithm and apply this to model the data obtained from our experiment. This chapter gives an overview of the mathematical preliminaries required to understand our model. Chapter 6 discusses the details of the method more deeply, in particular the computational aspects of the algorithm, and in Chapter 7 we discuss how we applied this theory to fit phase-type distributions to block delay data and discuss the results along with further mathematical extensions.

5.1 Continuous time Markov chains

We first briefly introduce a few basic concepts and results for Markov chains needed later on. Readers familiar with the basic properties of continuous time-homogeneous Markov chains on finite state spaces may skip this section. For proofs and a more rigorous, comprehensive treatment, see [21], [22], or [23].

The stochastic process underlying phase-type distributions is the continuous time Markov chain, also known as the Markov jump process. In essence, a stochastic process is a Markov process if its future trajectory depends only on the current state and not on any past state.

Definition 1 (Time-homogeneous Markov chains on finite state spaces). *A càdlàg stochastic process $\{X_t\}_{t \geq 0}$ which takes values in some finite set \mathcal{S} , is a continuous time Markov chain if it satisfies the Markov property:*

$$\mathbb{P}(X_{t_n} = j \mid X_{t_1} = i_1, \dots, X_{t_{n-1}} = i_{n-1}) = \mathbb{P}(X_{t_n} = j \mid X_{t_{n-1}} = i_{n-1}) \quad (5.1)$$

for all $j, i_1, \dots, i_{n-1} \in \mathcal{S}$, and every sequence $0 \leq t_1 < t_2 < \dots < t_n$. We define the transition probability for $0 \leq s \leq t$ as

$$p_{ij}(s, t) := \mathbb{P}(X_t = j \mid X_s = i). \quad (5.2)$$

Furthermore, a Markov chain is called time-homogeneous if $p_{ij}(s, t) = p_{ij}(0, t - s)$ for all $i, j \in \mathcal{S}$, and $0 \leq s \leq t$. We then simply write $p_{ij}(t) := p_{ij}(0, t)$, so that $p_{ij}(s, t) = p_{ij}(t - s)$.

In this thesis, we only consider time-homogeneous Markov chains on finite state spaces and assume all Markov chains are such from now on. Note that some regularity conditions have been omitted from the statements below, and they do not necessarily hold in generality for Markov chains with infinite state spaces.

The evolution of a Markov chain is dictated by the transition semigroup and its corresponding generator:

Definition 2 (Transition semigroup, generator, holding intensity). *The transition semigroup of a Markov chain, $\{X_t\}_{t \geq 0}$ on state space \mathcal{S} , is a family of matrices, $\{\mathbf{P}_t\}_{t \geq 0}$, such that for a time t , \mathbf{P}_t is the $|\mathcal{S}| \times |\mathcal{S}|$ matrix whose elements, $[\mathbf{P}_t]_{ij}$ are the transition probabilities, $p_{ij}(t)$. The generator, \mathbf{G} , of a Markov chain is defined as*

$$\mathbf{G} := \lim_{h \rightarrow 0} \frac{1}{h} (\mathbf{P}_h - \mathbf{I}). \quad (5.3)$$

Finally, define the holding intensity, λ_i , of a state $i \in \mathcal{S}$ as $\lambda_i := -G_{ii}$.

Lemma 3. *The generator satisfies $\mathbf{G}\mathbf{1} = \mathbf{0}$, and in particular, $\lambda_i = \sum_{j \in \mathcal{S} \setminus \{i\}} G_{ij}$.*

Proof. See [21, p. 267]. □

Definition 4 (Embedded chain and holding times). *Let $\{X_t\}_{t \geq 0}$ be a Markov chain. We define the embedded (discrete time) Markov chain $\{I_n\}_{n \in \mathbb{N}}$ and the holding times S_i , $i \in \mathbb{N}$ as follows. Let $I_0 := X_0$, and define $S_0 := \inf \{t \geq 0 \mid X_t \neq X_0\}$. Further define $I_{n+1} := X_{S_0 + \dots + S_n}$, and $S_{n+1} := \inf \{t \geq S_0 + \dots + S_n \mid X_t \neq I_n\}$. That is, I_n is the n -th state that X_t visits, and S_n is the time spent in state I_n before jumping to another state.*

An important property of the holding times is that they are exponentially distributed with parameter λ_i . We only state the result for S_0 , but it holds for any S_i , with some more notational clutter:

Lemma 5 (Exponentiality of holding times). *Let $\{X_t\}_{t \geq 0}$ be a Markov chain with generator \mathbf{G} and suppose $X_0 = i$. Then $S_0 \sim \exp(\lambda_i)$ and for $j \neq i$, $\mathbb{P}(X_{S_0} = j) = \frac{G_{ij}}{\lambda_i}$.*

Proof. See [21, p. 259]. □

Definition 6 (Recurrent, transient and absorbing states). *We call a state $i \in \mathcal{S}$ recurrent, if $\mathbb{P}(\{\exists n \geq 1, X_{I_n} = i\} \mid X_0 = i) = 1$, that is, if the chain returns with almost surely to that chain after leaving it. We call a state transient if it is not recurrent. Finally, a state is absorbing if $\mathbb{P}(\{\exists n \geq 1, X_{I_n} \neq i\} \mid X_0 = i) = 0$, that is, if the chain does not leave that state once hitting it.*

We now define the exponential of a matrix, defined by its Taylor series expansion:

Definition 7 (Matrix exponential). *For a square matrix \mathbf{A} , we define the matrix exponential,*

$$e^{\mathbf{A}} := \sum_{n \geq 0} \frac{1}{n!} \mathbf{A}^n. \quad (5.4)$$

It is not hard to show that the series converges for any square matrix, and so the exponential is defined for all \mathbf{A} [24, p. 160].

Theorem 8 (Matrix exponential as a solution to a differential equation). *Define the differential equation $\frac{\partial}{\partial y} \mathbf{X}(y) = \mathbf{A}y$ with initial condition $\mathbf{X}(0) = \mathbf{I}$. Then the equation is uniquely solved by $\mathbf{X}(y) = e^{\mathbf{A}y}$.*

Proof. See [24, p. 160]. □

Finally, we state the relationship between the transition semigroup and generator, which we need later in fitting phase-type distributions to data:

Theorem 9. *Subject to the boundary condition $\mathbf{P}_0 = \mathbf{I}$, we have*

$$\mathbf{P}_t = e^{\mathbf{G}t}. \quad (5.5)$$

Proof. See [21, p. 259]. □

5.2 Phase-type distributions

Phase-type distributions are a class of versatile probability distributions introduced by Erlang and popularised by Neuts starting in [25]. Since their inception, they have enjoyed widespread adoption and use in a range of stochastic modelling applications, in fields such as systems reliability modelling [26, 27]; artificial intelligence and data mining [28, 29]; machine learning [30, 31]; finance [32]; insurance pricing [33]; telecommunications [34]; population genetics [35]; maintenance engineering [36]; and healthcare modelling [37, 38].

This popularity is due to several factors. In some sense, they are a natural extension from exponential and Erlang distributions, and often problems which can be analytically solved when one assumes an exponential distribution are computationally tractable when replaced with a phase-type distribution [39]. In many applied cases, phase-type distributions can also aid in interpretability, when one assumes some kind of underlying state-based model. In addition to these desirable computational properties, phase-type distributions are dense in the set of all distributions on the non-negative reals in the sense of weak convergence (see Theorem 12), which further justifies their use as a parametrisation of unknown distributions.

In this thesis, we used phase-type distributions as a tool to empirically fit distributions onto observed delay data. This choice was somewhat arbitrary, although one could argue that given the structure of the Bitcoin network, phase-type distributions provide a natural model for the delay distribution. After all, the data are observations of hitting times of a very similar process to that of a continuous time Markov chain, although the transition times across any given link or node are not necessarily exponential, and the observations represent first hitting times of a group of observations. For a full introduction to phase-type distributions, see [40], or [41].

Definition 10 (Phase-type distribution). *Suppose $\{X_t\}_{t \geq 0}$ is a continuous time Markov chain with state space $\{0, \dots, p\}$, where states $1, \dots, p$ are transient and state 0 is absorbing. Due to the absorbing state at 0, the generator must then be of the form*

$$\mathbf{G} = \begin{pmatrix} 0 & \mathbf{0} \\ \mathbf{t} & \mathbf{T} \end{pmatrix}. \quad (5.6)$$

We call \mathbf{T} the phase-type generator and \mathbf{t} the exit rate vector. Furthermore, let $\boldsymbol{\pi}$ be some row vector defining the initial distribution on $1, \dots, p$, and consider τ , the time until absorption of this Markov chain:

$$\tau = \inf \{t \geq 0 \mid X_t = 0\}. \quad (5.7)$$

We say τ is phase-type distributed with order p (or with p phases) with initial distribution $\boldsymbol{\pi}$ and phase-type generator \mathbf{T} , denoted $\tau \sim \text{PH}(\boldsymbol{\pi}, \mathbf{T})$.

We write $T_{vw} := [\mathbf{T}]_{vw}$ for $v, w = 1, \dots, p$, and sometimes refer to the v -th element of \mathbf{t} as T_{v0} when this simplifies notation. Note however that specifying \mathbf{T} fully specifies \mathbf{t} :

Theorem 11 (Properties of phase-type distributions).

1. $\mathbf{t} = -\mathbf{T}\mathbf{1}$,
2. $\mathbf{P}_t = e^{\mathbf{Q}t} = \begin{pmatrix} 1 & \mathbf{0} \\ \mathbf{1} - e^{\mathbf{T}t}\mathbf{1} & e^{\mathbf{T}t} \end{pmatrix}$,
3. the distribution function is given by $F(y) = 1 - \boldsymbol{\pi}e^{\mathbf{T}y}\mathbf{1}$, and
4. the probability density function is given by $f(y) = \boldsymbol{\pi}e^{\mathbf{T}y}\mathbf{t}$.

Proof. For the first claim apply Lemma 3. For the second, apply Theorem 9 and the Taylor series expansion in the definition of the matrix exponential after block partitioning the generator. The second leads to the third as $F(y) = \mathbb{P}(X_y = 0) = \boldsymbol{\pi}(\mathbf{1} - e^{\mathbf{T}y}\mathbf{1}) = 1 - \boldsymbol{\pi}e^{\mathbf{T}y}\mathbf{1}$ as $\boldsymbol{\pi}$ is a probability distribution. For the last claim, take the derivative: $\frac{\partial}{\partial y}(1 - \boldsymbol{\pi}e^{\mathbf{T}y}\mathbf{1}) = -\boldsymbol{\pi}e^{\mathbf{T}y}\mathbf{T}\mathbf{1} = \boldsymbol{\pi}e^{\mathbf{T}y}\mathbf{t}$, by the first claim. \square

We finish this section by stating a fundamental result of phase-type distributions, which justifies using them for approximating arbitrary non-negative distributions.

Theorem 12 (Denseness of phase-type distributions). *The class of phase-type distributions is dense within the class of all distributions on the non-negative reals, in the sense of weak convergence.*

Proof. See [41, p. 183], or [40, p. 149]. \square

5.2.1 Examples of phase-type distributions

We now show some basic examples of well-known distributions formulated as phase-type distributions.

Example 13 (Exponential distribution). *Consider a phase-type distribution with one phase with $T_{11} = \lambda$ and initial distribution $\boldsymbol{\pi} = \mathbf{e}_1^\top$. Then the phase-type distribution with parameters $(\boldsymbol{\pi}, \mathbf{G})$ has the exponential distribution with parameter λ .*

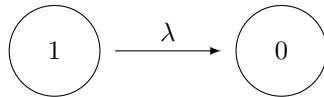


Figure 5.1: The underlying Markov chain of the exponential phase-type distribution

Example 14 (Generalised Erlang distribution). *Suppose X_1, \dots, X_n are independent exponential random variables with rates $\lambda_1, \dots, \lambda_n$, respectively. Then $Y := \sum_{i=1}^n X_i$ is said to have the generalised Erlang distribution, or $Y \sim \text{Erlang}_n(\lambda_1, \dots, \lambda_n)$. If $\lambda_i = \lambda$ for all i , then Y has the Erlang distribution, denoted $Y \sim \text{Erlang}(\lambda, n)$. Define $\boldsymbol{\pi} = \mathbf{e}_1^\top$ and set*

$$\mathbf{T} = \begin{pmatrix} -\lambda_1 & \lambda_1 & 0 & \dots & 0 \\ 0 & -\lambda_2 & \lambda_2 & & \vdots \\ \vdots & & \ddots & \ddots & 0 \\ & & & -\lambda_{n-1} & \lambda_{n-1} \\ 0 & \dots & 0 & 0 & -\lambda_n \end{pmatrix}, \quad (5.8)$$

then $\text{PH}(\boldsymbol{\pi}, \mathbf{T})$ has the $\text{Erlang}_n(\lambda_1, \dots, \lambda_n)$ distribution.



Figure 5.2: The underlying Markov chain of the generalised Erlang phase-type distribution

5.2.2 Coxian distributions

The class of all phase-type distributions is quite large (with $p(p+1) - 1$ parameters for a model with p phases), and as discussed later, this makes parameter estimation computationally difficult. To make model fitting somewhat easier and reduce the parameter space, we restricted ourselves to working with Coxian distributions, a rich sub-class of phase-type distributions:

Definition 15 (Coxian distributions). *A random variable X is said to have the Coxian distribution, if there exists \mathbf{T} of the form*

$$\mathbf{T} = \begin{pmatrix} -(\lambda_1 + \mu_1) & \lambda_1 & 0 & \dots & 0 \\ 0 & -(\lambda_2 + \mu_2) & \lambda_2 & & \vdots \\ \vdots & & \ddots & \ddots & 0 \\ & & & -(\lambda_{n-1} + \mu_{n-1}) & \lambda_{n-1} \\ 0 & \dots & 0 & 0 & -\lambda_n \end{pmatrix}, \quad (5.9)$$

such that with $\boldsymbol{\pi} = \mathbf{e}_1^\top$, $X \sim \text{PH}(\boldsymbol{\pi}, \mathbf{T})$.

Note that this class of distributions only has $2p - 1$ parameters. If we were to allow $\boldsymbol{\pi}$ to be arbitrary, this would give rise to the class of generalised Coxian distributions as defined in [33] with $3p - 2$ parameters.

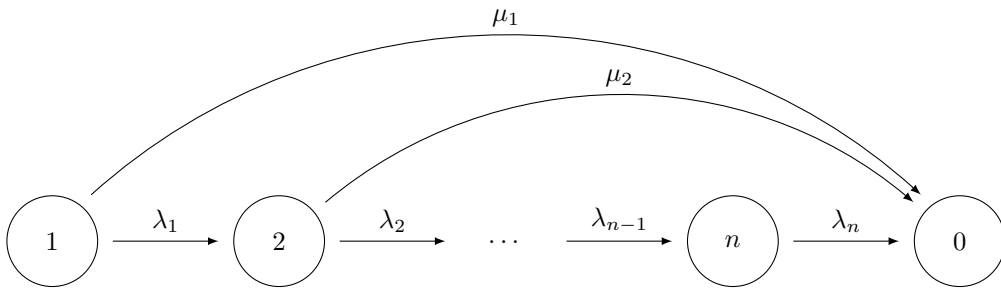


Figure 5.3: The underlying Markov chain of a Coxian distribution

5.3 The expectation-maximisation algorithm

The expectation-maximisation algorithm, or the EM-algorithm, is an iterative algorithm for maximum likelihood estimation when a model contains unobservable hidden variables, called latent variables. Due to its reduced complexity and desirable computational properties, it is also sometimes used

for maximum likelihood estimation even in cases where there are no inherent latent variables, by artificially formulating a problem as an incomplete-data problem [42]. The algorithm works by first initialising the parameter estimates with some starting values, then finding the log-likelihood of the full model given these parameter estimates and the observed data, then finally updating the estimates to maximise this log-likelihood. The algorithm iterates by repeating these two steps, known as the E- and the M-steps, respectively. Due to Jensen's inequality, the algorithm steps through parameter estimates with ever-increasing log-likelihoods, and under somewhat weak conditions converges to a stationary point. However, care must be taken when applying the algorithm as this may be merely a local maximum or a saddle point. See [43] for a systematic treatment of convergence results of the EM-algorithm under a variety of conditions.

Suppose \mathbf{X} is a random vector of the complete data of some experiment, and \mathbf{Y} is some observable subset of the data, with \mathbf{y} being the realisation of this observed data. Then under some unknown parameters $\boldsymbol{\theta} \in \Omega$ of interest, our objective is to compute the maximum likelihood estimator, that is, find $\boldsymbol{\theta}$ that maximises the likelihood function $\mathcal{L}(\boldsymbol{\theta}) := f(\mathbf{y}; \boldsymbol{\theta})$. Our complete log-likelihood is defined as

$$\log \mathcal{L}_c(\boldsymbol{\theta}) := \log f(\mathbf{x}; \boldsymbol{\theta}). \quad (5.10)$$

At the $k + 1$ -th iteration, the EM-algorithm consists of performing the following two steps. The first is the E-step, where we compute a function Q ; the expectation of the complete log-likelihood at $\boldsymbol{\theta}$ under our current parameter estimates, $\boldsymbol{\theta}^{(k)}$, and given our observable data $\mathbf{Y} = \mathbf{y}$,

$$Q(\boldsymbol{\theta}; \boldsymbol{\theta}^{(k)}) := \mathbb{E}_{\boldsymbol{\theta}^{(k)}} (\log \mathcal{L}_c(\boldsymbol{\theta}) \mid \mathbf{y}). \quad (5.11)$$

Following this, in the M-step, we update our parameter estimates to some maximiser of Q , that is,

$$\boldsymbol{\theta}^{(k+1)} \in \arg \max_{\boldsymbol{\theta} \in \Omega} Q(\boldsymbol{\theta}; \boldsymbol{\theta}^{(k)}). \quad (5.12)$$

The General EM-algorithm, as discussed in [40], is a small modification in which one need only choose some $\boldsymbol{\theta}^{(k+1)}$ such that $Q(\boldsymbol{\theta}^{(k+1)}; \boldsymbol{\theta}^{(k)}) \geq Q(\boldsymbol{\theta}^{(k)}; \boldsymbol{\theta}^{(k)})$. This may be a much more attainable task under computational constraints.

The EM-algorithm indeed monotonically increases our log-likelihood of the experiment, $\mathcal{L}(\boldsymbol{\theta}^{(k)})$, at each step. To see this, let $k(\mathbf{x} \mid \mathbf{y}; \boldsymbol{\theta})$ be the conditional density of \mathbf{x} given \mathbf{y} under parameters $\boldsymbol{\theta}$, and compute

$$\log \mathcal{L}_c(\boldsymbol{\theta}) = \log f(\mathbf{x}; \boldsymbol{\theta}) \quad (5.13)$$

$$= \log \mathcal{L}(\boldsymbol{\theta}) + \log k(\mathbf{x} \mid \mathbf{y}; \boldsymbol{\theta}). \quad (5.14)$$

Taking now the expectation given $\mathbf{Y} = \mathbf{y}$ under parameters $\boldsymbol{\theta}^{(k+1)}$, we have

$$Q(\boldsymbol{\theta}; \boldsymbol{\theta}^{(k)}) = \log \mathcal{L}(\boldsymbol{\theta}) + \mathbb{E}_{\boldsymbol{\theta}^{(k)}} (\log k(\mathbf{x} | \mathbf{y}; \boldsymbol{\theta}) | \mathbf{y}). \quad (5.15)$$

So now

$$\log \mathcal{L}(\boldsymbol{\theta}) = Q(\boldsymbol{\theta}; \boldsymbol{\theta}^{(k)}) - \mathbb{E}_{\boldsymbol{\theta}^{(k)}} (\log k(\mathbf{x} | \mathbf{y}; \boldsymbol{\theta}) | \mathbf{y}). \quad (5.16)$$

Consider now the difference $\log \mathcal{L}(\boldsymbol{\theta}^{(k+1)}) - \log \mathcal{L}(\boldsymbol{\theta}^{(k)})$. The first part of this difference will be non-negative by construction as we choose the next parameter estimate to satisfy $Q(\boldsymbol{\theta}^{(k+1)}; \boldsymbol{\theta}^{(k)}) \geq Q(\boldsymbol{\theta}^{(k)}; \boldsymbol{\theta}^{(k)})$. For the second part, let again $\boldsymbol{\theta} \in \Omega$ be arbitrary and note that the logarithm is concave, so apply Jensen's inequality,

$$\mathbb{E}_{\boldsymbol{\theta}^{(k)}} (\log k(\mathbf{x} | \mathbf{y}; \boldsymbol{\theta}) | \mathbf{y}) - \mathbb{E}_{\boldsymbol{\theta}^{(k)}} (\log k(\mathbf{x} | \mathbf{y}; \boldsymbol{\theta}^{(k)}) | \mathbf{y}) = \mathbb{E}_{\boldsymbol{\theta}^{(k)}} \left(\log \frac{k(\mathbf{x} | \mathbf{y}; \boldsymbol{\theta})}{k(\mathbf{x} | \mathbf{y}; \boldsymbol{\theta}^{(k)})} | \mathbf{y} \right) \quad (5.17)$$

$$\leq \log \mathbb{E}_{\boldsymbol{\theta}^{(k)}} \left(\frac{k(\mathbf{x} | \mathbf{y}; \boldsymbol{\theta})}{k(\mathbf{x} | \mathbf{y}; \boldsymbol{\theta}^{(k)})} | \mathbf{y} \right) \quad (5.18)$$

$$= 0. \quad (5.19)$$

The last equality follows from the definition of the pertinent expectation. Readers familiar with machine learning will recognise Equation 5.17 as the negative of the Kullback-Leibler divergence of the complete data given the observed data under $\boldsymbol{\theta}^{(k)}$ and the complete data given the observed data under $\boldsymbol{\theta}$, and so the computation reduces to showing that Kullback-Leibler divergence is non-negative.

Therefore, each iterate of $\boldsymbol{\theta}^{(k)}$ increases the likelihood, $\mathcal{L}(\boldsymbol{\theta}^{(k)})$.

5.4 Fitting phase-type distributions to data

Our aim now is to apply the EM-algorithm for fitting phase-type distributions to data by estimating the parameters $\boldsymbol{\pi}$ and \mathbf{T} . We first construct the problem as a complete data experiment, and then compute explicit formulas for the iterates to be computed at each step.

Consider the Markov process underlying a phase-type distribution of fixed order p . It is easy to write down the maximum likelihood estimator for the parameters of the phase-type distribution if we were able to observe the complete process. This would mean for each observation the number of jumps, N until the chain reaches the absorbing state 0, the holding times S_0, S_1, \dots, S_{N-1} (with $S_N = 0$), and the embedded Markov chain I_0, I_1, \dots, I_{N-1} . However, we only observe the absorption time $Y = S_0 + S_1 + \dots + S_{N-1}$. Framed this way, the problem can naturally be seen as an incomplete data problem, making it an apt application of the EM-algorithm.

Now consider a single observation $x = ((i_0, s_0), (i_1, s_1), \dots, (i_n, s_n))$ of the complete data. The s_k , for $k = 0, \dots, n$ are a realisation of an embedded Markov chain with transition probabilities $p_{jk} = \mathbb{P}(I_{t+1} = k | I_t = j)$, as follows. For $j, k = 1, \dots, p$ and $j \neq k$, we have

$$p_{jk} = \frac{T_{jk}}{\lambda_j}, \quad p_{j0} = \frac{t_j}{\lambda_j}. \quad (5.20)$$

The i_k , for $k = 0, \dots, n$ on the other hand are simply realisations of exponential random variables

with rates λ_{i_k} . The complete likelihood for a single sample is then given by

$$\mathcal{L}_c(\boldsymbol{\pi}, \mathbf{T}; x) = f(x; \boldsymbol{\pi}, \mathbf{T}) \quad (5.21)$$

$$= \pi_{i_0} \lambda_{i_0} e^{-\lambda_{i_0} s_0} p_{i_0 i_1} \cdots \lambda_{i_{n-1}} e^{-\lambda_{i_{n-1}} s_{n-1}} p_{i_{n-1} 0} \quad (5.22)$$

$$= \pi_{i_0} e^{-\lambda_{i_0} s_0} T_{i_0 i_1} \cdots e^{-\lambda_{i_{n-1}} s_{n-1}} T_{i_{n-1} 0}. \quad (5.23)$$

Given now a sample of L independent observations of the underlying complete process, $\mathbf{x} = (x^1, \dots, x^L)$, where superscripts denote the sample, we have the complete likelihood for that sample,

$$\mathcal{L}_c(\boldsymbol{\pi}, \mathbf{T}) = \prod_{l=1}^L f(x^l; \boldsymbol{\pi}, \mathbf{T}) \quad (5.24)$$

$$= \prod_{l=1}^L \pi_{i_0^l} e^{-\lambda_{i_0^l} s_0^l} T_{i_0^l i_1^l} \cdots e^{-\lambda_{i_{n-1}^l} s_{n-1}^l} T_{i_{n-1}^l 0}. \quad (5.25)$$

Rearranging, grouping into phases, and performing some substitutions, we get the following form for our complete likelihood:

$$\mathcal{L}_c(\boldsymbol{\pi}, \mathbf{T}) = \prod_{v=1}^p \pi_v^{B_v} \prod_{v=1}^p e^{T_{vv} Z_v} \prod_{v=1}^p \prod_{\substack{w=0 \\ w \neq v}}^p T_{vw}^{N_{vw}}. \quad (5.26)$$

The substitutions are as follows: $B_v = \sum_{l=1}^L \mathbf{1}_{\{i_0^l=v\}}$ is the total number of times that the processes started from state v ; $Z_v = \sum_{l=1}^L \sum_{j=1}^{n^l} s_j^l \mathbf{1}_{\{i_j^l=v\}}$ is the total time spent in state v ; and $N_{vw} = \sum_{l=1}^L \sum_{j=1}^{n^l-1} \mathbf{1}_{\{i_j^l=v, i_{j+1}^l=w\}}$ is the total number of transitions from v to w .

The B_v , Z_v , and N_{vw} are a sufficient statistic for $(\boldsymbol{\pi}, \mathbf{T})$ by the Fisher–Neyman factorization theorem. Furthermore, we can explicitly though laboriously compute the maximum likelihood estimators for $\boldsymbol{\pi}$ and \mathbf{T} by standard theory. The computations are reserved for Appendix A. For $v = 1, \dots, p$, and $w = 0, \dots, p$, $v \neq w$, the maximum likelihood estimators are given by

$$\hat{\pi}_v = \frac{B_v}{n}, \quad \hat{T}_{vw} = \frac{N_{vw}}{Z_v}, \quad \hat{T}_{vv} = - \sum_{w=0}^p \hat{T}_{vw}. \quad (5.27)$$

Since B_v , Z_v and N_{vw} are a sufficient statistic, it suffices for the E-step to compute the expectation of these under $(\boldsymbol{\pi}, \mathbf{T})^{(k)}$ and given $\mathbf{Y} = \mathbf{y}$. Also note that each of these statistics is a sum over the sample, and the realisations in the sample are independent, so it is enough for each statistic to sum the estimates for each sample, so we have

$$B_v^{(k+1)} = \sum_{l=1}^L \mathbb{E}_{(\boldsymbol{\pi}, \mathbf{T})^{(k)}} (B_v^l \mid y^l), \quad (5.28)$$

$$Z_v^{(k+1)} = \sum_{l=1}^L \mathbb{E}_{(\boldsymbol{\pi}, \mathbf{T})^{(k)}} (Z_v^l \mid y^l), \quad (5.29)$$

$$N_{vw}^{(k+1)} = \sum_{l=1}^L \mathbb{E}_{(\boldsymbol{\pi}, \mathbf{T})^{(k)}} (N_{vw}^l \mid y^l). \quad (5.30)$$

Here again $v = 1, \dots, p$, $w = 0, \dots, p$, and $v \neq w$. The estimates for the parameters are updated in the obvious way by substituting into Equation 5.27. Heavy computations are again recorded in Appendix B. We define the matrix-valued convenience function

$$\Gamma(y \mid \boldsymbol{\pi}, \mathbf{T}) = \int_0^y e^{\mathbf{T}(y-u)} \mathbf{t} \boldsymbol{\pi} e^{\mathbf{T}u} du. \quad (5.31)$$

Using this notation, our conditional expectations are given by

$$\mathbb{E}_{(\boldsymbol{\pi}, \mathbf{T})} (B_v \mid \mathbf{y}) = \sum_{l=1}^L \frac{\pi_v \mathbf{e}_v^\top e^{\mathbf{T}y^l} \mathbf{t}}{\boldsymbol{\pi} e^{\mathbf{T}y^l} \mathbf{t}}, \quad (5.32)$$

$$\mathbb{E}_{(\boldsymbol{\pi}, \mathbf{T})} (Z_v \mid \mathbf{y}) = \sum_{l=1}^L \frac{\Gamma_{vv}(y^l \mid \boldsymbol{\pi}, \mathbf{T})}{\boldsymbol{\pi} e^{\mathbf{T}y^l} \mathbf{t}}, \quad (5.33)$$

$$\mathbb{E}_{(\boldsymbol{\pi}, \mathbf{T})} (N_{v0} \mid \mathbf{y}) = \sum_{l=1}^L \frac{\boldsymbol{\pi} e^{\mathbf{T}y^l} \mathbf{e}_v t_v}{\boldsymbol{\pi} e^{\mathbf{T}y^l} \mathbf{t}}, \quad (5.34)$$

$$\mathbb{E}_{(\boldsymbol{\pi}, \mathbf{T})} (N_{vw} \mid \mathbf{y}) = \sum_{l=1}^L \frac{T_{vw} \Gamma_{vv}(y^l \mid \boldsymbol{\pi}, \mathbf{T})}{\boldsymbol{\pi} e^{\mathbf{T}y^l} \mathbf{t}}. \quad (5.35)$$

5.5 Properties of the algorithm

One of the main drawbacks in fitting phase-type distributions with the EM-algorithm is that phase-type distributions are heavily overparametrised [33] and exhibit a number of symmetries. This means that there exist several parameter sets, $(\boldsymbol{\pi}, \mathbf{T})$ that lead to the same distribution. For instance, simply permuting the underlying state space of the Markov chain leads to $p!$ parametrisations. In practice, this translates to increased complexity in the search space, leading to slower convergence, and a higher chance of converging to a local maximum or saddle point.

This algorithm has the convenient property that if some set of T_{vw} or π_v are set to 0, then at each iteration, that entry will remain 0. The advantage of this is that one can easily fit a sub-model using the same algorithm, simply by initialising the algorithm with a matrix that has a specified structure. For instance, to fit a Coxian distribution as in our case, one merely needs to initialise the algorithm with a matrix whose entries are zero except on the diagonal and superdiagonal and a initial distribution with $\pi_1 = 1$. The EM-algorithm will then only ever lead to fits which are also Coxian.

Slight changes to the method lead to ways for fitting phase-type distributions to continuous distributions, as well as to data that is censored (where only the interval that a data belongs in is observed rather than the exact value), or a combination of fully observed and censored data. For details on

these techniques, see [44] and [33].

5.6 Akaike’s Information Criterion

Up to now, we have discussed fitting various phase-type distributions to empirical data for a fixed number of phases, p . However, we have not yet discussed how to choose p , and how we can systematically compare fits with a different number of phases. If we were to simply fit several distributions with varying p and compare them based on some measure of error from the data, then increasing p would always decrease the error (in practice, convergence issues might cause larger models to lead to worse fits), as a model with $p - 1$ parameters is a sub-model of one with p parameters. However, this would not necessarily mean that we always find better approximations to the true underlying distribution, but rather that we have so many free parameters that our model is fitting around the randomness in our data. Simultaneously, we need to have a large enough p to capture the true shape of the distribution and avoid underfitting through not capturing the true distribution well enough. We need a method of model selection to balance out these two factors and get as close to the true model as possible.

Although there are several criteria for model selection, we used Akaike’s information criterion which amounts to choosing the model that minimises the number

$$AIC := 2k - 2 \log \mathcal{L}(\hat{\boldsymbol{\theta}}; \mathbf{y}) \quad (5.36)$$

where k is the number of parameters in the model and $\hat{\boldsymbol{\theta}}$ is the maximum likelihood estimator, so that $\log \mathcal{L}(\hat{\boldsymbol{\theta}}; \mathbf{y})$ is the maximum log-likelihood. We will not provide a full derivation of this criterion for brevity. For a thorough treatment, see [45], [46], or [47]. Roughly speaking, if we assume there exists some true distribution f that the underlying data originates from, then one can show that the model which minimises AIC also minimises the Kullback-Leibler divergence between that model and the true distribution. This result holds asymptotically in the number of samples under some important technical assumptions.

5.7 MapReduce

The MapReduce paradigm is a method for parallelising a big data workflow, whereby data is first partitioned into subsets, then handed off to worker queues where these workers apply some “mapping” to them. Once the workers have finished, the results of the computations are finally merged, or “reduced”. This is particularly useful in applications such as ours where there is a large number of computations that can easily be performed in parallel, without results interacting with each other except for in a final reduction step. We used the MapReduce paradigm to parallelise the algorithm and decrease the fitting time on multi-core computers.

Chapter 6

Computational aspects of phase-type fitting

In this chapter, we review some computational aspects of the EM-algorithm for fitting phase-type distributions. We also discuss the implementation we used, and the modifications we made to existing algorithms for our use-case to decrease the computational time on modern computing infrastructure.

The algorithm has two computationally heavy steps. The first is the computation of the integral $\mathbf{\Gamma}$ and the exponential $e^{\mathbf{T}y}$, and the second is when these two matrix-valued functions are evaluated for each observation and are used to compute the contribution of that observation to Equations 5.32 to 5.35.

Generally, the first of the two is the computationally demanding step. However, as the number of data points increases, as in our case, the second step also becomes increasingly difficult.

6.1 The integral $\mathbf{\Gamma}$

Traditionally, the most computationally difficult part has been the computation of the matrix-valued integral $\mathbf{\Gamma}$ of dimension $p \times p$ to a sufficient level of accuracy, and to a smaller extent in computing $e^{\mathbf{T}y}$, also of dimension $p \times p$. As the number of phases, p , is increased, this task quickly becomes very intensive. Most methods involve computing $\mathbf{\Gamma}(y \mid \boldsymbol{\pi}, \mathbf{T})$ for a fine grid of y -values, then interpolating between these when the expression needs to be approximated for a given y . This means that the computational time of this step increases linearly with the maximum observed time.

Recall that $\mathbf{\Gamma}$ is defined as

$$\mathbf{\Gamma}(y \mid \boldsymbol{\pi}, \mathbf{T}) = \int_0^y e^{\mathbf{T}(y-u)} \mathbf{t} \boldsymbol{\pi} e^{\mathbf{T}u} du. \quad (6.1)$$

A standard trick is to construct the block matrix

$$\mathbf{B} = \begin{pmatrix} \mathbf{T} & \mathbf{t} \boldsymbol{\pi} \\ \mathbf{0} & \mathbf{T} \end{pmatrix}, \quad (6.2)$$

from which one can verify that

$$e^{\mathbf{B}y} = \begin{pmatrix} e^{\mathbf{T}y} & \mathbf{\Gamma}(y \mid \boldsymbol{\pi}, \mathbf{T}) \\ \mathbf{0} & e^{\mathbf{T}y} \end{pmatrix}. \quad (6.3)$$

The calculation is reproduced in Appendix C. These kinds of integrals arise in several fields, including differential equations, numerical methods, and control theory (where they are known as Gramians). See [48] and [49] for an overview and [50] for a similar application.

This expression allows us to compute both $e^{\mathbf{T}y}$ and $\mathbf{\Gamma}$ by evaluating just one matrix exponential. However, computing matrix exponentials and their error bounds in general is a very difficult problem. See [51] for a discussion of several approaches to computing matrix exponential. Due to this, one generally attempts to create specialised methods by exploiting additional structure in the problem when high speed and accuracy are required. Unfortunately \mathbf{B} is a $2p \times 2p$ -dimensional matrix without much obvious structure. It is therefore reasonable to attempt to compute $\mathbf{\Gamma}$ directly by exploiting its structure; then compute $e^{\mathbf{T}y}$ separately.

There exist several methods to compute $\mathbf{\Gamma}$, including through this combined matrix exponential, as an ordinary differential equation, using standard quadrature methods, as well as using uniformisation methods.

6.1.1 The `EMpht.c` program

The original method for fitting phase-type distributions via EM-algorithm was introduced by Asmussen et al. in [39]. To accompany their paper, Olsson implemented an algorithm for computing the estimates using an ordinary differential equation method in ANSI-C [52], which we refer to as `EMpht.c`. In addition to $\mathbf{\Gamma}$, they defined the vector-valued helper functions

$$\mathbf{a}(y \mid \boldsymbol{\pi}, \mathbf{T}) = \boldsymbol{\pi} e^{\mathbf{T}y}, \quad (6.4)$$

$$\mathbf{b}(y \mid \mathbf{T}) = e^{\mathbf{T}y} \mathbf{t}. \quad (6.5)$$

Using these, the conditional expectations become

$$\mathbb{E}_{(\boldsymbol{\pi}, \mathbf{T})} (B_v \mid \mathbf{y}) = \sum_{l=1}^L \frac{\pi_v b_v(y^l \mid \mathbf{T})}{\boldsymbol{\pi} \mathbf{b}(y^l \mid \mathbf{T})}, \quad (6.6)$$

$$\mathbb{E}_{(\boldsymbol{\pi}, \mathbf{T})} (Z_v \mid \mathbf{y}) = \sum_{l=1}^L \frac{\Gamma_{vv}(y^l \mid \boldsymbol{\pi}, \mathbf{T})}{\boldsymbol{\pi} \mathbf{b}(y^l \mid \mathbf{T})}, \quad (6.7)$$

$$\mathbb{E}_{(\boldsymbol{\pi}, \mathbf{T})} (N_{v0} \mid \mathbf{y}) = \sum_{l=1}^L \frac{t_v a_v(y^l \mid \boldsymbol{\pi}, \mathbf{T})}{\boldsymbol{\pi} \mathbf{b}(y^l \mid \mathbf{T})}, \quad (6.8)$$

$$\mathbb{E}_{(\boldsymbol{\pi}, \mathbf{T})} (N_{vw} \mid \mathbf{y}) = \sum_{l=1}^L \frac{T_{vw} \Gamma_{wv}(y^l \mid \boldsymbol{\pi}, \mathbf{T})}{\boldsymbol{\pi} \mathbf{b}(y^l \mid \mathbf{T})}. \quad (6.9)$$

Subject to the initial conditions $\mathbf{a}(0 \mid \boldsymbol{\pi}, \mathbf{T}) = \boldsymbol{\pi}$, $\mathbf{b}(0 \mid \mathbf{T}) = \mathbf{t}$, and $\mathbf{\Gamma}(0 \mid \boldsymbol{\pi}, \mathbf{T}) = \mathbf{0}$, the solutions to these expressions can then be computed using a $p(p+2)$ -dimensional ordinary differential equation with

$$\frac{\partial}{\partial y} \mathbf{a}(y \mid \boldsymbol{\pi}, \mathbf{T}) = \mathbf{a}(y \mid \boldsymbol{\pi}, \mathbf{T}) \mathbf{T}, \quad (6.10)$$

$$\frac{\partial}{\partial y} \mathbf{b}(y \mid \mathbf{T}) = \mathbf{T} \mathbf{b}(y \mid \mathbf{T}), \quad (6.11)$$

$$\frac{\partial}{\partial y} \boldsymbol{\Gamma}(y \mid \boldsymbol{\pi}, \mathbf{T}) = \mathbf{T} \boldsymbol{\Gamma}(y \mid \boldsymbol{\pi}, \mathbf{T}) + \mathbf{t} \mathbf{a}(y \mid \boldsymbol{\pi}, \mathbf{T}). \quad (6.12)$$

The last derivative is by the Leibniz integral rule. Note that this is very similar to computing the matrix exponential in Equation 6.3.

Their program solves these equations using a hardcoded fourth order Runge-Kutta method. These equations are solved incrementally with some step size h up to the maximum value of the observation. The conditional expectations are computed within this loop and each y -value is rounded down to the nearest step. The new parameters are finally computed at the end of the routine.

We initially used the `EMpht.c` program to fit phase-type distributions to our data, but the program was too slow to process our whole dataset, or even a substantial sample from it. In addition, some of our data was very concentrated around zero, and had a long tail, which meant that stiffness of the differential equation became an issue. This was hard to work around as the solver algorithm was hardcoded and could not be tuned or changed. In particular, we found that $\boldsymbol{\Gamma}(y, \boldsymbol{\pi}, \mathbf{T})$ would occasionally evaluate to a negative value for some y , which then led to serious errors in the rest of the computation, drastically worsening the convergence rate and hence fitting performance.

6.1.2 The `EMpht.jl` program

In [33], Laub wrote a new implementation of the algorithm using the Julia programming language, and extended it in several ways. We will refer to this as the `EMpht.jl` program. The procedure was modified to use the general `OrdinaryDiffEq.jl` library for computing $\boldsymbol{\Gamma}$, giving easy access to a variety of stiff and non-stiff solvers. In addition to the original differential equation method, they also implemented several alternative ways of computing $\boldsymbol{\Gamma}$ for censored data, including quadrature methods and a uniformisation method discussed next.

6.1.3 Uniformisation methods

Uniformisation methods for general Markov chains were introduced by Jensen, and have been used extensively since then. The idea is the following.

If one defines a Poisson process $\{N_t\}_{t \geq 0}$ with fixed rate λ , and independent from this a discrete time Markov chain $\{I_n\}_{n \in \mathbb{N}}$ on a finite state space with transition matrix \mathbf{P} , then one can show that $\{I_{N_t}\}_{t \geq 0}$ is a continuous time Markov chain with generator $\lambda(\mathbf{P} - \mathbf{I})$ [53]. This is the idea of a Markov chain subordinate to a Poisson process.

Uniformisation, also known as the randomisation technique¹, is based on reversing this idea. We call a continuous time Markov chain uniformisable if the diagonal entries of its generator are uniformly bounded. In our case, as Markov chains have finite state spaces, this always holds. Suppose $\{X_t\}_{t \geq 0}$ is a continuous time Markov chain with generator \mathbf{Q} , and consider a Poisson process $\{N_t\}_{t \geq 0}$ with rate $\lambda := \sup_i \lambda_i$ where $\lambda_i = -Q_{ii}$ is the negative of the i -th diagonal entry of the generator. Suppose $\{I_n\}_{n \in \mathbb{N}}$ is an independent, discrete time Markov chain on the same state space with transition matrix $\mathbf{P} := \mathbf{Q}/\lambda + \mathbf{I}$. Now construct the Markov chain $\{I_{N_t}\}_{n \in \mathbb{N}}$ by subordinating this discrete time Markov

¹Markov chains subordinate to a Poisson process can be thought of as discrete time Markov chains with randomised jump times. The name originates from this.

chain, $\{I_n\}_{n \in \mathbb{N}}$, to the Poisson process $\{N_t\}_{t \geq 0}$. One can then show that again, $\{I_{N_t}\}_{n \in \mathbb{N}}$ is equivalent to $\{X_t\}_{t \geq 0}$ in the sense that they both have the same generator and all finite dimensional distributions coincide [53].

This idea can be conceptualised as a clever way to simulate $\{X_t\}_{t \geq 0}$ when one can only sample from one homogeneous Poisson process $\{N_t\}_{t \geq 0}$. Suppose the chain is initially in some state $i \in \mathcal{S}$: then the time until the next jump is distributed exponentially with rate equal to the holding intensity λ_i , and the probability of transitioning to a different state $j \in \mathcal{S}$, $j \neq i$ is Q_{ij}/λ_i (cf. Lemma 5). If the holding intensities were all equal, we could now simulate the whole of our Markov chain this way. However, when the holding intensities are not all equal, one can achieve the same outcome by sampling from an exponentially distributed random variable with intensity higher or equal to each of the holding intensities, and then thinning this Poisson process. If we are in state $i \in \mathcal{S}$, and sample from a Poisson process with rate $\lambda \geq \lambda_i$, then we first thin this process by ignoring the sample and staying in the same state with probability $P_{ii} = 1 - \lambda_i/\lambda$, and similarly to before, jumping to another state $j \in \mathcal{S}$, $j \neq i$ with probability $P_{ij} = \lambda_i/\lambda \times Q_{ij}/\lambda_i = Q_{ij}/\lambda$. This is exactly how the uniformisation technique works and the derivation shows how we arrive at the expression for the transition matrix, $\mathbf{P} = \mathbf{Q}/\lambda + \mathbf{I}$. For a more in-depth overview on uniformisation, see [54] or [53].

We can use this formula to derive an expression for $\pi e^{\mathbf{Q}t}$ as in [54] by conditioning on the number of jumps before a time t . We get

$$\pi e^{\mathbf{Q}t} = \sum_{n \geq 0} \pi \mathbf{P}^n \frac{(\lambda t)^n}{n!} e^{-\lambda t}. \quad (6.13)$$

The power of this method is that we can now explicitly express the truncation error in terms of a Poisson tail probability,

$$\left\| \pi e^{\mathbf{Q}t} - \sum_{n=0}^N \pi \mathbf{P}^n \frac{(\lambda t)^n}{n!} e^{-\lambda t} \right\|_{\infty} = \left\| \sum_{n>N} \pi \mathbf{P}^n \frac{(\lambda t)^n}{n!} e^{-\lambda t} \right\|_{\infty} \quad (6.14)$$

$$\leq \sum_{n>N} \frac{(\lambda t)^n}{n!} e^{-\lambda t}, \quad (6.15)$$

this follows directly as $\pi_i \leq 1$. In general, this method is superior to differential equation methods in computing transition probabilities for continuous time Markov chains [55].

In [55] and [56], Okamura implemented a complete uniformisation scheme for computing $\mathbf{\Gamma}$, based on [57]. The first paper, [55] deals with non-censored data and [56] extended this to all cases treated in the original papers of Asmussen [39] and Olsson [44].

In addition to tight guarantees on accuracy, Okamura proved that this improves the time complexity of the computation by a factor of p , a significant improvement. However, this comes at the cost of the time complexity depending on the number of data points.

In [33], the authors used `EMpht.jl` with an implementation of the uniformisation method by Okamura, which they fitted to purely interval data. Their data consisted of a life table, that is, a table showing for each age the probability of an individual of that age dying before reaching their next birthday. Their data was therefore “binned” to bins of one year each, that is, they only observed probability masses for yearly intervals. They only implemented these additional techniques for that case. We did not adapt these techniques to the non-censored case as their time complexity increases with the number of data points. By experimenting with the censored program, we found that the

time taken to compute solutions increased too quickly to handle all our data.

6.2 Our program

We based our final program on `EMpht.jl` by Laub, but modified it by implementing a hybrid approach combining the original differential equation approach with a quadrature method as a backup.

As mentioned earlier, the differential equations were often stiff in our case. We experimented with a number of stiff and non-stiff solvers, and eventually used an improved fifth order explicit Runge-Kutta solving technique based on [58], as implemented in `OrdinaryDiffEq.jl` [59].

In addition to using a slightly improved solver, a special case was added to the procedure, where if $\mathbf{\Gamma}$ erroneously evaluated to an negative value for some observation, then $\mathbf{\Gamma}(y^l; \boldsymbol{\pi}, \mathbf{T})$ was recomputed directly using the `HCubature.jl` library [60]. The library implements a quadrature algorithm based on [61]. This is an adaptive algorithm for numerical integration that successively subdivides a hyperrectangle until a given tolerance is achieved [60]. This algorithm is substantially slower than the other methods, but these problems arose in less than one percent of observations, so they did not significantly affect running times. These were mostly either observations very close to the origin or very close to the maximum observation. Furthermore, we found that the number of problems was reduced as the algorithm progressed in iterations, indicating numerical instability in early iterations which disappeared as the parameter estimates approached some maximum.

The original EM-algorithm, in both `EMpht.c` and `EMpht.jl` initialises $\boldsymbol{\pi}$ and \mathbf{T} using uniform random variables on the interval (0.1, 0.9), and following this, scales the values. $\boldsymbol{\pi}$ is scaled to be a probability distribution, and \mathbf{T} is scaled by multiplying by p/m where m is the median of the observations. In our case, this led to a large number of issues with stiffness, so we further divided this number by 10.

6.3 Computation of the conditional expectations

The computational aspects of the algorithm other than that of the various matrix integrals and exponentials has mostly been ignored in prior work. However, as the number of data points increases, just evaluating $\mathbf{\Gamma}$ through some interpolation method and updating the parameter estimates in a single thread of execution becomes computationally demanding.

The `EMpht.jl` program first solves the ordinary differential equation for $\mathbf{\Gamma}$, then for each observation y^l , computes $e^{\mathbf{T}y^l}$, evaluates $\mathbf{\Gamma}(y^l; \boldsymbol{\pi}, \mathbf{T})$ (interpolating from the solution), and updates Equations 5.32 to 5.35 by adding the contribution of that observation. We made the trade-off to compute instead a global solution to $e^{\mathbf{T}y}$ up to the maximum of the y , then interpolate this for each observation. This sacrificed some accuracy in the exponential, but allowed us to cache the solution for several time values and interpolate between them, which sped up the algorithm overall.

We also implemented a straightforward way to parallelise this computations using a MapReduce algorithm by applying standard techniques from computer science. In our instance, the mapping operation was the computation of each individual observation's contribution to the conditional expectations in Equations 5.32 to 5.35, and the reduction step consisted of summing each of these together and computing the new parameter estimates as by Equation 5.27. In the splitting step, the data points were randomly assigned to queues, one queue for each worker, and each worker then tallied up their contribution to the estimates. This procedure significantly decreased computational time, up to several orders of magnitude for large instances.

Chapter 7

Phase-type fits to propagation delays

In this section we fit phase-type distributions to the difference in block arrival times at Sydney and Northern Virginia for those blocks that arrived first at Northern Virginia. We chose these locations because blocks most commonly arrived at Northern Virginia first, and because Sydney is geographically far away from Virginia while also observing a large number of block arrivals. A histogram of the arrival time differences is shown in Figure 7.1.

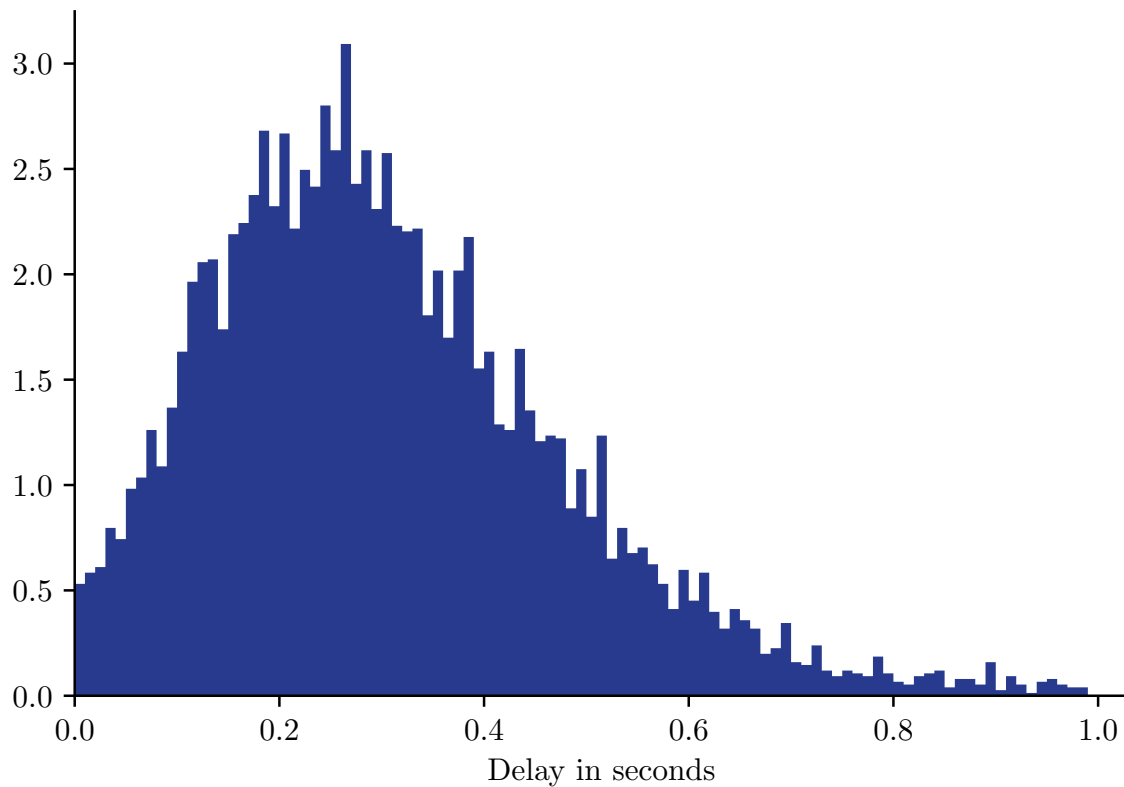


Figure 7.1: Histogram of arrival time differences between Northern Virginia and Sydney for blocks arriving first at Northern Virginia

7.1 Method

To perform the fits, we took the subset of blocks that were observed at both locations but arrived first at Northern Virginia, of which there were 7759, or approximately 52.4 %, then subtracted the time of observation at Northern Virginia from the time at which the block was first observed in Sydney.

We fitted Coxian phase-type distributions using our code for a varying number of phases, ranging from one to six phases. Our stopping criterion was for the log-likelihood to stop increasing by more than 1×10^{-6} on average over the past 100 iterations of the EM-algorithm. We only fitted to the bottom 98 % of data, as this coincided almost exactly with 1 second, and the complexity of the EM-algorithm grows with the maximum observation value, so fitting to the large outliers would have caused the fits to take much longer to compute.

For each model, we ran the algorithm six times with random initial parameters. When fitting with no more than four phases, the algorithm completed very quickly, took less than ten thousand iterations, and always converged to the same estimates of \mathbf{T} (the initial distribution is fixed for Coxian distributions). With both $p = 5$ and $p = 6$, the code started taking longer and in two of the six runs, failed to converge to the same value as the other four runs. Figure 7.2 shows the average running times and number of iterations per run for successful runs.

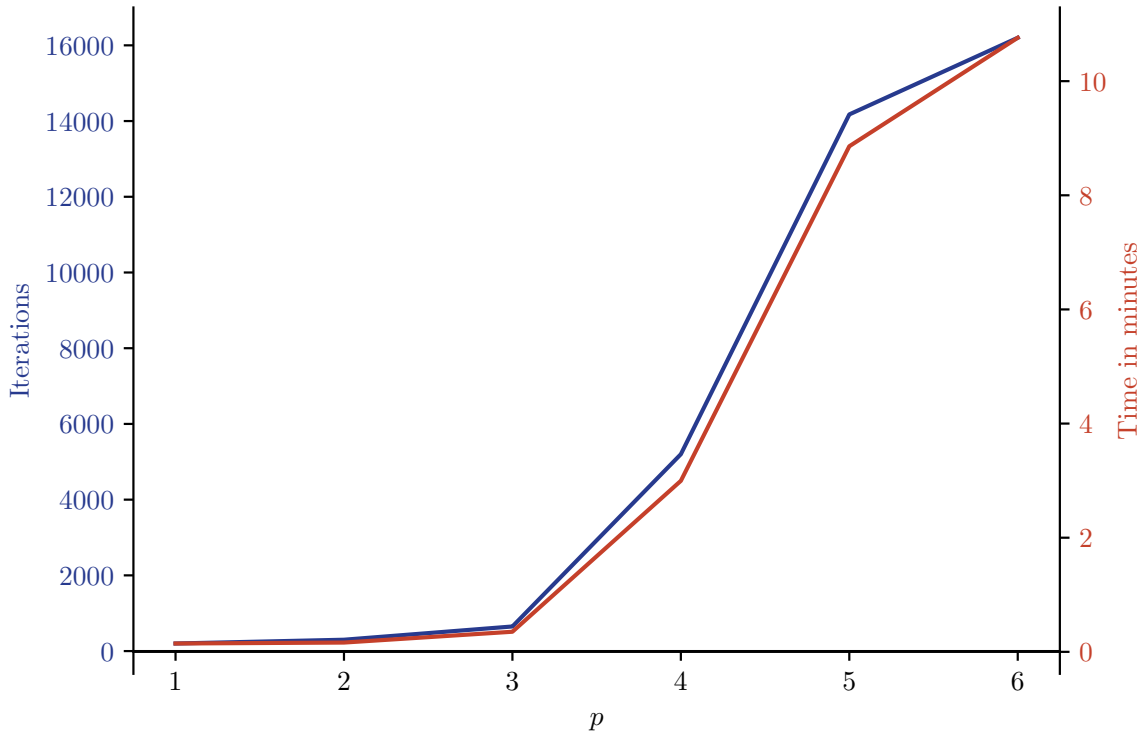


Figure 7.2: Average running time and number of iteration per run for successful runs

It seems that the runs with six phases did not converge completely.

7.2 Model selection

We performed model selection using Akaike's information criterion discussed in Section 5.6. The number of parameters when fitting Coxian distributions is $k = 2p - 1$, so the AIC is given by

$$4p - 2 - 2 \log \mathcal{L}(\hat{\theta}; \mathbf{y}). \quad (7.1)$$

We computed the AIC values for each model, which are shown in Figure 7.3. We stopped fitting larger models after $p = 6$ as we found that the AIC had already started increasing at $p = 4$, and because the fitting time was roughly exponential in the number of phases, making it difficult to continue further.

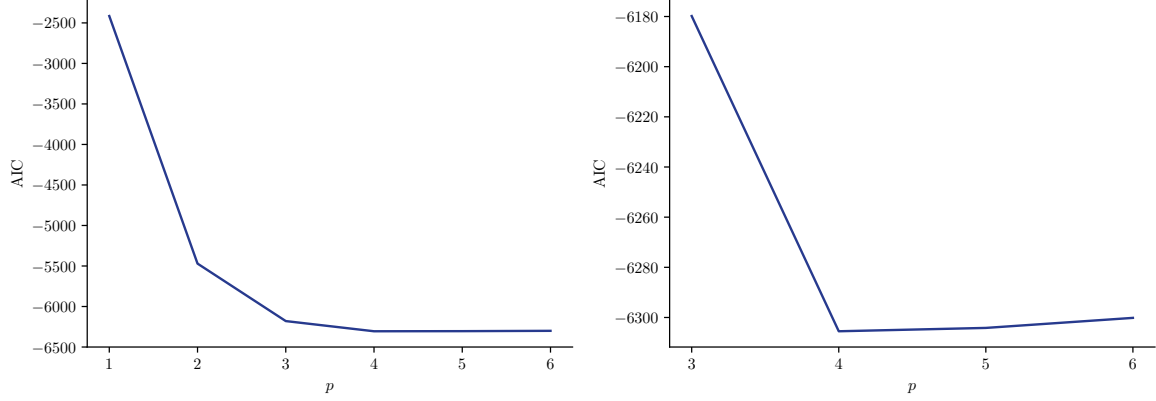


Figure 7.3: AIC of models

The AIC values dropped quickly until $p = 4$, then slowly started growing again. We therefore chose $p = 4$ as the best fitting model, which attained the minimum AIC of -6305.5 .

7.3 Discussion

Figure 7.4 shows the fits for each value of p . For $p = 1$, we simply have an exponential distribution as expected, and its rate parameter is approximately 3.18. The distribution for $p = 2$ at first resembles the sum of two independent and identical exponentials, or an Erlang distribution with shape parameter equal to 2. In fact, looking at its estimated phase-type generator, it is very close:

$$\mathbf{T}_2 = \begin{pmatrix} -6.346 & 6.332 \\ 0 & -6.346 \end{pmatrix}. \quad (7.2)$$

The sum of two exponentials would have the same form, but have the top right-hand element equal to the negative of the diagonals.

We can also see that the fit gets better as p increase from 1 to 4, but that there is not much of a difference between the fits with $p = 4$ to $p = 6$. Maybe the most noticeable difference is in the behaviour near zero, where the fit with four phases differs slightly from the other two. The estimated phase-type generator of the fit with $p = 4$ is

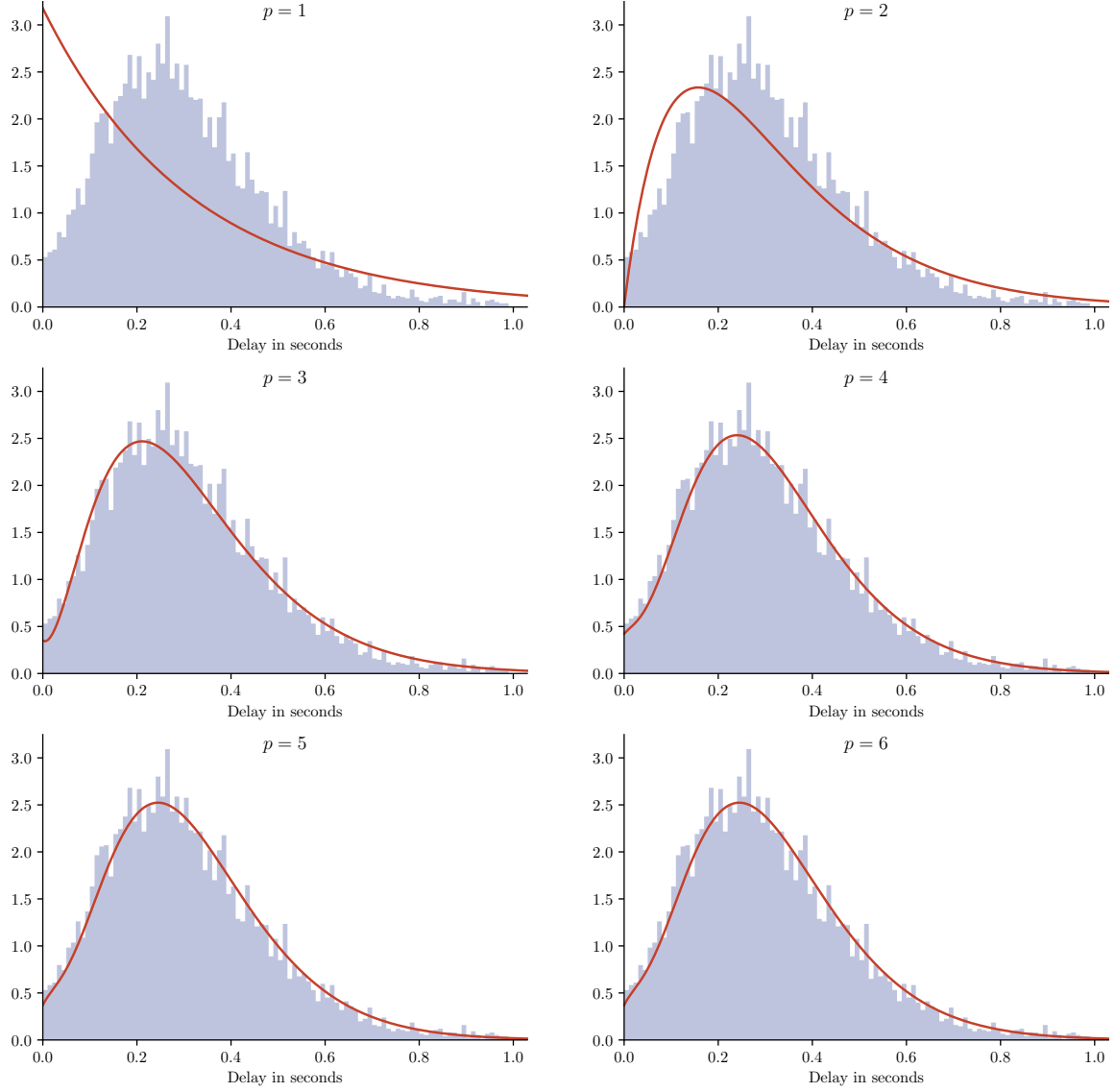


Figure 7.4: The phase-type distribution fits

$$\mathbf{T}_4 = \begin{pmatrix} -12.122 & 11.698 & 0 & 0 \\ 0 & -12.121 & 11.210 & 0 \\ 0 & 0 & -11.688 & 11.687 \\ 0 & 0 & 0 & -11.691 \end{pmatrix}. \quad (7.3)$$

The parameter estimates were equal for each run. We can now also see why the differential equations were stiff: there are several states that are almost instantaneous, where the underlying Markov chain resides for a very short amount of time before jumping into the next state.

7.3.1 Basic statistics

The mean of our final fit with four phases is 0.3148, and its variance is 0.0304, its mode is 0.2896, and its median is 0.2896. The 99-th percentile is at 0.832, which means that if the Bitcoin block

propagation delay in general followed this same distribution (discussed next), then 99 % of the nodes on the network would receive a new block within 0.832 seconds.

7.3.2 Interval-censoring and censoring of the tail

Another approach to fitting phase-type distributions to this data would have been to bin the values to intervals, say for each millisecond, then apply the interval-censored methods as in [33]. Given that our data had 7923 observations, binning would most likely not have made a big difference in computational speed, especially when the computationally intensive step was computed in parallel. However, when fitting to larger datasets with lower requirements for accuracy, binning could be a worthwhile.

As discussed earlier, we computed fits to only the bottom 98 % of the data, cutting out the tail. We could have included this data by treating it as right-censored and applying the methods in [44].

7.3.3 Interpretation as propagation delay

If we assume that the blocks that arrived first at Northern Virginia were mined close to Northern Virginia, and that the arrival time there is close to the time at which the block was mined, then one can interpret this fit as an approximation of the propagation delay between Northern Virginia and Sydney. However, it is not obvious why these assumptions should be true, and it is hard to justify and judge the extent to which this models real behaviour. We now propose a better way of interpreting the results through an extension of the model.

7.3.4 Further extensions

Consider now a single block and the arrival times of that block at each of the observational locations. We do not know the exact time at which this block was mined, but we can instead consider our observation as consisting of $\mathbf{X} = \mathbf{Y} - M\mathbf{1}$ where \mathbf{Y} is the vector of true propagation delays and $M = \min \mathbf{Y}$. Let us stay within our framework of phase-type distributions by assuming that the marginal distributions of \mathbf{Y} are phase-type distributed. This gives rise to two interesting models.

Assuming independence

Let us for a moment consider a simpler model and assume that the arrival times at each of the observational locations are independent and distributed identically. Then one can perform the computations in Appendix B for the conditional expectations, but conditioning instead on \mathbf{Y} and M . In fact, by the tower property of expectation, one can simply take the estimators for B_v , Z_v , N_{v0} and N_{vw} and condition on \mathbf{Y} and M . We then need to apply the law of total probability and integrate over all the values of the minimum, M . This gives a form similar to the standard E-step, but the expressions include a second integral. For instance, for the conditional expectation of B_v^l with respect to the observed times $\mathbf{X} = \mathbf{x}$, we get

$$\mathbb{E}(B_v^l | \mathbf{x}) = \int_{x^l}^{\infty} \mathbf{e}_v^{\top} e^{\mathbf{T}y} \mathbf{t} \pi_v \frac{\pi e^{\mathbf{T}(y-x^l)} \mathbf{t}}{\pi e^{\mathbf{T}y} \mathbf{t}} dy. \quad (7.4)$$

Here we are actually integrating with respect to y^l , but have dropped the superscript for brevity. Similarly, one can compute the other conditional expectations. For instance, for Z_v^l , we get

$$\mathbb{E}(Z_v^l | \mathbf{x}) = \int_{x^l}^{\infty} \int_0^{\infty} \mathbf{e}_v^{\top} e^{\mathbf{T}(y-u)\mathbf{t}} \boldsymbol{\pi} e^{\mathbf{T}u} \mathbf{e}_v du \frac{\boldsymbol{\pi} e^{\mathbf{T}(y-x^l)\mathbf{t}}}{\boldsymbol{\pi} e^{\mathbf{T}y\mathbf{t}}} dy. \quad (7.5)$$

It may be possible to compute these integrals numerically, from which one could then compute the maximum likelihood estimators for the parameters through an EM-algorithm as before. This would, however, be very computationally demanding, and we have not attempted to do so yet.

Multivariate phase-type distributions

An even better model would be to not assume independence of the marginals at all, but rather assume that \mathbf{Y} follows some kind of multivariate phase-type distribution.

Suppose \mathbf{Y} has n components. One idea would be to consider a Markov chain and choose n absorbing subsets of the state space, such that once the chain has entered one of these subsets it cannot escape. We then observe the times at which this Markov chain hits each of these n sets, giving rise to the multivariate distribution for \mathbf{Y} . We need the subsets to have a non-empty intersection for the marginals to be distributions. The marginal distributions are then all phase-type distributions. Furthermore, one can see that the fully independent case is a submodel of this construction, for instance by constructing the obvious Markov chain on the cartesian product of the state spaces of the marginal phase-type distributions. It would be very interesting to study the dependent, joint distribution of delays through this technique.

Part III

Exploratory Data Analysis and Further Questions

Chapter 8

Patterns in the dataset

In this part, we explore the dataset further through a non-rigorous exploratory data analysis. Through our research, we found several interesting patterns in the data that opened up a number of interesting questions, but have not yet embarked on exploring or explaining them in detail. We present some cursory thoughts and educated guesses on what might have caused them but attempt by no means a thorough study of them.

8.1 Inter-arrival times of blocks

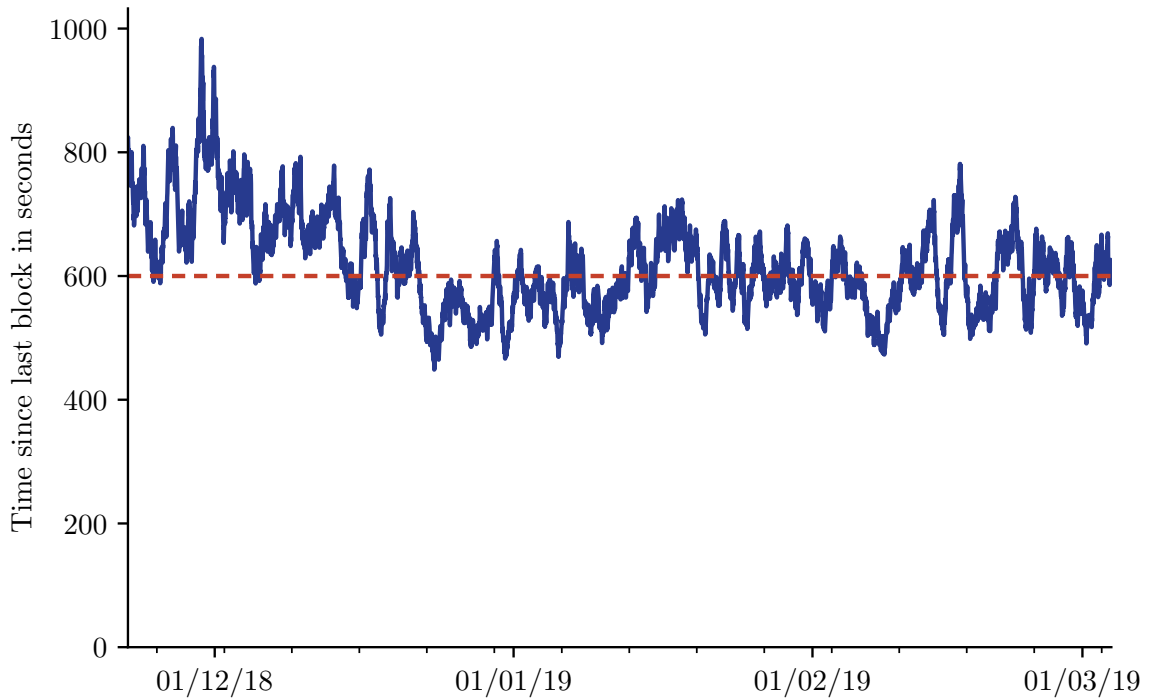


Figure 8.1: Daily rolling mean of inter-arrival times of blocks over the observed time period

As discussed in Section 2.2.3, the mining difficulty is adjusted about every two weeks to keep the time between block at approximately 10 minutes. Figure 8.1 shows our observed inter-arrival times, along with the objective of a 10 minute arrival time. In the first month of our experiment, the

inter-arrival times were on average higher than the 10 minute objective, then dipped for a few weeks below it, and then finally stayed at approximately 10 minutes for the rest of the experiment. One possible reason for these fluctuations is the exchange rate of Bitcoin, which dropped steadily from mid-November until mid-December, which would incentivise some miners to stop mining if their operation became unprofitable. Similarly, exchange rate increased again in the third week of December. When miners stop mining, the total computational power of the network decreases and blocks become more rare until the difficulty is adjusted to take this into account.

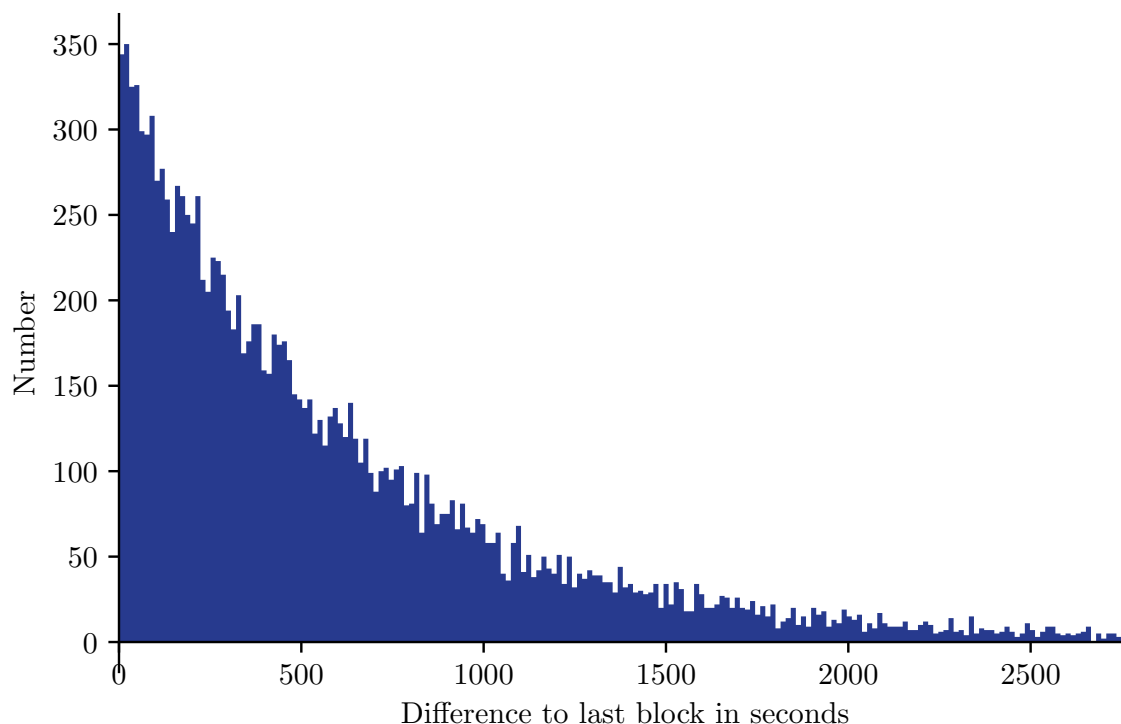


Figure 8.2: Distribution of inter-arrival times

A histogram of the inter-arrival times is shown in Figure 8.2. In the paper that introduce Bitcoin, Nakamoto argues that the arrival process should be a Poisson process [1] which would lead to exponential inter-arrival times. Our data fits to an exponential distribution with a mean of 606.2 quite well. Bowden et al. however argue in [2] that this process is in fact not a Poisson process, and present a refined model. We did not investigate how the arrival times fit to this model.

8.2 Difference between timestamp in the block header and the arrival time

Figure 8.3 shows a histogram of the difference between the arrival time of a block and the timestamp in the block header for each observed block. The Bitcoin protocol does not enforce strict rules on the timestamp, such as requiring it to be in the past; however, there are some restrictions on how far it can deviate from the median of previous blocks.

The majority of these differences are positive, meaning that the timestamp in the block header is before the time at which we observed it. However, the magnitude of the difference is much higher than what seems plausible under propagation delay. One explanation for this is if the mining pools require

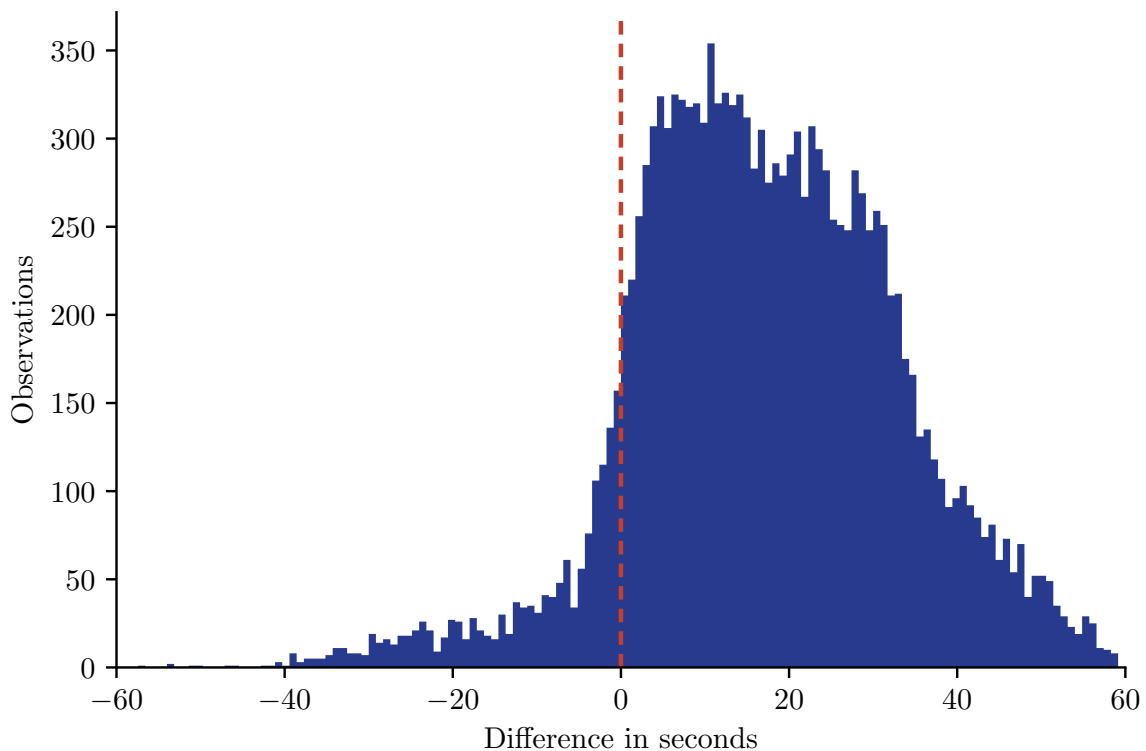


Figure 8.3: Time difference between observed arrival time and the timestamp in block header

their miners to mine on the exact block template that has been sent by the pool, but recompute and circulate a new block template infrequently. This would mean that the timestamp would only be updated occasionally, leading to the observed behaviour of a large number of positive differences. However, it is not clear why the timestamp wouldn't be updated by miners in the pool independently.

It seems that it would be advantageous for mining pools to claim that blocks are mined further apart than they really are in order to have the mining difficulty adjusted to be easier, hence giving them higher rewards. However, this would cause a runaway effect where the “clock” of the blockchain would forever have to advance faster than time in the real world. Although it seems that miners do not do this, it may be that some miners include a timestamp in the future (giving a negative difference in the graphs) in order to balance this out.

8.3 Empty and full blocks, size and weight

The weight of a block is a measurement of the size of the block, which accounts normal transactions and SegWit transactions separately (see Section 2.2.7). In this section, we define a block as empty if its weight is less than 50 thousand bytes, or 1.25 % of the maximum weight, which is four million weight units. Similarly, we define a block as full if its size is no more than 50 thousand bytes from the maximum weight limit, in other words, over 98.75 % full. Figure 8.4 shows the proportion of full blocks, empty blocks, and those that are neither full nor empty. Empty blocks are discussed later along with mining pools.

Blocks that are neither full nor empty seem to have an approximately uniform distribution. We do not know why some miners create partially full blocks. An explanation for this would be if the Bitcoin system processed all transactions and the memory pool was empty; however the network has

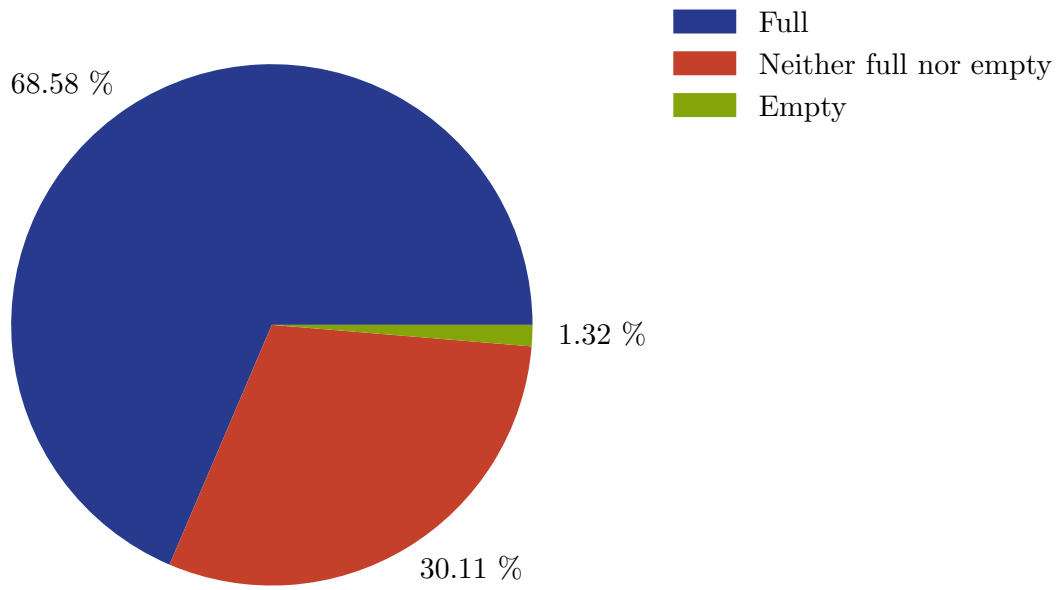


Figure 8.4: Proportion of full blocks, empty blocks, and blocks that are partially full

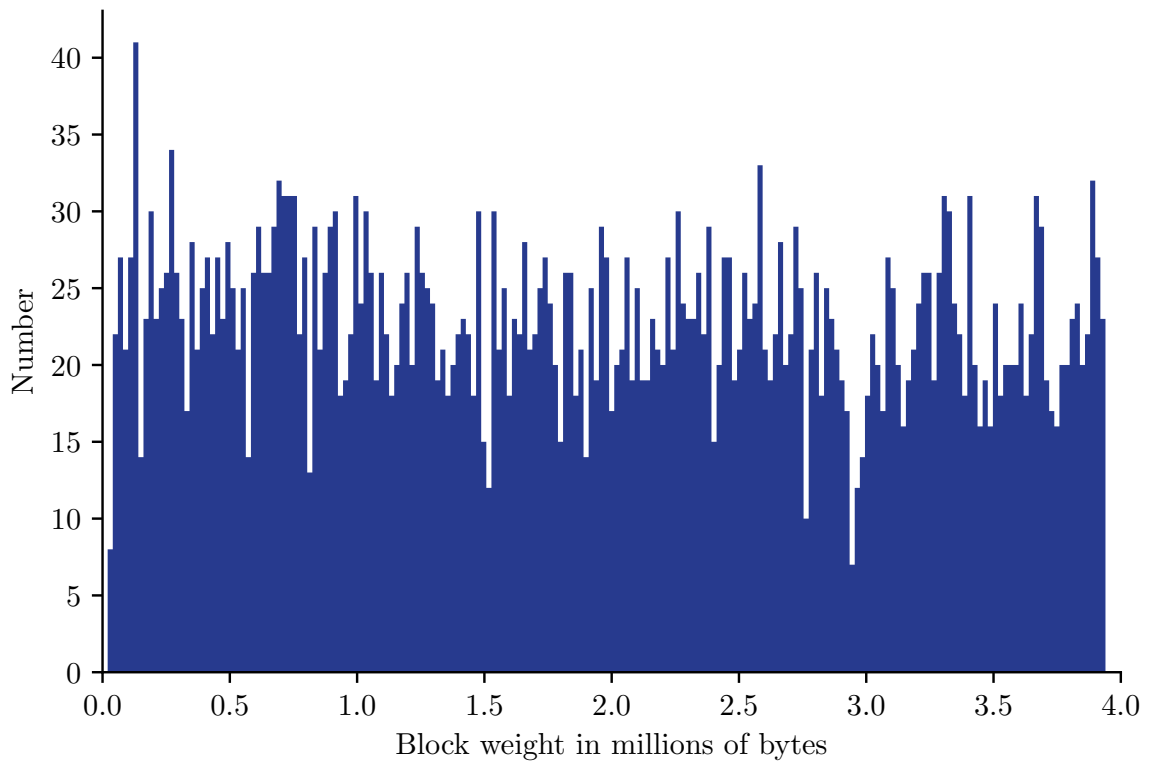


Figure 8.5: Distribution of block weights for blocks that are neither full nor empty

been overloaded with transactions for several years now.

8.4 Block size and number of transactions

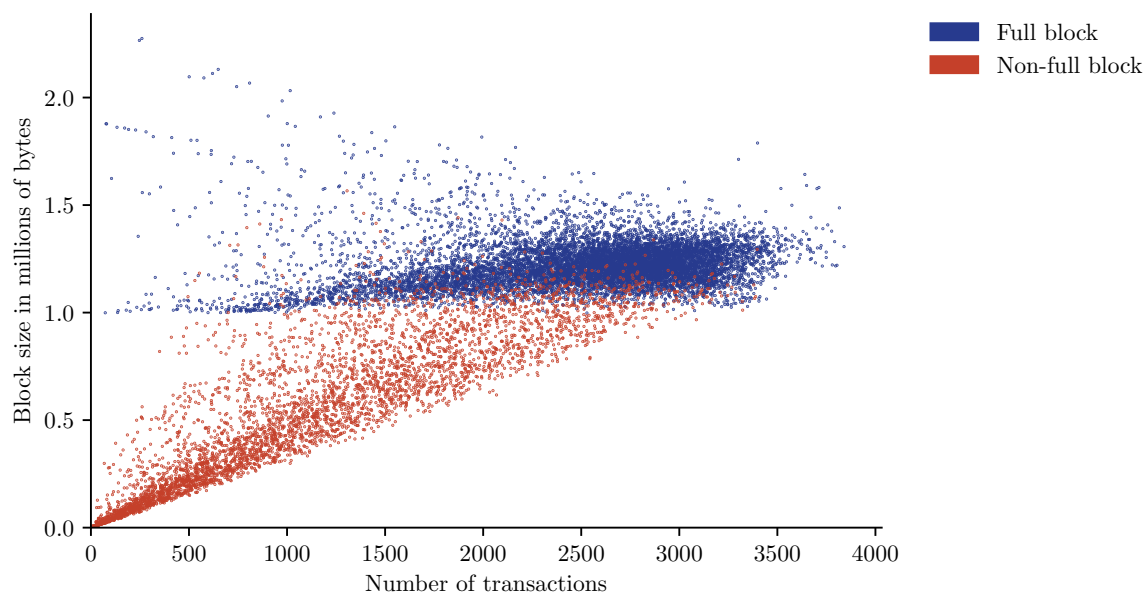


Figure 8.6: Number of transactions versus actual block size

Figure 8.6 shows a figure of the number of transactions in a block versus its size. Blocks with a block size larger than one million bytes contain witness data, which is not counted in the block size limit equally, as discussed in Section 2.2.7. Non-full blocks show the expected trend of increasing size with number of transactions. Transactions can be of different sizes, so this is not an exact linear relationship. The majority of full blocks show a slight linear trend in size increasing from about 1 to 1.3 million bytes as the number of transactions increases. This linear trend could be explained by a constant proportion of SegWit transactions.

The full blocks with only a few transactions, but with a large size are caused by very large SegWit transactions. Those transactions close to one million bytes in size are large non-SegWit transactions. Large transactions involve a large number of inputs and outputs, moving Bitcoins between very many different addresses, but are all bundled in a single transaction. Such large transactions are sometimes used by entities to obscure the origin of Bitcoins, akin to laundering money, often as a part of a “coin laundry” service. A large transaction pools all the Bitcoins to be spent together (inputs), and then splits them apart into all the outgoing addresses (outputs), without pairing inputs and outputs together. This makes it very difficult to determine which addresses moved Bitcoins to which addresses.

8.5 Empty blocks and mining pools

Figure 8.7 shows the percentage of blocks that each pool mined that were empty. According to [62], mining pools mine empty blocks during the time it takes them to validate the new block and create a new block template. There are three delays associated with this: the first is the time it takes for the mining pool’s control node to receive a new block in full after first receiving only the block header. The second is the processing delay taken to validate the new block, remove the transactions in that block from the memory pool of the control node, and create a new block template to mine on. The third delay is the time it takes for that mining pool to distribute a new block template to its mining

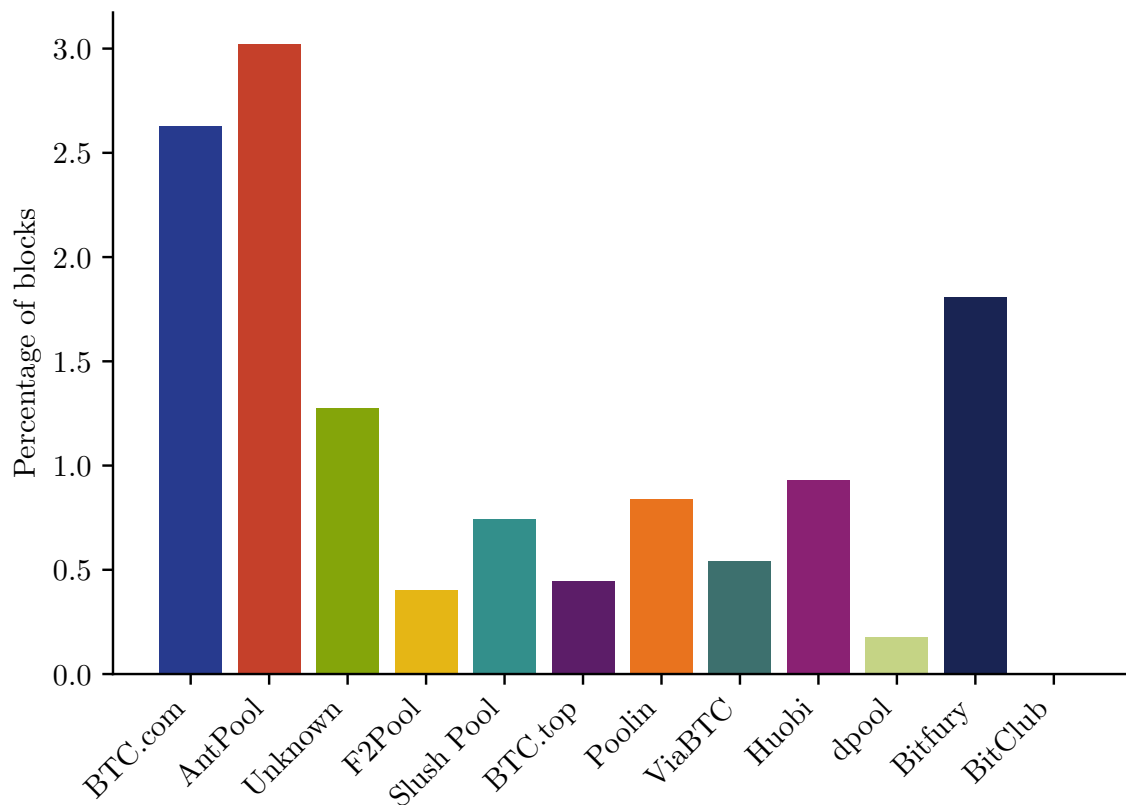


Figure 8.7: Percentage of empty blocks by each mining pool

hardware and miners.

Most pools are open to the public: a miner downloads the software, then connects to the mining pool that sends it the header of a block template to mine on. It would seem plausible that this software were itself connected to the Bitcoin network, and could be programmed to start mining on an empty block (which it could easily construct independently without needing a copy of the whole blockchain) as soon as it observed a block header whose hash was correct. Independently of this, when the mining pool operator would learn about the new block, they would construct a new header and distribute it to all miners. Furthermore, this would remove the need for the miner and mining pool operator to have a low latency connection. This hypothesis is supported by the fact that BTC.com and AntPool are both very large pools open to the public, which presumably have a large number of miners distributed over large geographical areas. F2Pool on the other hand, which has a small percentage of empty blocks, is a small Chinese miner which is concentrated in a small geographical area. The large, distributed pools have a large number of empty blocks, whereas the small, concentrated pool has a low number of empty blocks.

8.6 Causes of delay

We attempted to explore the causes of propagation delay. To do this, we restricted ourselves to the blocks that were first observed at Northern Virginia. We then computed the median time at which each of the roughly 700 peers of the Northern Virginia observational location relayed the block to the observational node. There are two reasons for using the median: the first is that the distribution is

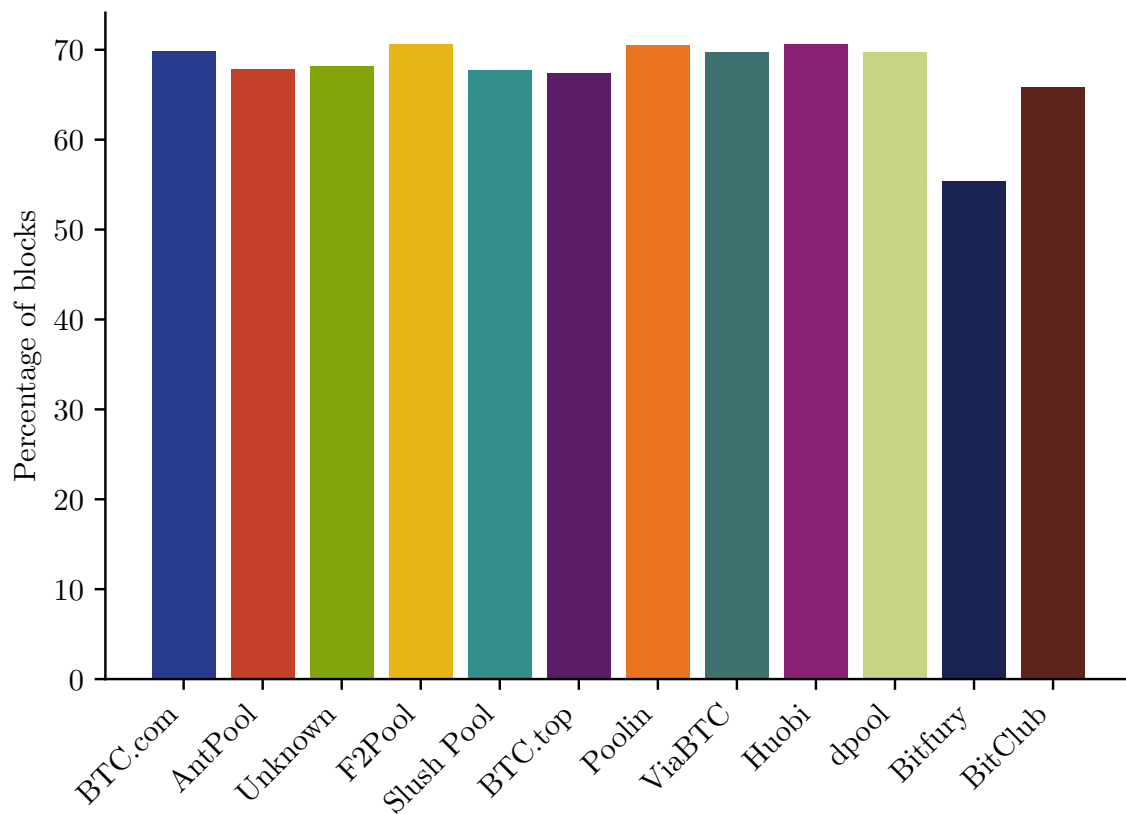


Figure 8.8: Percentage of full blocks by each mining pool

heavy tailed, so using the median is a better estimate of the centre than the mean. Secondly, the median of the times it takes for a set of nodes to receive a block can be conveniently interpreted as the time it takes for half of those nodes to reach consensus on the current state of the chain.

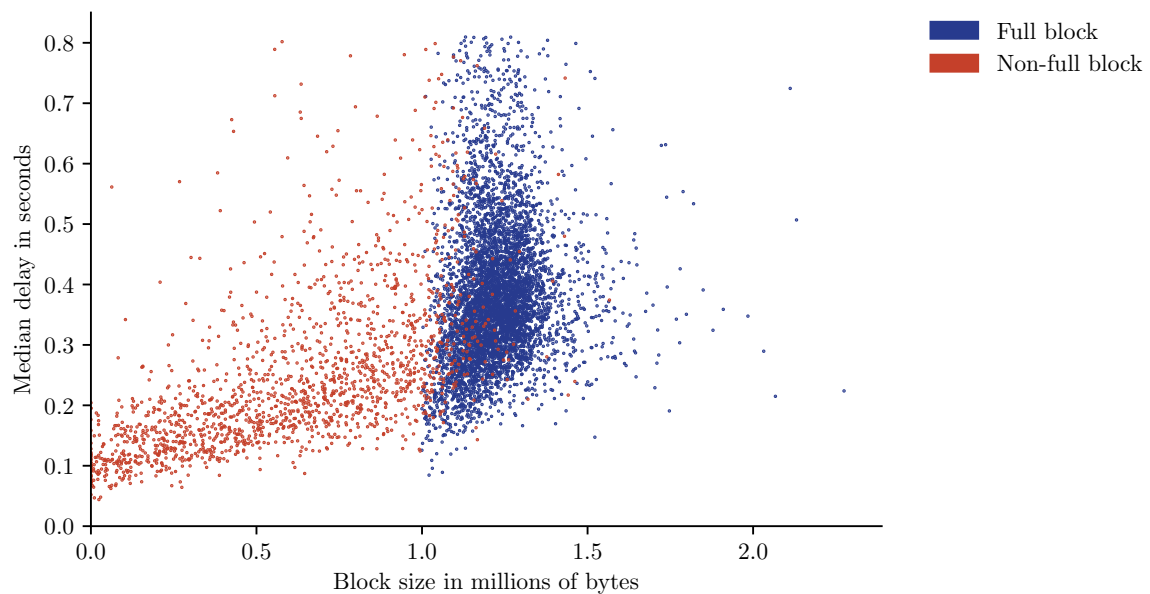


Figure 8.9: Block size versus median delay of blocks

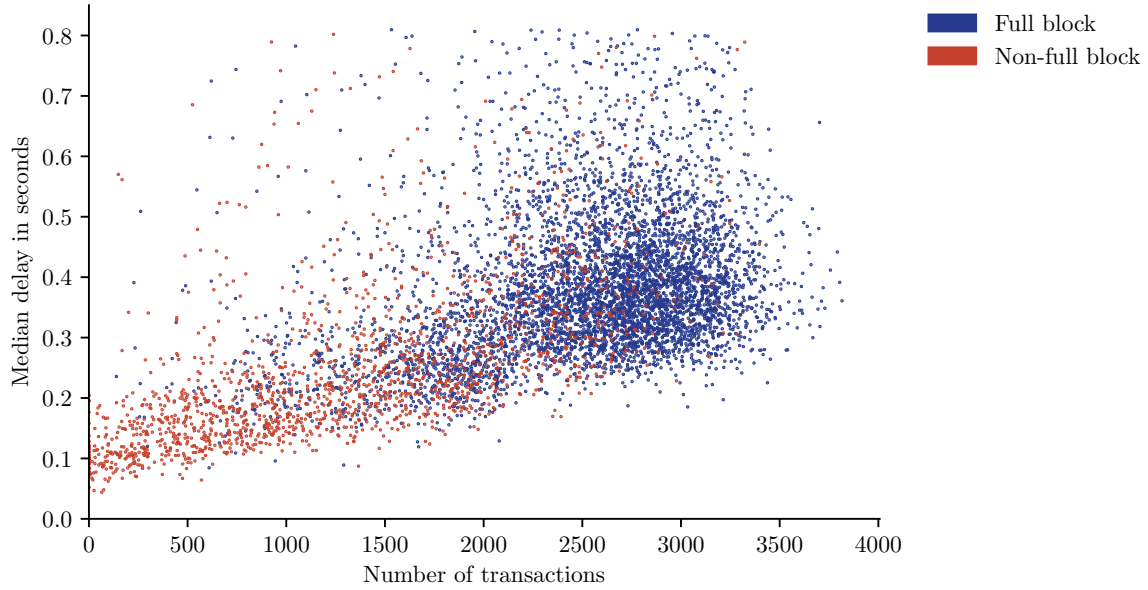


Figure 8.10: Number of transactions versus median delay of blocks

Figure 8.9 shows this median as a function of the size of the block, and Figure 8.10 shows it as a function of the number of transactions in the block. Note that the size and number of transactions in a block are related, as discussed in Section 8.4.

The first figure does not seem to have a very clear trend, except that larger blocks take longer to propagate. On the contrary, the latter figure shows a much clearer trend, and it seems that the delay increases linearly with the number of transactions.

There are generally two sources of propagation delay: the network delay between nodes, and the processing delay. The former is the time taken to relay the block from one node to another and latter is the time it takes for a node to verify that a block header and all the transactions in that block are valid.

These graphs seem to support the hypothesis that propagation delay is not caused by network delays, but rather by processing delays, and in particular, in verifying transactions. One of the most intensive computational steps in verifying a transaction is the verification of the cryptographic signature within it. It would be interesting to compute the number of signatures to be verified in each block, and plot these against the median delay, as each transaction does not always the same number of signatures.

8.7 Delay and location

Figure 8.12 shows the total number of peers per country from whom we received block messages from.

We were interested in the role of geography on the propagation delay. We first computed for each message the delay between that message and the first time we received a message about that particular block. We then computed the median of this delay for each node. We removed nodes with less than 10 messages. Finally, we performed a reverse geo-location based on the IP address of each node and took the median of the values for each node in a country. Figure 8.13 shows this; note the exponential scale. Figure 8.14 shows a histogram of all of these median delays. These are not necessarily good measures summaries of the distribution of propagation delays, as the observations

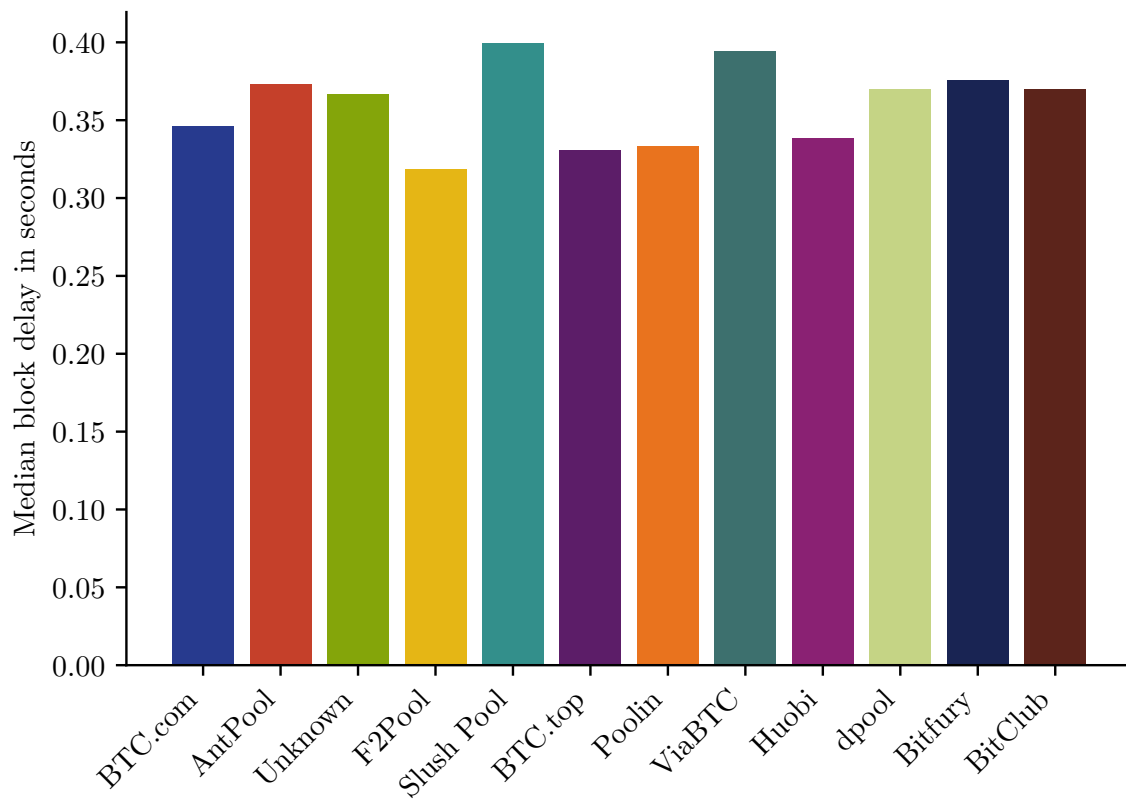


Figure 8.11: Median block delay for each mining pool

are heavily dependent.

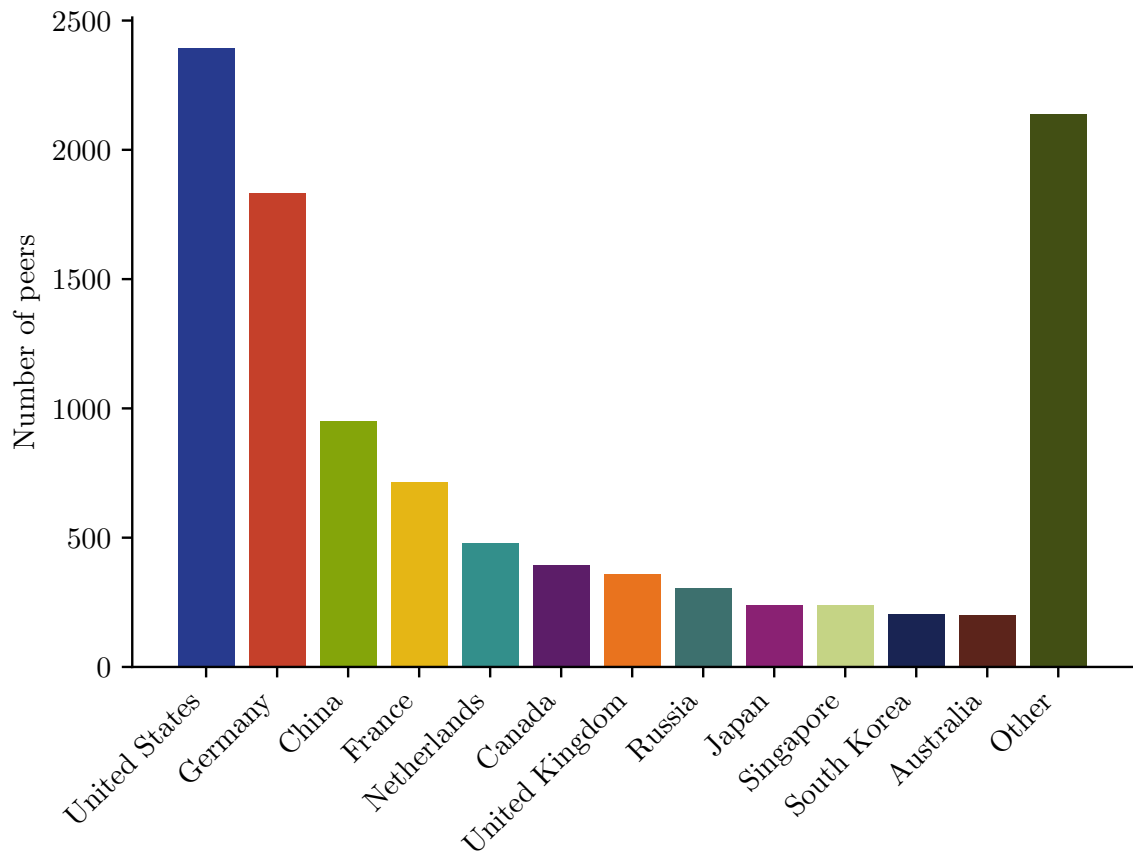


Figure 8.12: Number of peers per country

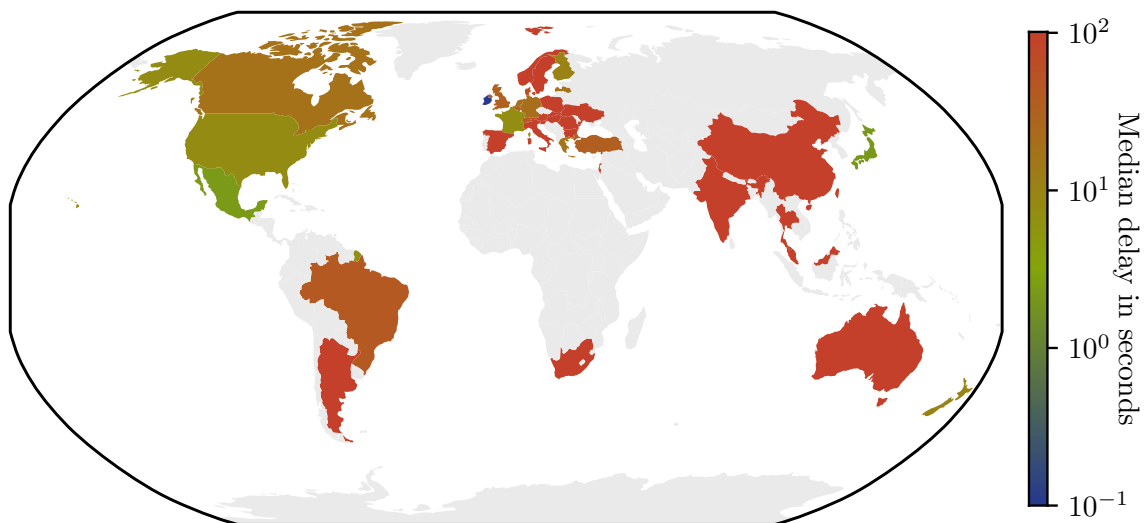


Figure 8.13: Map of median delay by country

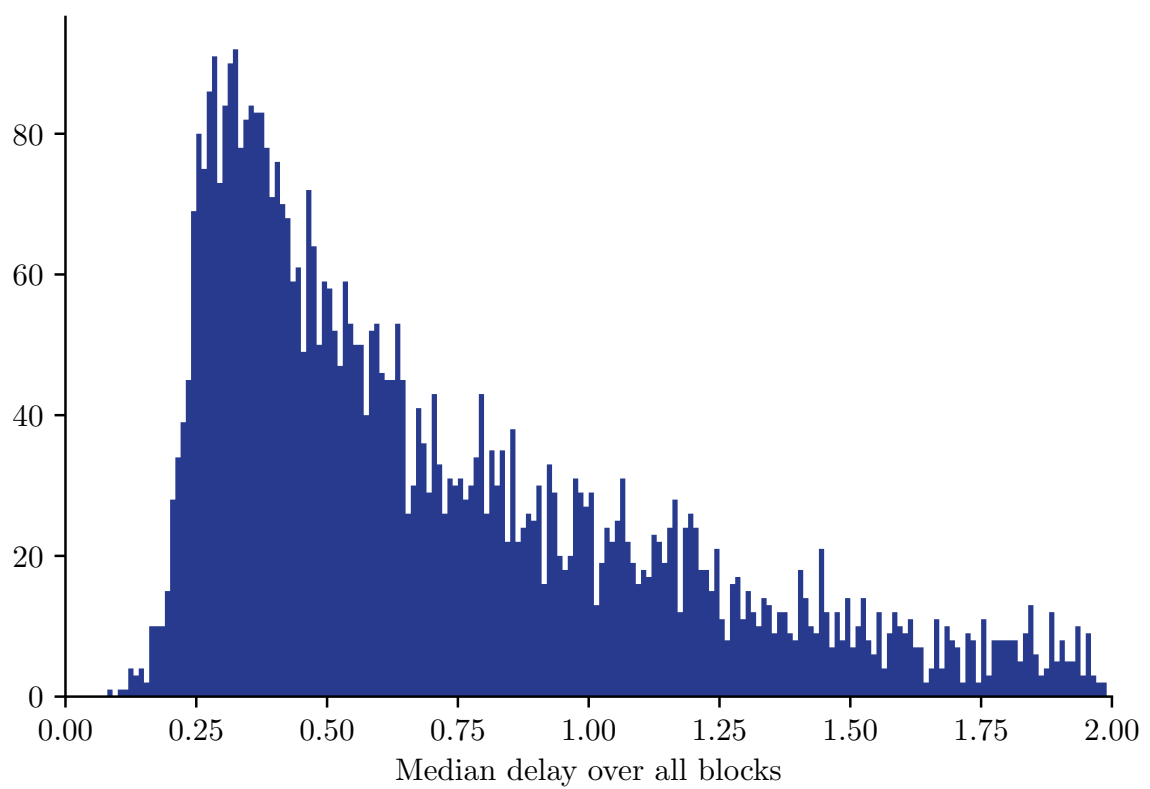


Figure 8.14: Histogram of median delay for nodes

Conclusion

In this thesis, we explored aspects of blockchain technology by studying the block propagation process of Bitcoin. We created a tool and built a globally distributed data collection system to observe the block propagation patterns of blocks on the network. We then used the EM-algorithm to fit phase-type distributions onto a subset of the data. We discussed model selection and the quality of the fits, along with further mathematical extensions to the method for more accurate models. Finally, we presented an exploratory data analysis of some of the data to shed some light on the patterns within it and to open up further questions.

We made three contributions: an open dataset of cleaned, pre-processed Bitcoin network data with covariates extracted from the blockchain; a phase-type model for the block propagation delay; and an improvement to the implementation of the EM-algorithm in [33] for large datasets. The data, source code, and some additional complementary material is available on the accompanying website at <https://bitcoin.aapeliuorinen.com/>.

Part IV

Appendices

Appendix A

Maximum likelihood estimators for transition rates and initialisation probabilities of a Markov chain

Our complete likelihood function is given in Equation 5.26,

$$\mathcal{L}_c(\boldsymbol{\pi}, \mathbf{T}) = \prod_{v=1}^p \pi_v^{B_v} \prod_{v=1}^p e^{T_{vv} Z_v} \prod_{v=1}^p \prod_{\substack{w=0 \\ w \neq v}}^p T_{vw}^{N_{vw}}. \quad (\text{A.1})$$

Therefore our complete log-likelihood, say ℓ_c , is given by

$$\ell_c(\boldsymbol{\pi}, \mathbf{T}) = \sum_{v=1}^p B_v \log \pi_v + \sum_{v=1}^p T_{vv} Z_v + \sum_{v=1}^p \sum_{\substack{w=0 \\ w \neq v}}^p N_{vw} \log T_{vw} \quad (\text{A.2})$$

$$= \sum_{v=1}^p B_v \log \pi_v + \sum_{v=1}^p \sum_{\substack{w=0 \\ w \neq v}}^p (N_{vw} \log T_{vw} - Z_v T_{vw}). \quad (\text{A.3})$$

Note that $\boldsymbol{\pi}$ and \mathbf{T} are decoupled in this equation, so it suffices to maximise with respect to each variable individually. Computing first the derivative with respect to T_{vw} for $v = 1, \dots, p$, $w = 0, \dots, p$ with $v \neq w$, we get

$$\frac{\partial \ell_c(\boldsymbol{\pi}, \mathbf{T})}{\partial T_{vw}} = \frac{N_{vw}}{T_{vw}} - Z_v. \quad (\text{A.4})$$

When this derivative vanishes, we have

$$T_{vw} = \frac{N_{vw}}{Z_v}. \quad (\text{A.5})$$

We then need to find a probability vector $\boldsymbol{\pi}$ that maximises $\sum_{v=1}^p B_v \log \pi_v$, subject to the probability constraint, $\sum_{v=1}^p \pi_v = 1$. For this, let ψ be a Lagrange multiplier, and consider

$$\mathcal{L}(\boldsymbol{\pi}, \mathbf{B}, \psi) = \sum_{v=1}^p B_v \log \pi_v - \psi \left(\sum_{v=1}^p \pi_v - 1 \right). \quad (\text{A.6})$$

The derivatives are given by

$$\frac{\partial \mathcal{L}(\boldsymbol{\pi}, \mathbf{B}, \psi)}{\partial \pi_v} = \frac{B_v}{\pi_v} - \psi, \quad \frac{\partial \mathcal{L}(\boldsymbol{\pi}, \mathbf{B}, \psi)}{\partial \psi} = 1 - \sum_{v=1}^p \pi_v. \quad (\text{A.7})$$

Setting these to zero, and solving the linear system of equations gives us

$$\pi_v = \frac{B_v}{n}. \quad (\text{A.8})$$

Furthermore, all second order derivatives vanish except for

$$\frac{\partial^2 \ell_c(\boldsymbol{\pi}, \mathbf{T})}{\partial T_{vw}^2} = -N_{vw} T_{vw}^{-2}, \quad \frac{\partial^2 \ell_c(\boldsymbol{\pi}, \mathbf{T})}{\partial \pi_v} = -B_v \pi_v^{-2}. \quad (\text{A.9})$$

These are both negative, and so the solution is a maximiser. Therefore, for $v = 1, \dots, p$, and $w = 0, \dots, p$, $v \neq w$, the maximum likelihood estimators are given by

$$\hat{\pi}_v = \frac{B_v}{n}, \quad \hat{T}_{vw} = \frac{N_{vw}}{Z_v}, \quad \hat{T}_{vv} = - \sum_{w=0}^p \hat{T}_{vw}. \quad (\text{A.10})$$

Appendix B

Computation of conditional expectations

Consider a single realisation of the absorption time $Y = y$ arising from a phase-type distribution with parameters $(\boldsymbol{\pi}, \mathbf{T})$, and let J_u be the state of the underlying continuous time Markov chain at time u . We drop the extra superscripts and subscripts for clarity. First compute the conditional expectation of B_v :

$$\mathbb{E}(B_v \mid y) = \mathbb{P}(J_0 = v \mid Y = y) \quad (\text{B.1})$$

$$= \frac{\mathbb{P}(J_0 = v, Y \in dy)}{\mathbb{P}(Y \in dy)} \quad (\text{B.2})$$

$$= \frac{\mathbb{P}(Y \in dy \mid J_0 = v) \mathbb{P}(J_0 = v)}{\mathbb{P}(Y \in dy)} \quad (\text{B.3})$$

$$= \frac{\mathbf{e}_v^\top e^{\mathbf{T}y} \mathbf{t} \pi_v}{\boldsymbol{\pi} e^{\mathbf{T}y} \mathbf{t}}. \quad (\text{B.4})$$

Similarly, we compute

$$\mathbb{E}(Z_v \mid y) = \mathbb{E}\left(\int_0^y \mathbf{1}_{\{J_u=v\}} du \mid y\right) \quad (\text{B.5})$$

$$= \int_0^y \mathbb{E}(\mathbf{1}_{\{J_u=v\}} \mid y) du \quad (\text{B.6})$$

$$= \int_0^y \mathbb{P}(J_u = v \mid Y = y) du \quad (\text{B.7})$$

$$= \int_0^y \frac{\mathbb{P}(Y \in dy \mid J_u = v) \mathbb{P}(J_u = v)}{\mathbb{P}(Y \in dy)} du \quad (\text{B.8})$$

$$= \int_0^y \frac{\mathbf{e}_v^\top e^{\mathbf{T}(y-u)} \mathbf{t} \boldsymbol{\pi} e^{\mathbf{T}u} \mathbf{e}_v}{\boldsymbol{\pi} e^{\mathbf{T}y} \mathbf{t}} du. \quad (\text{B.9})$$

Here we may interchange the integral and expectation as the integrand is non-negative. Before embarking on the most difficult task of computing the conditional expectation of N_{vw} , let us compute the easier conditional expectation of N_{v0} :

$$\mathbb{E}(N_{v0} \mid y) = \mathbb{P}(J_{y-} = v \mid Y = y) \quad (\text{B.10})$$

$$= \frac{\mathbb{P}(Y \in dy \mid J_{y-} = v) \mathbb{P}(J_{y-} = v)}{\mathbb{P}(Y \in dy)} \quad (\text{B.11})$$

$$= \frac{t_v \boldsymbol{\pi} e^{\mathbf{T}y} \mathbf{e}_v}{\boldsymbol{\pi} e^{\mathbf{T}y} \mathbf{t}}. \quad (\text{B.12})$$

Finally we compute the conditional expectation of N_{vw} . Consider first an approximation N_{vw}^ε to this random variable for $\varepsilon > 0$ where we count the number of jumps from v to w at consecutive windows of size ε . We have

$$\mathbb{E}(N_{vw}^\varepsilon \mid y) = \mathbb{E}\left(\sum_{k=0}^{\lfloor y/\varepsilon \rfloor - 1} \mathbf{1}_{\{J_{k\varepsilon}=v, J_{(k+1)\varepsilon}=w\}} \mid y\right) \quad (\text{B.13})$$

$$= \sum_{k=0}^{\lfloor y/\varepsilon \rfloor - 1} \frac{\mathbb{P}(J_{k\varepsilon} = v, J_{(k+1)\varepsilon} = w, Y \in dy)}{\mathbb{P}(Y \in dy)} \quad (\text{B.14})$$

$$= \sum_{k=0}^{\lfloor y/\varepsilon \rfloor - 1} \frac{\mathbb{P}(Y \in dy \mid J_{(k+1)\varepsilon} = w) \mathbb{P}(J_{(k+1)\varepsilon} = w \mid J_{k\varepsilon} = v) \mathbb{P}(J_{k\varepsilon} = v)}{\mathbb{P}(Y \in dy)} \quad (\text{B.15})$$

$$= \sum_{k=0}^{\lfloor y/\varepsilon \rfloor - 1} \frac{\mathbf{e}_w^\top e^{\mathbf{T}(y-(k+1)\varepsilon)} \mathbf{t} \mathbf{e}_v^\top e^{\mathbf{T}\varepsilon} \mathbf{e}_w \boldsymbol{\pi} e^{\mathbf{T}k\varepsilon} \mathbf{e}_v}{\boldsymbol{\pi} e^{\mathbf{T}y} \mathbf{t}} \quad (\text{B.16})$$

$$= \frac{1}{\boldsymbol{\pi} e^{\mathbf{T}y} \mathbf{t}} \sum_{k=0}^{\lfloor y/\varepsilon \rfloor - 1} \varepsilon \mathbf{e}_w^\top e^{\mathbf{T}(y-(k+1)\varepsilon)} \mathbf{t} \mathbf{e}_v^\top \left(\frac{e^{\mathbf{T}\varepsilon} - \mathbf{I}}{\varepsilon} \right) \mathbf{e}_w \boldsymbol{\pi} e^{\mathbf{T}k\varepsilon} \mathbf{e}_v. \quad (\text{B.17})$$

In the last step we used the fact that $v \neq w$ so $\mathbf{e}_v^\top \mathbf{e}_w = 0$, and we have added nothing to the equation. Now $e^{\mathbf{T}u}$ is continuous, and we have

$$\lim_{\varepsilon \rightarrow 0^+} \frac{e^{\mathbf{T}\varepsilon} - \mathbf{I}}{\varepsilon} = \mathbf{T}. \quad (\text{B.18})$$

Combining these and interpreting the conditional expectation as an approximation of the Riemann integral, we have as ε vanishes that

$$\mathbb{E}(N_{vw}^\varepsilon \mid y) \rightarrow \frac{1}{\boldsymbol{\pi} e^{\mathbf{T}y} \mathbf{t}} \int_0^y \mathbf{e}_w^\top e^{\mathbf{T}(y-u)} \mathbf{t} T_{vw} \boldsymbol{\pi} e^{\mathbf{T}u} \mathbf{e}_v du. \quad (\text{B.19})$$

Since this approximation is bounded above by N_{vw} and $N_{vw}^\varepsilon \rightarrow N_{vw}$ almost surely, we conclude by the dominated convergence theorem for conditional expectation that

$$\mathbb{E}(N_{vw} \mid y) = \frac{T_{vw}}{\boldsymbol{\pi} e^{\mathbf{T}y} \mathbf{t}} \int_0^y \mathbf{e}_w^\top e^{\mathbf{T}(y-u)} \mathbf{t} \boldsymbol{\pi} e^{\mathbf{T}u} \mathbf{e}_v du. \quad (\text{B.20})$$

Collating these results together gives us the conditional expectations

$$\mathbb{E}(B_v \mid y) = \frac{\pi_v \mathbf{e}_v^\top e^{\mathbf{T}y} \mathbf{t}}{\boldsymbol{\pi} e^{\mathbf{T}y} \mathbf{t}}, \quad (\text{B.21})$$

$$\mathbb{E}(Z_v \mid y) = \frac{1}{\boldsymbol{\pi} e^{\mathbf{T}y} \mathbf{t}} \int_0^y \mathbf{e}_v^\top e^{\mathbf{T}(y-u)} \mathbf{t} \boldsymbol{\pi} e^{\mathbf{T}u} \mathbf{e}_v du, \quad (\text{B.22})$$

$$\mathbb{E}(N_{v0} \mid y) = \frac{\boldsymbol{\pi} e^{\mathbf{T}y} \mathbf{e}_v t_v}{\boldsymbol{\pi} e^{\mathbf{T}y} \mathbf{t}}, \quad (\text{B.23})$$

$$\mathbb{E}(N_{vw} \mid y) = \frac{T_{vw}}{\boldsymbol{\pi} e^{\mathbf{T}y} \mathbf{t}} \int_0^y \mathbf{e}_w^\top e^{\mathbf{T}(y-u)} \mathbf{t} \boldsymbol{\pi} e^{\mathbf{T}u} \mathbf{e}_v du. \quad (\text{B.24})$$

Finally, to write them in cleaner form, define the matrix-valued function

$$\boldsymbol{\Gamma}(y \mid \boldsymbol{\pi}, \mathbf{T}) = \int_0^y e^{\mathbf{T}(y-u)} \mathbf{t} \boldsymbol{\pi} e^{\mathbf{T}u} du. \quad (\text{B.25})$$

Then our conditional expectations take the form

$$\mathbb{E}(B_v \mid y) = \frac{\pi_v \mathbf{e}_v^\top e^{\mathbf{T}y} \mathbf{t}}{\boldsymbol{\pi} e^{\mathbf{T}y} \mathbf{t}}, \quad (\text{B.26})$$

$$\mathbb{E}(Z_v \mid y) = \frac{\Gamma_{vv}(y \mid \boldsymbol{\pi}, \mathbf{T})}{\boldsymbol{\pi} e^{\mathbf{T}y} \mathbf{t}}, \quad (\text{B.27})$$

$$\mathbb{E}(N_{v0} \mid y) = \frac{\boldsymbol{\pi} e^{\mathbf{T}y} \mathbf{e}_v t_v}{\boldsymbol{\pi} e^{\mathbf{T}y} \mathbf{t}}, \quad (\text{B.28})$$

$$\mathbb{E}(N_{vw} \mid y) = \frac{T_{vw} \Gamma_{vw}(y \mid \boldsymbol{\pi}, \mathbf{T})}{\boldsymbol{\pi} e^{\mathbf{T}y} \mathbf{t}}. \quad (\text{B.29})$$

Appendix C

Computations for the integral Γ as the exponential of a block matrix

Define

$$\Gamma(y \mid \boldsymbol{\pi}, \mathbf{T}) = \int_0^y e^{\mathbf{T}(y-u)} \mathbf{t}\boldsymbol{\pi} e^{\mathbf{T}u} du, \quad (\text{C.1})$$

$$\mathbf{B} = \begin{pmatrix} \mathbf{T} & \mathbf{t}\boldsymbol{\pi} \\ \mathbf{0} & \mathbf{T} \end{pmatrix}. \quad (\text{C.2})$$

We wish to show that

$$e^{\mathbf{B}y} = \begin{pmatrix} e^{\mathbf{T}y} & \Gamma(y \mid \boldsymbol{\pi}, \mathbf{T}) \\ \mathbf{0} & e^{\mathbf{T}y} \end{pmatrix}. \quad (\text{C.3})$$

Firstly, by writing out the Taylor series expansion defining the matrix exponential (see Definition 7), we can easily verify that the diagonal blocks of $e^{\mathbf{B}y}$ are equal to $e^{\mathbf{T}y}$, and the bottom left block is zero. Let the remaining top right block be $\mathbf{G}(y)$, we then have

$$\frac{\partial}{\partial y} e^{\mathbf{B}y} = \mathbf{B} e^{\mathbf{B}y} \quad (\text{C.4})$$

$$= \begin{pmatrix} \mathbf{T} & \mathbf{t}\boldsymbol{\pi} \\ \mathbf{0} & \mathbf{T} \end{pmatrix} \begin{pmatrix} e^{\mathbf{T}y} & \mathbf{G}(y) \\ \mathbf{0} & e^{\mathbf{T}y} \end{pmatrix} \quad (\text{C.5})$$

$$= \begin{pmatrix} \mathbf{T}e^{\mathbf{T}y} & \mathbf{T}\mathbf{G} + \mathbf{t}\boldsymbol{\pi}e^{\mathbf{T}y} \\ \mathbf{0} & \mathbf{T}e^{\mathbf{T}y} \end{pmatrix}. \quad (\text{C.6})$$

Apply the Leibniz integral rule to $\Gamma(y \mid \boldsymbol{\pi}, \mathbf{T})$, to get

$$\frac{\partial}{\partial y} \Gamma(y \mid \boldsymbol{\pi}, \mathbf{T}) = \mathbf{t}\boldsymbol{\pi} e^{\mathbf{T}y} + \mathbf{T} \int_0^y e^{\mathbf{T}(y-u)} \mathbf{t}\boldsymbol{\pi} e^{\mathbf{T}u} du \quad (\text{C.7})$$

$$= \mathbf{t}\boldsymbol{\pi} e^{\mathbf{T}y} + \mathbf{T} \Gamma(y \mid \boldsymbol{\pi}, \mathbf{T}). \quad (\text{C.8})$$

Recall from Theorem 8 that the matrix exponential, $e^{\mathbf{B}y}$ may be computed as the unique solution $\mathbf{X}(y)$ to the equation $\frac{\partial}{\partial y}\mathbf{X}(y) = \mathbf{B}y$ with initial condition $\mathbf{X}(0) = \mathbf{I}$.

Combining this with the fact that $\mathbf{\Gamma}(0 \mid \boldsymbol{\pi}, \mathbf{T}) = \mathbf{0}$, we have that $\mathbf{\Gamma}(y \mid \boldsymbol{\pi}, \mathbf{T})$ satisfies the ordinary differential equation arising from the top right-hand block of $e^{\mathbf{B}y}$. Therefore, we have $\mathbf{G}(y) = \mathbf{\Gamma}(y \mid \boldsymbol{\pi}, \mathbf{T})$, and so Equation C.3 holds, as required.

Bibliography

- [1] Satoshi Nakamoto. Bitcoin: A peer-to-peer electronic cash system. 2009.
- [2] R. Bowden, H. P. Keeler, A. E. Krzesinski, and P. G. Taylor. Block arrivals in the Bitcoin blockchain. *arXiv e-prints*, page arXiv:1801.07447, Jan 2018.
- [3] Pierre Goffard. Fraud risk assessment within blockchain transactions. 2018.
- [4] Ittay Eyal and Emin Gün Sirer. Majority is not enough: Bitcoin mining is vulnerable. In Nicolas Christin and Reihaneh Safavi-Naini, editors, *Financial Cryptography and Data Security*, pages 436–454, Berlin, Heidelberg, 2014. Springer Berlin Heidelberg.
- [5] J. Göbel, H.P. Keeler, A.E. Krzesinski, and P.G. Taylor. Bitcoin blockchain dynamics: The selfish-mine strategy in the presence of propagation delay. *Performance Evaluation*, 104:23 – 41, 2016.
- [6] Yoad Lewenberg, Yoram Bachrach, Yonatan Sompolsky, Aviv Zohar, and Jeffrey S. Rosen-schein. Bitcoin mining pools: A cooperative game theoretic analysis. In *Proceedings of the 2015 International Conference on Autonomous Agents and Multiagent Systems*, AAMAS ’15, pages 919–927, Richland, SC, 2015. International Foundation for Autonomous Agents and Multiagent Systems.
- [7] Miles Carlsten, Harry Kalodner, S. Matthew Weinberg, and Arvind Narayanan. On the instability of bitcoin without the block reward. In *Proceedings of the 2016 ACM SIGSAC Conference on Computer and Communications Security*, CCS ’16, pages 154–167, New York, NY, USA, 2016. ACM.
- [8] Matthias Grundmann, Till Neudecker, and Hannes Hartenstein. Exploiting transaction accumulation and double spends for topology inference in bitcoin. In Aviv Zohar, Ittay Eyal, Vanessa Teague, Jeremy Clark, Andrea Bracciali, Federico Pintore, and Massimiliano Sala, editors, *Financial Cryptography and Data Security*, pages 113–126, Berlin, Heidelberg, 2019. Springer Berlin Heidelberg.
- [9] Péter L. Juhász, József Stéger, Dániel Kondor, and Gábor Vattay. A Bayesian approach to identify Bitcoin users. *PLoS ONE*, 13(12):e0207000, Dec 2018.
- [10] T. Neudecker, P. Andelfinger, and H. Hartenstein. Timing analysis for inferring the topology of the Bitcoin peer-to-peer network. In *2016 Intl IEEE Conferences on Ubiquitous Intelligence Computing, Advanced and Trusted Computing, Scalable Computing and Communications, Cloud and Big Data Computing, Internet of People, and Smart World Congress (UIC/ATC/ScalCom/CBDCCom/IoP/SmartWorld)*, pages 358–367, July 2016.

- [11] G. Zanzottera, P. Fragneto, and B. Rossi. A topological model for the blockchain. In *2018 IEEE 24th International Conference on Parallel and Distributed Systems (ICPADS)*, pages 1016–1021, Dec 2018.
- [12] Vincent Gramoli. From blockchain consensus back to byzantine consensus. *Future Generation Computer Systems*, 2017.
- [13] Hung Dang, Tien Tuan Anh Dinh, Dumitrel Loghin, Ee-Chien Chang, Qian Lin, and Beng Chin Ooi. Towards Scaling Blockchain Systems via Sharding. *arXiv e-prints*, page arXiv:1804.00399, Apr 2018.
- [14] Bitcoin Core Developers. Bitcoin reference client. <https://github.com/bitcoin/bitcoin>, 2019.
- [15] Erik De Win and Bart Preneel. *Elliptic Curve Public-Key Cryptosystems — An Introduction*, pages 131–141. Springer Berlin Heidelberg, Berlin, Heidelberg, 1998.
- [16] Certicom Research. SEC 1: Elliptic curve cryptography. 2009.
- [17] Certicom Research. SEC 2: Recommended elliptic curve domain parameters. 2010.
- [18] Adam Back. A partial hash collision based postage scheme. <http://www.hashcash.org/papers/announce.txt>, 1997.
- [19] Bitcoin core developers. Seeds utility. <https://github.com/bitcoin/bitcoin/tree/176aa5a/contrib/seeds>, 2018.
- [20] Peter Todd. python-bitcoinlib. <https://github.com/petertodd/python-bitcoinlib>, 2019.
- [21] Geoffrey Grimmett and David Stirzaker. *Probability and Random Processes*. Oxford University Press, 2001.
- [22] Masaaki Kijima. *Continuous-time Markov chains*, pages 167–241. Springer US, Boston, MA, 1997.
- [23] Daniel W. Stroock. *Markov Processes in Continuous Time*, pages 99–136. Springer Berlin Heidelberg, Berlin, Heidelberg, 2014.
- [24] *Linear Systems and Stability of Nonlinear Systems*, pages 145–224. Springer New York, New York, NY, 2006.
- [25] Marcel F. Neuts. Computational uses of the method of phases in the theory of queues. *Computers & Mathematics with Applications*, 1(2):151 – 166, 1975.
- [26] Marcel F. Neuts and Kathleen S. Meier. On the use of phase type distributions in reliability modelling of systems with two components. *Operations-Research-Spektrum*, 2(4):227–234, Dec 1981.
- [27] D. Peng, L. Fang, and C. Tong. A multi-state reliability analysis of single-component repairable system based on phase-type distribution. In *2013 International Conference on Management Science and Engineering 20th Annual Conference Proceedings*, pages 496–501, July 2013.
- [28] Adele Marshall, Sally McClean, Mary Shapcott1, and Peter Millard. Learning dynamic Bayesian belief networks using conditional phase-type distributions. In Djamel A. Zighed, Jan Komorowski, and Jan Żytkow, editors, *Principles of Data Mining and Knowledge Discovery*, pages 516–523, Berlin, Heidelberg, 2000. Springer Berlin Heidelberg.

- [29] Håkan L. S. Younes and Reid Simmons. Solving generalized semi-Markov decision processes using continuous phase-type distributions. pages 742–748, 01 2004.
- [30] Adele H. Marshall and Barry Shaw. Computational learning of the conditional phase-type (c-ph) distribution. *Computational Management Science*, 11(1):139–155, Jan 2014.
- [31] L. J. Perreault, M. Thornton, R. Goodman, and J. W. Sheppard. A swarm-based approach to learning phase-type distributions for continuous time Bayesian networks. In *2015 IEEE Symposium Series on Computational Intelligence*, pages 1860–1867, Dec 2015.
- [32] Alexander Herbertsson. Modelling default contagion using multivariate phase-type distributions. *Review of Derivatives Research*, 14(1):1–36, Apr 2011.
- [33] Søren Asmussen, Patrick J. Laub, and Hailiang Yang. Phase-type models in life insurance: Fitting and valuation of equity-linked benefits. *Risks*, 7(1), 2019.
- [34] M. K. Boroujeny, Y. Ephraim, and B. L. Mark. Phase-type bounds on network performance. In *2018 52nd Annual Conference on Information Sciences and Systems (CISS)*, pages 1–6, March 2018.
- [35] Asger Hobolth, Arno Siri-Jégousse, and Mogens Bladt. Phase-type distributions in population genetics. *arXiv e-prints*, page arXiv:1806.01416, Jun 2018.
- [36] C. Wang, Y. Zhang, G. Wang, and L. Wang. Reliability modeling of protection system based on phase-type distribution. In *2012 3rd IEEE PES Innovative Smart Grid Technologies Europe (ISGT Europe)*, pages 1–5, Oct 2012.
- [37] Adele H. Marshall and Sally I. McClean. Using Coxian phase-type distributions to identify patient characteristics for duration of stay in hospital. *Health Care Management Science*, 7(4):285–289, Nov 2004.
- [38] Vincent A Knight and Paul R Harper. Modelling emergency medical services with phase-type distributions. *Health Systems*, 1(1):58–68, Jun 2012.
- [39] Søren Asmussen, Olle Nerman, and Marita Olsson. Fitting phase-type distributions via the EM algorithm. *Scandinavian Journal of Statistics*, 23(4):419–441, 1996.
- [40] Mogens Bladt and Bo Friis Nielsen. *Estimation of Phase-Type Distributions*, pages 671–701. Springer US, Boston, MA, 2017.
- [41] *Phase-Type Distributions*, pages 169–184. Springer Netherlands, Dordrecht, 2005.
- [42] Shu Kay Ng, Thriyambakam Krishnan, and Geoffrey J. McLachlan. *The EM Algorithm*, pages 139–172. Springer Berlin Heidelberg, Berlin, Heidelberg, 2012.
- [43] C. F. Jeff Wu. On the convergence properties of the EM algorithm. *Ann. Statist.*, 11(1):95–103, 03 1983.
- [44] Marita Olsson. Estimation of phase-type distributions from censored data. *Scandinavian Journal of Statistics*, 23(4):443–460, 1996.
- [45] H. Akaike. A new look at the statistical model identification. *IEEE Transactions on Automatic Control*, 19(6):716–723, December 1974.

- [46] Ritei Shibata. *Statistical Aspects of Model Selection*, pages 215–240. Springer Berlin Heidelberg, Berlin, Heidelberg, 1989.
- [47] Kenneth P. Burnham and David R. Anderson, editors. *Information and Likelihood Theory: A Basis for Model Selection and Inference*, pages 49–97. Springer New York, New York, NY, 2002.
- [48] C. Van Loan. Computing integrals involving the matrix exponential. *IEEE Transactions on Automatic Control*, 23(3):395–404, June 1978.
- [49] F. Carbonell, J.C. Jiménez, and L.M. Pedroso. Computing multiple integrals involving matrix exponentials. *Journal of Computational and Applied Mathematics*, 213(1):300 – 305, 2008.
- [50] Sophie Hautphenne and Mark Fackrell. An EM algorithm for the model fitting of Markovian binary trees. *Computational Statistics & Data Analysis*, 70:19 – 34, 2014.
- [51] C. Moler and C. Van Loan. Nineteen dubious ways to compute the exponential of a matrix, twenty-five years later. *SIAM Review*, 45(1):3–49, 2003.
- [52] Marita Olsson. *The EMpht-programme*, June 1998.
- [53] Donald Gross and Douglas R. Miller. The randomization technique as a modeling tool and solution procedure for transient Markov processes. *Operations Research*, 32(2):343–361, 1984.
- [54] W.K. Grassmann. Transient solutions in markovian queueing systems. *Computers & Operations Research*, 4(1):47 – 53, 1977.
- [55] Hiroyuki Okamura, Tadashi Dohi, and Kishor S. Trivedi. A refined EM algorithm for PH distributions. *Performance Evaluation*, 68(10):938 – 954, 2011.
- [56] Hiroyuki Okamura, Tadashi Dohi, and Kishor S. Trivedi. Improvement of expectation–maximization algorithm for phase-type distributions with grouped and truncated data. *Applied Stochastic Models in Business and Industry*, 29(2):141–156, 4 2013.
- [57] Andrew Reibman and Kishor Trivedi. Numerical transient analysis of Markov models. *Computers & Operations Research*, 15(1):19 – 36, 1988.
- [58] Ch. Tsitouras. Runge–Kutta pairs of order 5(4) satisfying only the first column simplifying assumption. *Computers & Mathematics with Applications*, 62(2):770 – 775, 2011.
- [59] OrdinaryDiffEq.jl. <https://github.com/JuliaDiffEq/OrdinaryDiffEq.jl>, 2019.
- [60] Steven G. Johnson. HCubature.jl. <https://github.com/stevengj/HCubature.jl>, 2019.
- [61] A.C. Genz and A.A. Malik. Remarks on algorithm 006: An adaptive algorithm for numerical integration over an N-dimensional rectangular region. *Journal of Computational and Applied Mathematics*, 6(4):295 – 302, 1980.
- [62] Pascal Gauthier. Why do some Bitcoin mining pools mine empty blocks? <https://bitcoinmagazine.com/articles/why-do-some-bitcoin-mining-pools-mine-empty-blocks-1468337739/>, 2016.